Université de Montréal

Photoresponsive Supramolecular Polymer Films - Comparison of the Hydrogen and Ionic Bonding Strategies

Par
Mahnaz Kamaliardakani

Département de Chimie
Faculté des arts et des sciences

Mémoire présenté à la Faculté des études supérieures et postdoctorales en vue de l'obtention du grade de maître ès sciences (M.Sc.) en chimie

Août 2018

Résumé

Les complexes supramoléculaires dans lesquels un azobenzène photoactif est lié de manière non-covalente à un polymère représentent des alternatives simples, économiques et flexibles par rapport aux matériaux photosensibles traditionnels de type azopolymères à chaînes latérales. La photoisomérisation rapide et réversible des azobenzènes permet d'exercer un contrôle externe efficace des propriétés du matériau hôte et peut donner lieu à des déplacements moléculaires à grande échelle, tels que le transport de masse macroscopique photoinduit sous illumination par de la lumière polarisée. Les phénomènes induits par la lumière dans les azomatériaux offrent un grand potentiel dans divers domaines d'application allant de la photonique à la biologie. Les matériaux supramoléculaires photosensibles sont souvent basés sur des liaisons hydrogène mais l'utilisation des liaisons ioniques entre des composés de charges opposées est également une approche supramoléculaire intéressante pour concevoir des complexes azopolymères.

Dans ce mémoire, les assemblages supramoléculaires du poly(4-vinylpyridine) (P4VP) photopassif et de son dérivé quaternisé (P4VPMe) sont liés par des liaisons hydrogène et ioniques à de petites molécules photoactives analogues, respectivement le 4-hydroxy-4'-diméthylamino-azobenzène (azoOH) et l'orange de méthyle (MO), qui présente un groupement sulfonate à la place de la fonction OH. Ces complexes photoactifs sont étudiés avec les objectifs suivants :

1. Comprendre l'effet du type d'interaction sur les propriétés photoinduites des azocomplexes, en particulier leur orientation moléculaire et l'efficacité de diffraction de leurs réseaux de relief de surface (SRG).

2. Déterminer le rôle de la masse molaire du polymère (5,2 kg/mol, 50 kg/mol et 200 kg/mol) sur la photosensibilité des azocomplexes.

La complexation entre les composants est d'abord confirmée par spectroscopie infrarouge statique (IR) et RMN ^{1}H. La spectroscopie UV-visible de film minces irradiés par un faisceau laser à 488 nm polarisé linéairement confirme l'absence de séparation de phases et révèle un pourcentage minimum d'isomères *cis* à l'état photostationnaire similaire pour les deux séries de complexes (respectivement 14% et 20 % pour azoOH et MO).

La spectroscopie IR d'absorption structurale avec modulation de la polarisation (PM-IRSAS) est ensuite utilisée pour étudier l'impact du type d'interaction supramoléculaire et de la masse molaire du polymère sur l'orientation photoinduite des azocomplexes. Leurs mouvements macroscopiques photoinduits par un patron d'interférence de lumière polarisée circulairement à 488 nm sont également étudiés en mesurant *in situ* l'efficacité de diffraction lors de l'inscription de SRG.

Nous avons trouvé que les complexes ioniques répondent à la lumière beaucoup plus fortement que les complexes analogues liés par liaisons H, à la fois en termes d'orientation et d'efficacité de diffraction. Les résultats de PM-IRSAS montrent également une contribution beaucoup plus grande de la redistribution angulaire sur la déplétion angulaire sélective (angular hole burning) pour les complexes de MO. Par contre, la masse molaire du polymère hôte n'a pas d'impact important sur la photo-orientation moléculaire, alors qu'elle a un effet substantiel sur l'efficacité de l'inscription des SRG, le complexe de faible masse molaire présentant une performance supérieure à celle des deux autres complexes. Nous concluons que l'enchevêtrement des chaînes joue un rôle plus important que la température de transition vitreuse pour le phototransport dans ces systèmes.

Le mémoire fournit des connaissances fondamentales sur l'effet de la nature et de la force des interactions supramoléculaires sur la photosensibilité des azocomplexes, contribuant ainsi à améliorer la conception de polymères photosensibles supramoléculaires efficaces.

Mots-clés : fonctionnalisation supramoléculaire, azobenzène, complexe azopolymère, photo-orientation, photoisomérisation, réseau de relief de surface.

Abstract

Supramolecular non-covalently bonded azobenzene-containing complexes are easy-to-prepare alternatives to covalently bonded azopolymers as photoresponsive materials. The rapid and reversible nanoscale photoisomerization of azobenzenes enables effective external control of the host material's properties and they can give rise to large-scale motions, such as macroscopic mass transport with polarized illumination. The light-induced phenomena in azomaterials offer great potential in various areas ranging from photonics to biology. Photoresponsive supramolecular materials often hydrogen bond between a passive polymer and a photoactive small molecule. However, ionic bonding between oppositely-charged components is also a versatile supramolecular approach to design azobenzene-containing systems.

In this M.Sc. thesis, supramolecular assemblies of photopassive poly(4-vinylpyridine) (P4VP) and its quaternized derivative (P4VPMe) are hydrogen-bonded (H-bonded) and ionically bonded (i-bonded), respectively, with analogous photoactive small molecules. The small molecules studied are 4-hydroxy-4′-dimethylaminoazobenzene (azoOH) and methyl orange (MO), respectively, where the OH functionality of azoOH is replaced by a sulfonate group in MO. These photoactive complexes are studied with the following objectives:

1. To understand the effect of the bonding type on the photoinduced properties of azocomplexes, in particular their molecular orientation and their surface relief grating (SRG) diffraction efficiency (DE).
2. To determine the role of the polymer molecular weight (5.2, 50, and 200 kg/mol) on the photosensitivity of the azocomplexes.

The complexation between components is first confirmed using static infrared (IR) spectroscopy and ^{1}H NMR. UV-visible spectroscopy studies under illumination of linearly polarized 488-nm laser light of spin-coated thin films confirms the absence of phase separation in both series of complexes and reveals a similar minimum percentage of *cis* isomers (14% vs. 20% for azoOH and MO, respectively).

Polarization modulation infrared structural absorbance spectroscopy (PM-IRSAS) is then used to investigate the impact of the supramolecular interaction type and the polymer molecular weight (MW) on the molecular-level photoinduced orientation ($<P_2>$) of the azocomplexes using

linearly polarized 488-nm light. Then, their photoinduced macroscopic-scale motion that produces surface relief gratings (SRG) is investigated using an interference pattern of circularly polarized 488-nm light.

We find that i-bonded complexes respond to light more strongly than their analogous H-bonded complexes, both in terms of $<P_2>$ and DE values. The PM-IRSAS results also show a much larger contribution of angular redistribution over angular hole burning for the MO-based complexes. In addition, the host polymer MW does not impact the molecular photo-orientation, while it does affect the SRG inscription efficiency. The low MW complex shows a higher DE than the two higher MW complexes. We can conclude that chain entanglement plays a more important role than the glass transition temperature for phototransport in these systems.

The M.Sc. thesis provides fundamental knowledge of the effect of the supramolecular interaction type and strength on the photosensitivity of azocomplexes. This knowledge contributes to practical guidelines for the design of efficient supramolecular photoresponsive polymers.

Keywords : supramolecular functionalization, azobenzene, azopolymer complex, photo-orientation, photoisomerization, photoinduced surface relief grating.

Table of contents

List of Figures

List of Tables

List of Schemes

List of Abbreviations

A_0	Structural absorbance
A_p	Absorbance parallel to the pump beam polarization
A_s	Absorbance perpendicular to the pump beam polarization
A_{ini}	Initial absorbance before irradiation
A_{irr}	Maximum absorbance under irradiation
AFM	Atomic force microscopy
AHB	Angular hole burning
AR	Angular redistribution
ATR	Attenuated total reflection
ATRP	Atom transfer radical polymerization
azoOH	4-Hydroxy-4′-dimethylaminoazobenzene
azoOH/P4VP	Hydrogen-bonded azocomplex
d	Film thickness
DE	Diffraction efficiency
DE_{res}	Residual diffraction efficiency
DFT	Density functional theory
DMF	Dimethylformamide
DMSO	Dimethyl sulfoxide
DN	Degree of neutralization
DR1	Disperse Red 1
DR1M	Disperse Red 1 methacrylate

DSC	Differential scanning calorimetry
FT-IR	Fourier transform infrared
h	Planck's constant
H-bonding	Hydrogen bonding
^{1}H NMR	Proton nuclear magnetic resonance
I	Intensity of the transmitted light
I_0	Intensity of the incident light
i-bonding	Ionic bonding
IR	Infrared
IRLD	Infrared linear dichroism
k	Boltzmann constant
k	Rate constant
LC	Liquid crystalline
MO	Methyl orange: 4-[(4-dimethylamino)phenylazo]benzene sulfonate
MO/P4VPMe	Ionically bonded azocomplex
MW	Molecular weight
NHA	4-Nitro-4′-hydroxyazobenzene
OD	Optical density
p	Parallel direction to the electric field of polarization
P_{cis}	*Cis* content
PADA	4-(2-Pyridylazo)-*N,N*-dimethylaniline
PAZO	Poly(1-[4-(3-carboxy-4-hydroxyphenylazo)benzenesulfonamido]-1,2-ethanediyl sodium salt)

PCMS	Poly(chloromethylstyrene)
PDM	Poly(dimethylaminoethyl methacrylate)
PDMQ	Quaternized PDM
PDR1A	Poly(Disperse Red 1 acrylate)
PDR1M	Poly(Disperse Red 1 methacrylate)
PIB	Photoinduced birefringence
pK_a	Acid dissociation constant on logarithmic scale
PMEA	Poly[4-[2-(methacryloyloxy)ethyl]azobenzene]
PMMA	Poly(methyl methacrylate)
PM-IRLD	Polarization modulation infrared linear dichroism
PM-IRSAS	Polarization modulation infrared structural absorbance spectroscopy
Psi	Polysiloxane
PVPh	Poly(4-vinyl phenol)
P4VP	Poly(4-vinylpyridine)
P4VPEt	Ethylated poly(4-vinylpyridine)
P4VPMe	Methylated poly(4-vinylpyridine)
R	Dichroic ratio
RD	Rotational diffusion
s	Perpendicular direction to the electric field polarization
SRG	Surface-relief grating
t	Time
T	Temperature
T_g	Glass transition temperature

THF	Tetrahydrofuran
UV	Ultraviolet
UV-vis	Ultraviolet-visible spectroscopy
X-bonding	Halogen bonding
α	Angle between the transition dipole moment and the molecular main axis
ΔA	Dichroic difference
$\lvert\Delta n\rvert$	Absolute birefringence
λ	Wavelength
λ_{max}	Maximum wavelength of absorption
v	Photon frequency
τ	Time constant
$\langle P_2 \rangle$	Orientation parameter
$\langle P_2 \rangle_{max}$	Maximum orientation
$\langle P_2 \rangle_{res}$	Residual orientation
$\langle T_2 \rangle$	Normalized linear dichroism
2NHA	[(2,5-Dimethoxy-4-((4-nitrophenyl)diazenyl)phenyl)diazinyl]phenol

Acknowledgements

This research wouldn't have been possible without the guidance of my supervisors, Prof. C. Géraldine Bazuin and Prof. Christian Pellerin. I would like to express my deepest gratitude to them for welcoming me to their laboratories and treating me friendly during my master's study. I also would like to thank them sincerely for their patient discussions about my project and their detailed corrections for my manuscript and thesis. I will never forget it.

Many acknowledgements are addressed to the postdoctoral fellow, Dr. Jaana Vapaavuori, for her kind personality, endless understanding, professional help and for giving me her time in listening to me and helping me work out my problems during my master's program.

I thank Dr. Xiaoxiao Wang for his great idea during the synthesis of materials used for this research and his generous help.

I am grateful to Prof. R. Georges Sabat at the Royal Military College of Canada (RMC) for allowing me to gain valuable experience by giving me the opportunity to do some parts of experiments in his laboratory at RMC.

I acknowledge the support personnel in the Chemistry Department, particularly Sylvain Essiembre for their valuable and professional help and kind behavior.

I am appreciative to all the students in the groups of Bazuin and Pellerin, particularly Catherine Lanthier, who offered a lot of help to let me accommodate myself to this new francophone environment. I also thank Zeinab Kara Ali and Anna Gittsegrad for their help during my master's program.

I express my appreciation to all those who helped me in the laboratory during my experiments.

Finally, I express my heartfelt gratitude to my beloved family for loving considerations and great confidence in me all through these years, and my great thanks to my parents for their encouragement, constant support, trust, and love.

Chapter 1: Introduction

1.1. Supramolecular materials

It is more than two centuries that molecular chemistry has been widely used to create molecules and complicated materials from atoms through covalent bonds, which can be termed "molecular chemistry". Beyond molecular chemistry, supramolecular chemistry has paved the way to construct highly sophisticated, functional chemical systems from components held together by intermolecular forces. The concept of supramolecular functionalization was first introduced by Jean-Marie Lehn in the late 1960s and then developed by him, Donald J. Cram and Charles J. Pedersen who shared the Nobel Prize in Chemistry in 1987.[1]

The principle of this procedure is the connection of components having molecular receptors that are capable of selectively binding one another via non-covalent interactions, such as hydrophobic interactions, metal coordination, π-π stacking, hydrogen bonding, and electrostatic forces. According to Lehn "*supramolecular polymers are reversible, constitutionally dynamic materials, capable of modifying their constitution by exchanging, recombining, incorporating components*".[2] The supramolecular functionalization strategy can be considered as a powerful tool that gives rise to many subfields, such as molecular self-assembly, molecular recognition, template-directed synthesis, mechanically interlocked molecular architectures, biomimetics, and molecular machinery.[3,4]

In addition to the variety of supramolecular non-covalent bonding types, the strength of interactions is also variable. They range from strong ionic bonds that have comparable strength of a covalent bond, 350 kJ/mol, to very weak hydrogen bonds, with strengths on the order of 5 kJ/mol. [3,5] They can also be used with different molecular architectures to form network, rodlike, fibrous, disclike, helical, lamellar and various chainlike structures, as shown in Figure 1.1.[6] Thus, a variety of materials with different shapes and numerous potential applications can be prepared with the help of the dynamic and often reversible character of the supramolecular bonds. Amongst all these material systems, assemblies between polymers with side chain functional groups and appropriately functionalized small molecules (Figure 1.2c) are of particular interest to researchers.

These functional materials can be constructed easily by mixing readily available or easily modifiable components, as opposed to the time-consuming synthesis of covalent functional side-chain polymers (Figure 1.2b).[7] This synthetic strategy combines the simplicity of doping (mixing small molecules with polymers, Figure 1.2a) while retaining the robustness of the covalently bonded side-chain polymers.[8,9]

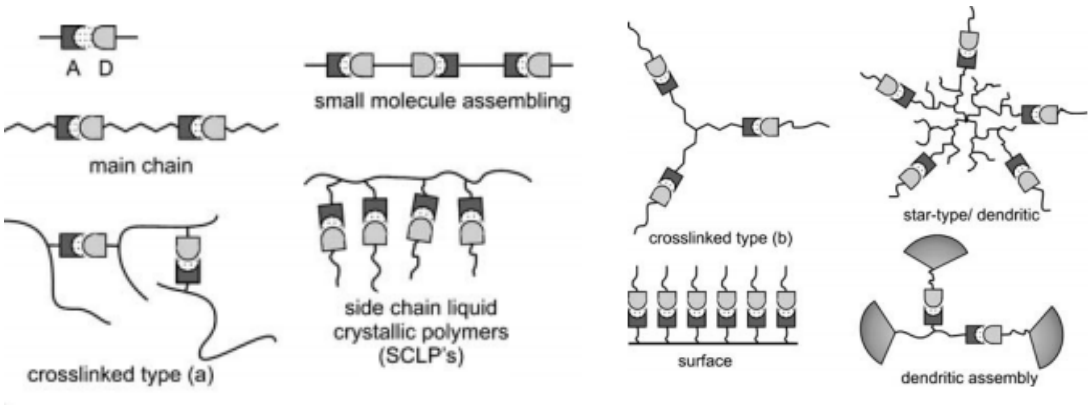

Figure 1.1. Architectures of different supramolecular hydrogen-bonded polymers (A: hydrogen-bonding acceptor, D: hydrogen-bonding donor). Reproduced with permission from Ref. 6, Copyright 2006 Springer-Verlag Berlin Heidelberg.

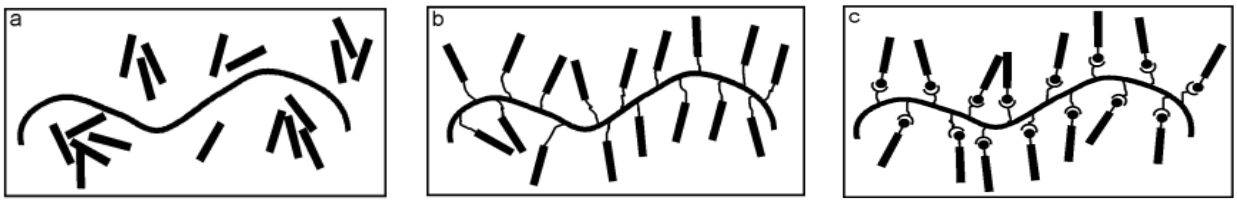

Figure 1.2. Schematic representations of three types of polymer materials: (a) conventional non-bonded guest-host system (also called doping), (b) covalently linked side-chain system, and (c) side-chain system formed by supramolecular interactions. Reprinted with permission from Ref. 10, Copyright 2005 American Chemical Society.

Considering the above, there are three substantial advantages to applying supramolecular chemistry instead of conventional methods for attaching functionalized small guest molecules to a polymer host:

(1) The supramolecular strategy either prevents or decreases aggregation and crystallization, or macro-phase separation, of the functionalized small molecules. This is in contrast to conventional non-bonded guest-host methods (mixing of the small molecules with a polymer matrix; Figure 1.2a).[10,11]

(2) The easy preparation of material systems through the supramolecular technique makes it a more convenient method compared to the synthesis of polymers with covalently attached side chains (Figure 1.2b).

(3) The dynamic character of non-covalent supramolecular bonds allows the possibility of non-destructive detachment and removal of the small molecules using appropriate solvents. For instance, selective detachment of a strongly coloured chromophore, attached to a polymer via supramolecular hydrogen bonds, from films inscribed with surface relief gratings (SRG, defined in section 1.6) without changing their periodic structures has been done by Zettsu et al.[12] to improve its efficiency as an optical element (Figure 1.3).

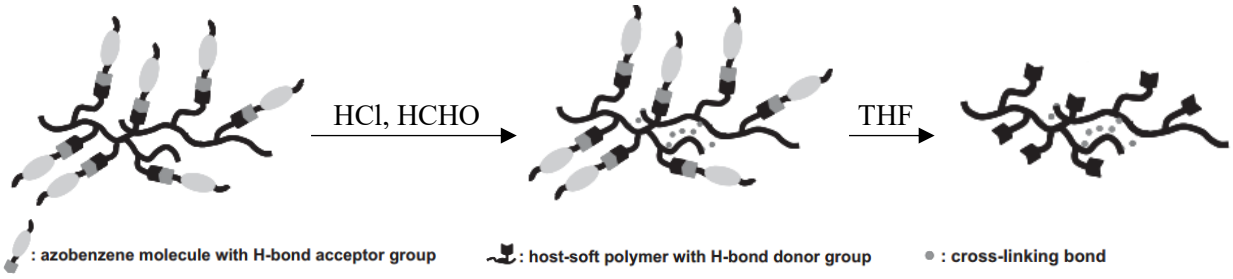

Figure 1.3. Schematic illustration of a hydrogen-bonded (H-bond) supramolecular polymer film and the selective detachment of chromophore units from the SRG-inscribed films. Adapted with permission from Ref. 12, Copyright 2008 John Wiley & Sons, Inc.

1.2. Supramolecular interactions

Supramolecular complexes can be categorized by the nature and strength of the interactions between the polymer host and the guest molecules. Among the different types of supramolecular interactions, the hydrogen bond, the ionic bond, and the halogen bond have received the most attention for developing and studying supramolecular complexes.

1.2.1. Hydrogen bonding (H-bonding)

According to the IUPAC definition,[13] *"the hydrogen bond is an attractive interaction between a hydrogen atom from a molecule or a molecular fragment* $X-H$ *in which X is more electronegative than H, and an atom or a group of atoms in the same or a different molecule, in which there is evidence of bond formation."* Connecting two components through a hydrogen bond can be done by attraction between a hydrogen-bond acceptor, which is an atom with a lone-pair or π-electrons, and an unprotected proton in the covalent bond $X-H$, which acts as a hydrogen-bond donor. These monovalent hydrogen bonds can be used, for example, to build dimeric, oligomeric, and polymeric building blocks into supramolecular main-chain liquid crystalline polymers.[6] Supramolecular side-chain hydrogen-bonded polymers with different structures, such as lamellar, mesoporous, and fibrous, can be synthesized in a similar manner. To achieve such architectures, an assembled structure of molecules bind through hydrogen bonding to a covalently synthesized main chain (a homopolymer or a block copolymer, for example) containing molecular recognition units as side groups, as shown in Figure 1.4.[8] For instance, side-chain liquid crystalline materials can be prepared by attaching side-chain mesogenic units to the polymer backbone.[14,15] Supramolecular polymers and networks can also be formed via multiple hydrogen bonds (Figure 1.5).[6]

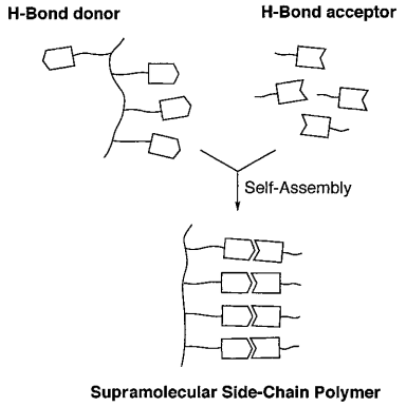

Figure 1.4. Self-assembly of supramolecular side-chain polymers consisting of a functionalized polymer backbone as the hydrogen-bond donor and functionalized small molecules as hydrogen-bond acceptors. Reproduced with permission from Ref. 14, Copyright 2001 John Wiley & Sons, Inc.

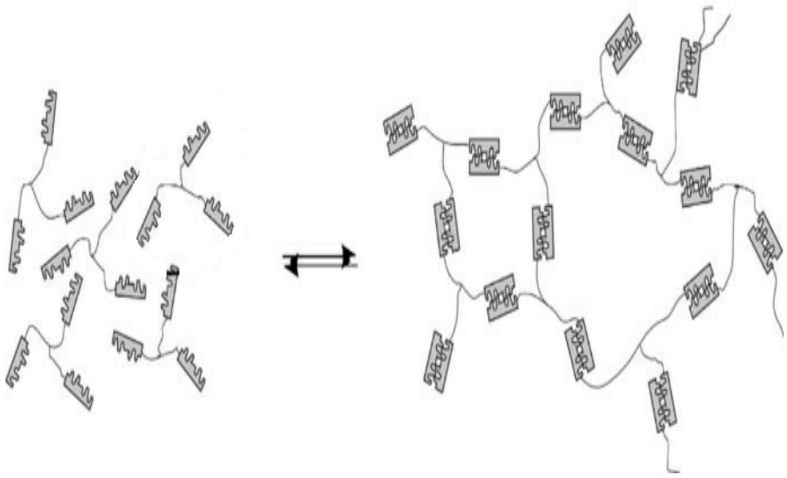

Figure 1.5. Formation of supramolecular polymers and networks via self-complementing quadrupolar hydrogen bonds. Adapted with permission from Ref. 6, Copyright 2006 Springer-Verlag Berlin Heidelberg.

One of the characteristics of the hydrogen bond that influences packing modes in crystals is its directional nature. This is related to the preference of the $X-H\cdots Y$ interaction towards linearity.[13] This directional nature of the hydrogen bond, as well as the structural diversity of hydrogen-bonding systems, render H-bonding as one of the most-commonly used interactions to prepare material systems through supramolecular chemistry.

H-bonding systems can be divided into three categories based on their strength:[6] strong hydrogen bonds with both a strong directional nature and association energies higher than ~40 kJ/mol, medium or weak hydrogen bonds where directionality is partially lost and the bond energies are less than ~40 kJ/mol, and either nonclassical or unconventional hydrogen bonds (Figure 1.6). The strength of the directional hydrogen bond depends on the nature of the hydrogen-bond donor and acceptor atoms (D and A), such as electron-withdrawing capacity and atomic radius, as well as the external environment, such as the solvent used. The strength of the hydrogen-bonding system is also related to the number of individual hydrogen bonds per molecule in the system. Therefore, the strength of the H-bonded complexes can be tuned by the number of hydrogen bonds and internal or external parameters. These lead to a highly controllable level of inter-molecular ordering. This property also makes the hydrogen bond a prominent non-covalent bond to design supramolecular systems, even though it is not the strongest non-covalent interaction.[6,16]

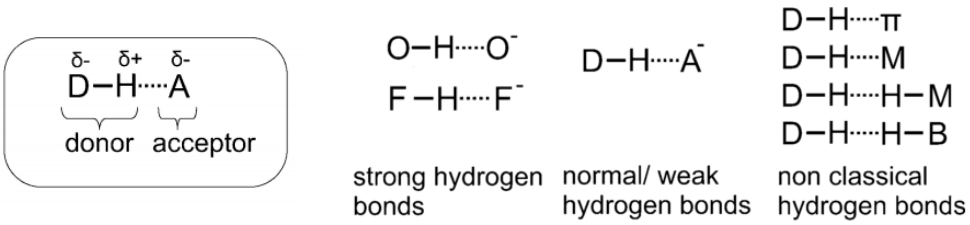

Figure 1.6. Presentation of three different classes of hydrogen bonds (D: hydrogen-bonding donor, A: hydrogen-bonding acceptor; M: metal; B: boron). Adapted with permission from Ref. 6, Copyright 2006 Springer-Verlag Berlin Heidelberg.

To summarize, hydrogen bonds are used not only as molecular tools to guide the supramolecular assembly of polymer-based materials into a certain order, but they are also used to tune material properties, depending on (a) the hydrogen bond strength, (b) the directionality and the recognition capability, and (c) the reversible nature of the interaction using external stimuli, such as solvents, temperature, and external fields (shear, electric fields, magnetic fields). These characteristics allow the design of a diversity of materials with practical and new properties through H-bonded supramolecular chemistry.[6]

1.2.2. Ionic bonding (i-bonding)

Another interaction exploited to design supramolecular functional materials is ionic bonding, whose strength is similar to that of the covalent bond. The ionic bond is defined as an electrostatic attraction between two opposite charges.[17] In contrast to the H-bond, the ionic bond is non-directional. There are two ways to obtain non-directional bonding interaction: a) through a proton transfer procedure, which often involves some H-bonding, for example from a sulfonic acid group to pyridine, or from carboxylic acid to a tertiary amine, and b) through an ion exchange procedure between two salts.[3]

The ionic bond has been used for a wide range of charged pairs, such as dye-surfactant,[18,19] surfactant-polyelectrolyte,[20,21] and dye-polyelectrolyte[22-24] to form self-assembled, ordered structures (Figure 1.7). Among the variety of systems are ionic dye-polyelectrolyte materials in solution form[25,26] and in the solid state,[22-24,27,28] including Langmuir-Blodgett films,[29-31] and layer-

by-layer films.[32,33] They are of interest because of properties, such as liquid crystallinity, rigidity, possibility of high dye loading, and photosensitivity. According to different applications, a variety of ionically bonded complexes can be formulated by the selection of readily available or easily modified and inexpensive commercial constituents.[34]

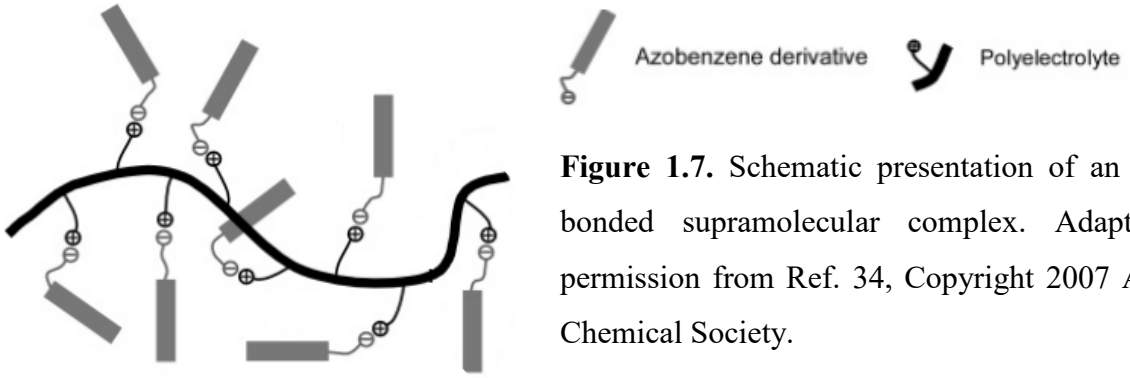

Figure 1.7. Schematic presentation of an ionically bonded supramolecular complex. Adapted with permission from Ref. 34, Copyright 2007 American Chemical Society.

By comparing hydrogen-bonded systems with ionically bonded systems, the principal differences between these two binding mechanisms can be summarized as follows:

I. The i-bond is a non-directional interaction whose strength ranges from 50 to 250 kJ/mol, whereas the H-bond is a directional bond with a strength of 5 to 65 kJ/mol.[5]
II. Ionic systems can be formed by a cooperative zipper-like binding between the guest units and polymer hosts, whereas H-bonding is always non-cooperative and leads to random binding of the components.[5]
III. H-bonding allows for a convenient control over the guest content by easy adjustment of the mixing ratio of two components. In the ionic architectures, cooperative binding usually leads to 1:1 stoichiometry between the components or parts of the components if they are not in equimolar proportion.[5]

1.2.3. Halogen bonding (X-bonding)

Halogen bonding is an emerging non-covalent interaction for supramolecular assembly.[35-40] According to the definition by IUPAC,[41] *"a halogen bond occurs when there is evidence of a*

net attractive interaction between an electrophilic region associated with a halogen atom in a molecular entity and a nucleophilic region in another, or the same, molecular entity." Although hydrogen bonds and halogen bonds, where covalently-bonded hydrogens ($R-H$) or halogens ($R-X$) are attached to sites with partial negative charge (lone electron pair or π-electrons), are very similar in nature, they also differ from each other. First, halogen bonds lead to greater linearity than hydrogen bonds: in the former, the $R-X\cdots A$ link is typically linear or near-linear with bond angles close to 180°, whereas in the latter the $R-H\cdots A$ link is more likely to be nonlinear with bond angles usually considerably less than 180°. Examples of H-bonding between H_2O molecules and of X-bonding between a CH_3Br and a H_2O molecule are shown in Figure 1.8. Second, the interaction strength of the X-bond scales with the polarizability of the halogen atom, so the bond strength order develops as I > Br > Cl. Thus, the strength of the halogen bond interaction can be tuned by a single-atom mutation.[35,42-45]

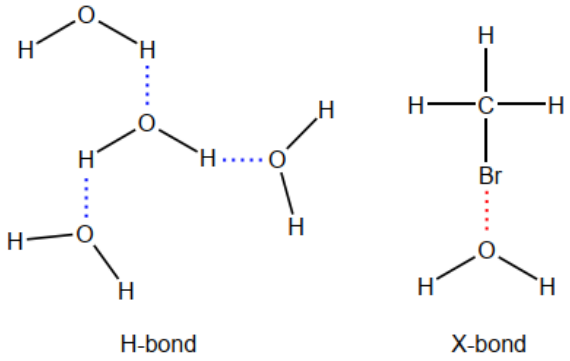

Figure 1.8. Schematic presentation of bond angles of H-bonding and X-bonding. Reproduced from Ref. 42, Copyright 2014.

The unique features of halogen bonding, directionality and tunable interaction strength, renders halogen bonding a useful tool in designing functional supramolecular materials. Priimagi et al.[35] highlighted the recent advances of using halogen bonding in the design of functional materials. In addition, Cavallo and co-workers[46] have summarized the specific advantages of using the halogen bond in various fields, including material sciences, biomolecular recognition, and drug design.

1.3. Photoresponsive polymer complexes

Supramolecular bonding between a variety of polymers and small molecules are widely used to prepare photoresponsive assemblies. Usually, these involve a passive polymer (often termed host) and photoactive small molecules based on azobenzene (often termed guests). Azobenzene derivatives are the most commonly utilized small molecules to prepare azopolymer complexes, with poly(4-vinyl pyridine) (P4VP) as a popular polymer host.[3] In the following, the relevant characteristics of azobenzene derivatives will be reviewed and then various polymer complexes involving azo-based small molecules, with a particular emphasis on P4VP-based hosts, will be presented.

1.3.1. Azobenzenes

Azobenzenes, also called azo dyes or azo chromophores, are diazene (HN=NH) derivatives where phenyls replace both hydrogens. According to Rau,[47] these chromophores can be divided into three categories, distinguishable by their spectroscopic characteristics as well as their colours based on the benzene ring substitutions, as shown in Figure 1.9a:[7,48,49]

a. Azobenzene molecules with yellow colour: unsubstituted azobenzene and azobenzene derivatives with non-polar substituents, such as long aliphatic groups.
b. Aminoazobenzene molecules with orange colour: *ortho*- or *para*-substituted azobenzenes with an electron-donating group (usually an amino, $–NH_2$, hydroxy, –OH, or alkoxy, –OR).
c. Pseudostilbene azo molecules with red colour: *para*-substituted azobenzenes with an electron-donating group (such as an amino group) at one end and an electron-withdrawing group (such as a nitro group, $–NO_2$) at the other end, giving them an electronic *push-pull* character. Molecules with weak electronic *push-pull* quality, e.g. 4-nitro-4′-hydroxy-azobenzene, can be classified under the aminoazobenzene category. The classification scheme relies more on their absorption spectrum and photophysical properties rather than on their chemical structure.

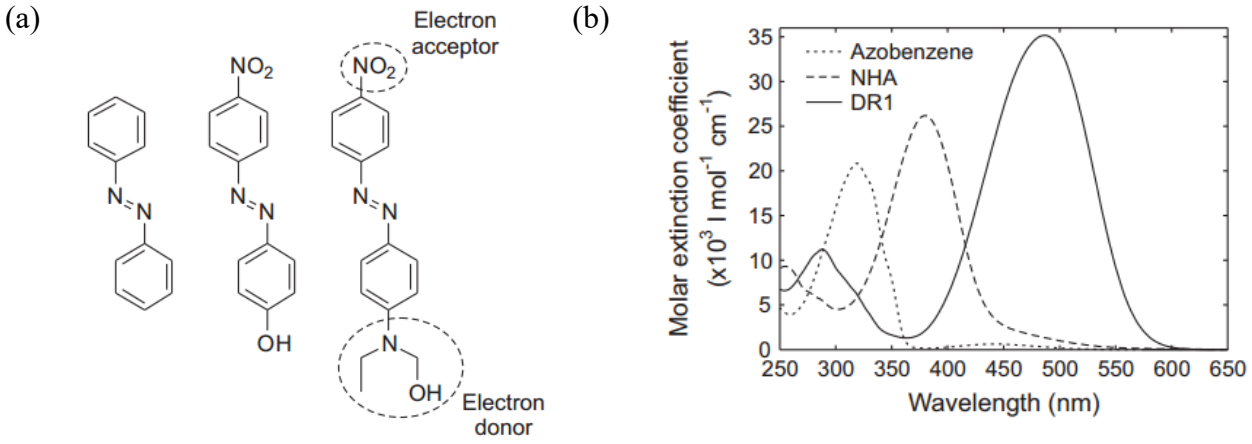

Figure 1.9. (a) Chemical structures representative of three categories of azobenzene derivatives: an azobenzene (unsubstituted azobenzene, left), an aminoazobenzene (4-nitro-4′-hydroxy-azobenzene (NHA), center), and a pseudostilbene (Disperse Red 1 (DR1), right) chromophore. (b) Absorption spectra of azobenzene, NHA and DR1 in dilute tetrahydrofuran solution. Reprinted with permission from Ref. 48, Copyright 2009 Helsinki University of Technology.

One of the common features of azobenzene molecules is their strong electronic absorption in the ultraviolet and visible wavelength region due to the extended conjugated π system. The substitution pattern of azobenzenes has a strong effect on their spectral and photophysical properties. Figure 1.9b shows the difference in the absorption spectra of the three different azobenzenes. This difference is related to the relative energies of the n-π^* and π-π^* transitions, where the former originates from the non-bonding pairs of electrons localized on the nitrogen atom and the latter results from the excitation of a delocalized π-electron of the N=N moiety. For example, azobenzene molecules have an intense π-π^* band in the near UV and a weak n-π^* band in the visible region. For aminoazobenzenes, the π-π^* band is red-shifted region and thus partly overlaps the n-π^* band. For pseudostilbenes, the n-π^* band almost completely overlaps with the intense π-π^* transition.[7,48] Indeed, the colour change from yellow to orange to red is a consequence of the red-shift of the dominant absorption band from the UV to the visible region.

Another common and important characteristic of azobenzene derivatives is the clean, efficient, and reversible isomerization between a rod-like, thermally stable *trans* isomer and a

globular, metastable *cis* isomer that can be distinguished by a twisting of the phenyl rings relative to the plane of the azo bond and a 44% reduction in the distance between the 4 and 4′ positions, as indicated in Figure 1.10a.[7,48] For the parent azobenzene, the *trans* isomer is more stable by about 50 kJ/mol in comparison with the *cis* form, making the former the predominant form at room temperature.[47] *Trans-cis* isomerization occurs after exposing the molecules to external triggers, such as irradiation with UV-visible light,[47] mechanical stress,[50] or electrostatic stimulation,[51] while thermal *cis-trans* isomerization can happen spontaneously in the dark due to the higher thermodynamic stability of the *trans* isomer.[52] The photoisomerization of azobenzenes is the origin of many interesting phenomena used in different applications, such as molecular machines[53,54] and holographic recording devices.[55,56]

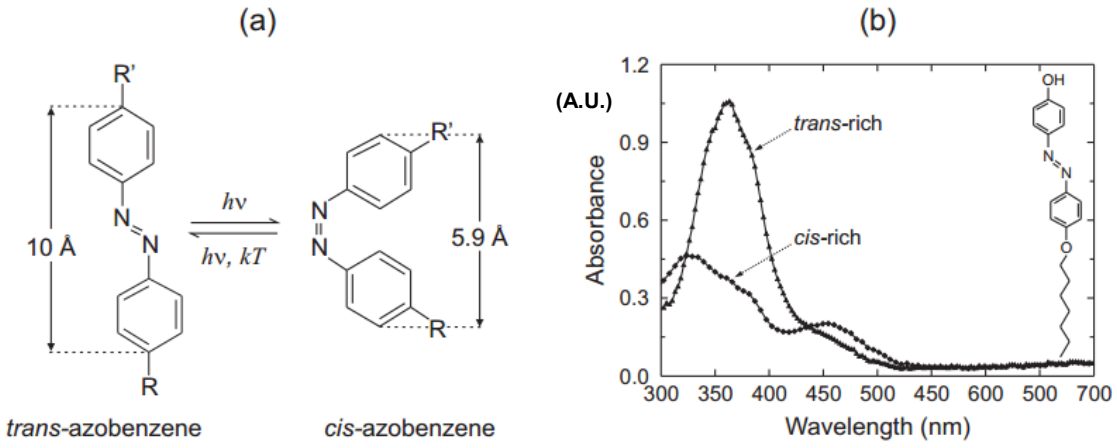

Figure 1.10. (a) *Trans-cis* photoisomerization reaction of azobenzene. (b) Absorption spectra of thin films of the *trans*-rich and *cis*-rich states of 4-(4′-heptyloxyphenyl)azophenol, shown in the inset, before and after irradiating with light. Reprinted with permission from Ref. 48, Copyright 2009 Helsinki University of Technology.

Absorption of a photon with an energy hν where *h* is Planck's constant and *v* is the photon's frequency (usually in the UV range), triggers *trans-cis* photoisomerization that crosses an energy barrier of around 200 kJ/mol within a timescale of picoseconds. The *cis-trans* relaxation occurs either thermally (kT, the product of the Boltzmann constant, *k*, and the temperature, *T*) with an energy barrier on the order of 100-150 kJ/mol or radiatively by absorbing a photon with an energy

hν (in the visible range).[7,42] The timescale for the thermally-driven back isomerization is on the order of hours, minutes and seconds for azobenzenes, aminoazobenzenes, and pseudostilbenes, respectively. In other words, the *cis* lifetime is strongly dependent on the electronic structure and substitution pattern of the azo derivative as well as on surrounding conditions, such as temperature and solvent.[7,16] Yager and Barrett[57] have summarized the *cis* lifetimes of different main-chain and side-chain azobenzene-containing materials, which range from 4 days up to 6 years. Upon *trans*-*cis* photoisomerization, the π-π^* band of the *trans* isomer is slightly blue-shifted and its intensity is significantly reduced, while the n-π^* band of the cis state appears, as illustrated in Figure 1.10b.[48] Continuous illumination of a solution or solid azobenzene-containing sample culminates in a photostationary state between the photoinduced and thermally-driven reactions.[7,16]

Based on X-ray diffraction methods and computational techniques applied to azobenzenes, the *trans* form has a planar structure with C_{2h} symmetry, whereas the *cis* state adopts a non-planar conformation with C_2 symmetry.[58-61] Therefore, photoisomerization leads to large structural changes in the azobenzene conformation that results in substantial effects on the spectroscopic and physical properties of the azobenzene-containing systems. The photochemical properties of the pseudostilbenes are of additional interest because the nature of their substituents leading to an asymmetric electron distribution induces a strong nonlinear optical response. Moreover, both isomerization processes can be driven by a single illumination wavelength that results in continuous cycling between the two isomeric forms. This is a required property for many photoinduced phenomena, such as photo-orientation.[7]

The n-π^* and π-π^* transitions excite the singlet state (S_0) of the ground state of the azobenzene molecules to the first S_1 ($n\pi^*$) and the second S_2 ($\pi\pi^*$) singlet excited vibrational states. Both $S_0 \rightarrow S_1$ and $S_0 \rightarrow S_2$ excitation can lead to photoisomerization and the S_1 state can be created by direct $S_0 \rightarrow S_1$ excitation or intersystem $S_2 \rightarrow S_1$ relaxation. Ultrafast time-resolved spectroscopic studies indicate that both $S_2 \rightarrow S_1$ and $S_1 \rightarrow S_0$ relaxation occur after $S_0 \rightarrow S_2$ excitation of the *trans* isomer, as shown in Figure 1.11.[58]

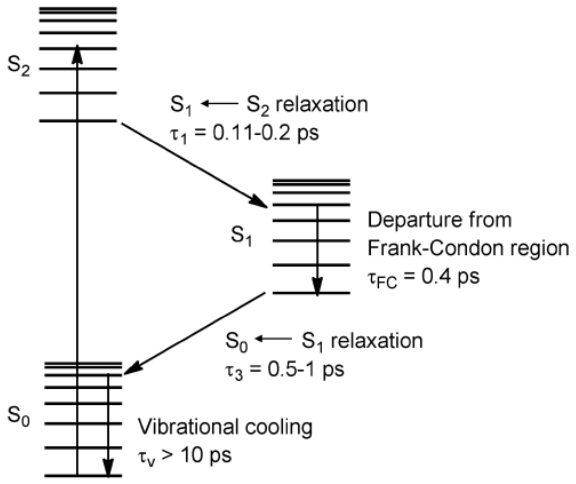

Figure 1.11. A simplified Jablonski diagram to show the S_0, S_1 and S_2 states of the *trans* isomer. Excitation to the S_2 state is followed by rapid relaxation to the S_1 state. Then, departure from the Frank-Condon region and $S_1 \rightarrow S_0$ relaxation takes place accompanied by *trans-to-cis* isomerization. Finally, vibrational cooling of the S_0 state occurs. Reprinted with permission from Ref. 58, Copyright 2012 Royal Society of Chemistry.

The photoisomerization mechanism of azobenzenes has been the subject of interest and controversy since isolation of the *cis* isomer nearly eighty years ago.[62] The isomerization mechanism is affected by different parameters, such as the isomeric state (*cis* vs. *trans*), the excitation mode (thermal vs. radiation), the illumination wavelength, the solvent, the substitution pattern of the azobenzene, the temperature, and the pressure. Four different mechanisms have been proposed for the photoisomerization of azobenzenes: rotation, inversion, concerted inversion, and inversion-assisted rotation, as shown in Figure 1.12. However, it is clear that a single mechanism cannot satisfactorily explain all aspects of the isomerization process of different azo chromophores.[58]

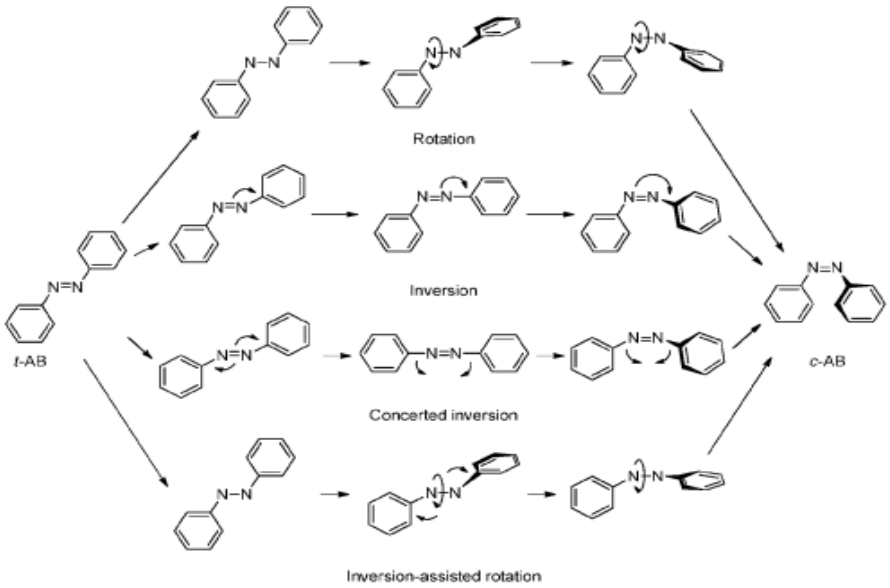

Figure 1.12. Four proposed mechanisms for the *trans-to-cis* photoisomerization of azobenzene molecules. Reprinted with permission from Ref. 58, Copyright 2012 Royal Society of Chemistry.

Azobenzenes can be functionalized not only by different substituents as indicated above, but also by substituents that either provide acidic or basic properties or that participate in supramolecular interactions.[42] Moreover, *trans* azobenzenes can be used as effective mesogenic cores to design side-chain liquid crystalline azopolymers.[3,63] *Trans* azobenzenes often act as mesogens for creating liquid crystalline (LC) materials due to their rigid rod-like structure, whereas *cis* azobenzenes are generally not mesogenic. In general, photoisomerization can drive reversible order-disorder phase transitions between the liquid crystalline phase of *trans* isomers and the non-mesogenic, isotropic phase of *cis* isomers, resulting in different photo-responsive applications, such as photoinduced alignment, photochemical phase transitions and photo-triggered molecular cooperative motion.[64] Photoinduced transitions generally are more restricted in a polymer matrix than in solution. This can be related to the limited free volume available in the bulk state and reduced segmental motion of the polymer chains, as well as steric constraints. Furthermore, the polymer matrix can prevent chromophore aggregation by hindering excessive interactions between neighbouring azo molecules.[7]

Their collective practical properties render azobenzene derivatives as one of the most prominent components of photoresponsive supramolecular complexes.

1.3.2. Polymer-azobenzene complexes

Azobenzene guests have been attached to many different architectures of polymeric hosts, such as linear random copolymers,[12,65,66] linear block copolymers,[67,68] hyperbranched polymers and dendrimers,[69] and crosslinked polymers.[34,70,71] In this work, we utilize the linear homopolymer poly(4-vinylpyridine) (P4VP) as the host for functionalized azobenzene-based guests. The azobenzene molecules are non-covalently attached as side chains to linear polymer chains by supramolecular bonds. Keeping the architecture of the host material fixed and simple enables a comparison of fundamental properties of azocomplexes. Thus, we focus on supramolecularly functionalized linear homopolymer P4VPs.

The oldest evidence regarding vinylpyridine dates to World War II when vinylpyridine was used as a comonomer with butadiene in the synthetic rubber program.[72] In 1950, Fitzgerald and Fuoss[72] developed different mechanisms, such as bulk polymerization and emulsion polymerization, to synthesize P4VP. Living anionic polymerization of P4VP was developed much

later by Varshney et al.[73] and Creutz et al.,[74] whereas controlled radical polymerization and atom transfer radical polymerization (ATRP) was achieved by Bohrisch et al.[75] and Xia et al.,[76] respectively to obtain polymers with narrow polydispersities and controlled molecular weights.

P4VP is a widely used polymer host or matrix for the study of photoresponsive properties of azobenzene-containing complexes due to several characteristics.[3] The lone electron pair on the tertiary nitrogen atom, that does not participate in the conjugation of the pyridine ring, confers a weak basic property ($pK_a = 5.25 \pm 0.01$) to the ring.[77] This endows P4VP with the capability of complexing with many other materials through different interactions, including hydrogen bonding,[3,78] ionic interactions[23,24] and halogen bonding.[79] This makes the comparison of different azobenzene complexes easier, as libraries of azo molecules can be used to complex with the same polymer backbone via the same or different interactions. Furthermore, the polymer can be dissolved in different organic solvents, such as dimethyl sulfoxide (DMSO), dimethylformamide (DMF), methanol, ethanol, isopropanol, chloroform, as well as solvent mixtures.

It may be mentioned that the basic property of pyridine also leads to P4VP complexes based on metal ion coordination with different metal cations, such as Zn^{2+}, Ca^{2+}, Cu^{2+}, Co^{2+} and Ni^{2+}.[80,81] Such metallosupramolecular P4VP systems can be used, for example, either to remove heavy metals, such as copper II from wastewater[81] or to obtain a mesomorphic liquid crystal using zinc II cation coordination.[80] To our knowledge, metal coordination has not been used to date to prepare azopolymer complexes.

Hydrogen-bonded azobenzene-P4VP complexes studied to date are almost all based on phenol-pyridine interactions. In these systems, the free electron pair on the nitrogen atom of the pyridine is the H-bond acceptor and the phenol group on the azobenzene derivative is the H-bond donor (Figures 1.13a and 1.14).[3,78] Priimagi et al.[10,11,82,83] have investigated various such supramolecular azopolymer complexes, including the opposite functionality (Figure 1.13b), constructed by hydrogen bonding between small-molecule azo derivatives and polymer hosts since 2005. The phenol-pyridine hydrogen bond is relatively strong, with a bond energy of 16-60 kJ/mol, and it can reach close to equimolar proportion- i.e. one chromophore for each polymer repeat unit- without aggregating and phase separating. Thus, this is an easy approach for controlling azobenzene doping in the solid state without detrimental chromophore-chromophore aggregation affecting the photonic properties.[84] In contrast, COOH-functionalized molecules, especially when

linear as in *p*-substituted azos, generally lead to low levels of H-bonding with P4VP due to the high driving force crystallization of these molecules.[85-88] Hydrogen-bond formation can be verified by infrared spectroscopy, for example, by the shift of the 993 cm^{-1} band of pure P4VP, which is related to the vibrational stretching mode of the free pyridine ring, to higher wavenumbers, typically 1005-1010 cm^{-1}, in P4VP complexes.[89,90]

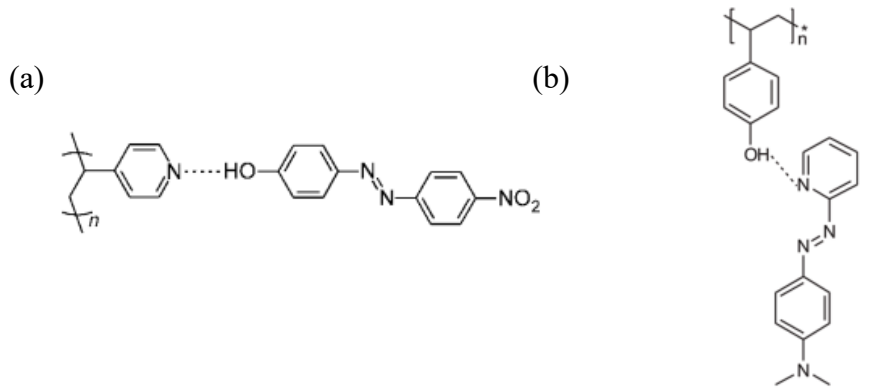

Figure 1.13. Formation of the phenol-pyridine hydrogen bond between polymer host and azobenzene derivative. The dashed line depicts the phenol-pyridine hydrogen bonding. (a) Adapted with permission from Ref. 83, Copyright 2008 American Chemical Society. (b) Adapted with permission from Ref. 82, Copyright 2009 American Chemical Society.

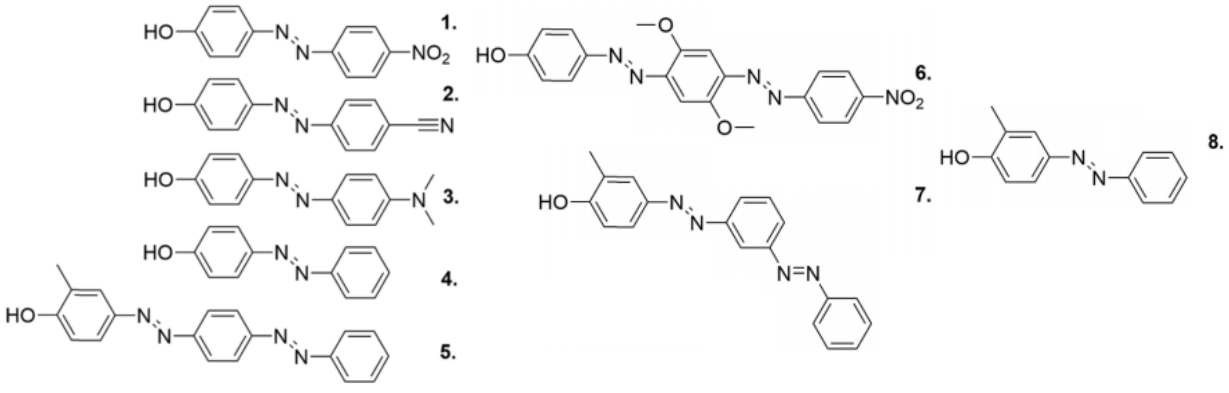

Figure 1.14. A library of different azobenzenes for phenol-pyridine hydrogen-bonding to P4VP. Reproduced with permission from Ref. 3, Copyright 2018 Royal Society of Chemistry.

Similarly, P4VP can function as a halogen-bond acceptor. In this case, the nitrogen atom acts as a nucleophilic site that halogen bonds with the electrophilic region associated with a halogen atom covalently attached to an azobenzene moiety (Figure 1.15). Recently, Priimagi et al.[91] found that the response to light of halogen-bonded P4VP-azobenzene complexes is stronger than that of the analogous hydrogen-bonded complexes. They showed more efficient light-induced surface relief gratings (SRG), a phenomenon that will be introduced in section 1.6.

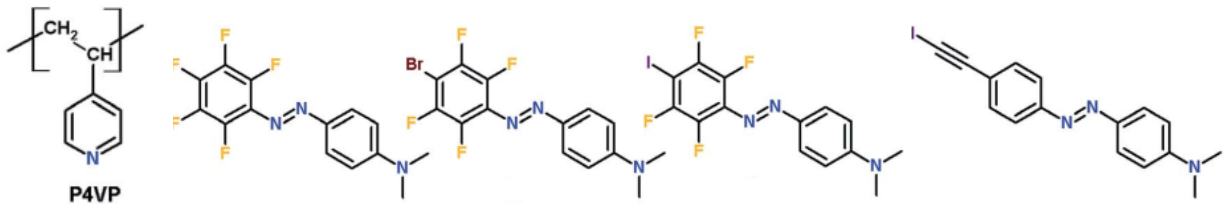

Figure 1.15. Chemical structures of halogenated azobenzenes used to complex with P4VP. Adapted with permission from Ref. 79, Copyright 2015 Royal Society of Chemistry.

To form supramolecular ionic complexes, P4VP is generally first converted into a polycation. This conversion can occur through an acid-base reaction between the lone electron pair of the nitrogen atom of the pyridine ring and the proton of Bronsted acids (HCl, HBr, HI, H_2SO_4, H_3PO_4)[92] or organic sulfonic acids[93,94] to form protonated P4VP. It is also often achieved through quaternization of P4VP with alkyl halogen compounds to obtain alkylated P4VP. Following this modification, an azo derivative functionalized by a negatively charged moiety, typically a sulfonate group, can be complexed to the alkylated P4VP through an ion exchange procedure. For optimal complexation, the starting counterions must be eliminated. This two-step procedure was used to obtain the ionic photoresponsive side-chain liquid crystalline polymers shown in Figures 1.16 and 1.17, as well as the library depicted in Figure 1.18.[23,24,95]

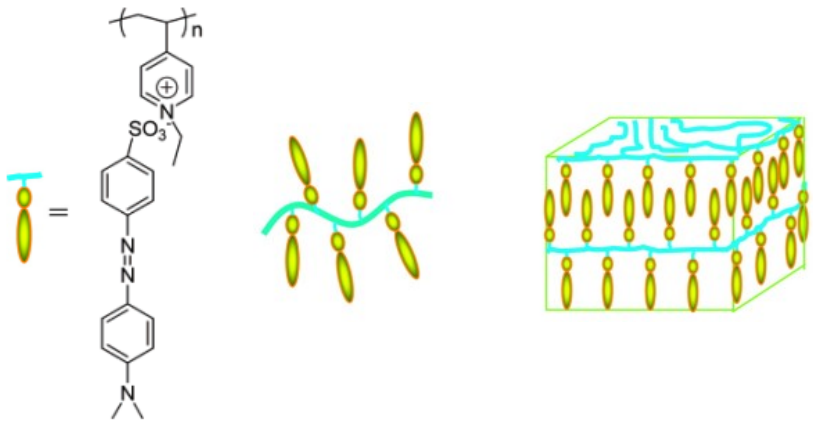

Figure 1.16. Schematic presentation of the ionic complex between ethylated P4VP and MO. Adapted with permission from Ref. 95, Copyright 2007 American Chemical Society.

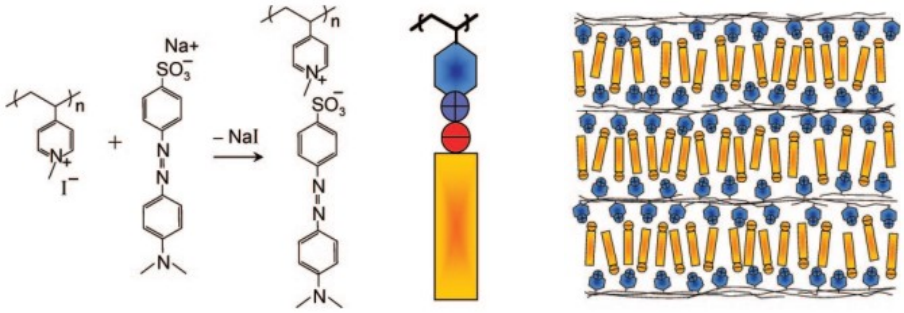

Figure 1.17. Schematic representation of the ionic complex between methylated P4VP and MO. Adapted with permission from Ref. 23, Copyright 2008 American Chemical Society.

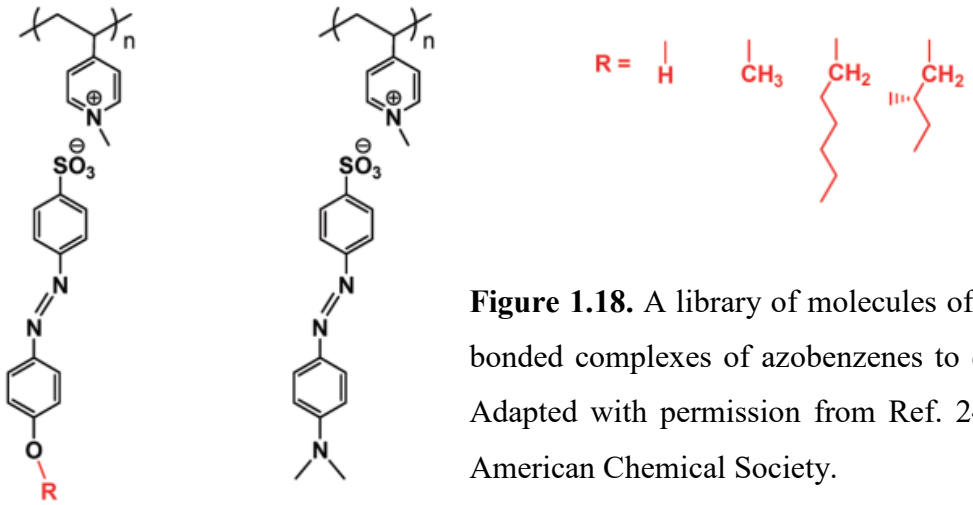

Figure 1.18. A library of molecules of different ionically bonded complexes of azobenzenes to quaternized P4VP. Adapted with permission from Ref. 24, Copyright 2009 American Chemical Society.

Another approach is to directly protonate the P4VP by the small molecule component in a one-step procedure. This was used by Zhu et al.[94] to synthesize complexes between P4VP and wedge-shaped mesogenic sulfonic acids to form liquid crystalline supramolecular materials with lamellar and cylindrical morphologies, depending on the molar ratio of the components (Figure 1.19).

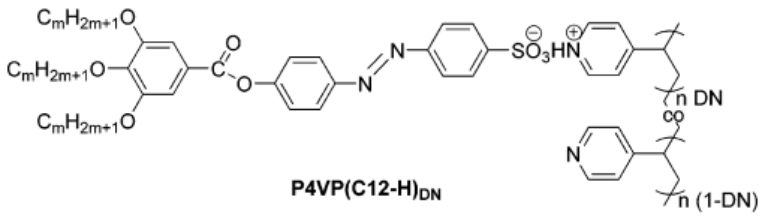

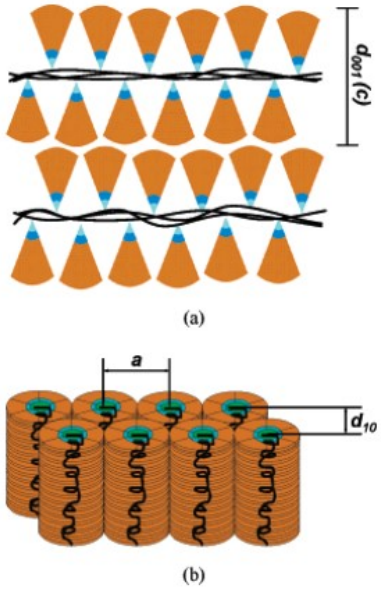

Figure 1.19. Structure of P4VP complexed with wedge-shaped sulfonic acid (P4VP(C12-H)$_{DN}$, upper left), where DN refers to the degree of neutralization. (a) and (b) Proposed packing model of the complex in the lamellar phase (0.5 ≥ DN, top right) and in the hexagonal columnar phase (DN ≥ 0.8, bottom right). Adapted with permission from Ref. 94, copyright 2006 American Chemical Society.

The use of ionic self-assembly for supramolecular materials including photosensitive azobenzene-containing complexes and photomobile azobenzene-based materials, was reviewed by Faul[96] as well as Ube and Ikeda,[97] and was developed by Xiao et al.[95] and Zhang et al.[23,24] The latter used similar systems of ionically bonded complexes, between methyl orange (MO) and ethylated poly(4-vinylpyridine) (P4VPEt) (Figure 1.16) and between MO and methylated P4VP (P4VPMe) (Figure 1.17), respectively. They found that both of the azopolymer complexes form a liquid crystalline smectic A mesophase and that they show high photoinduced birefringence. On the other hand, azobenzene-containing photosensitive supramolecular materials fabricated through ionic bonding show stronger photoinduced orientation in comparison with covalently bonded polymers. This was attributed to the high charge density that leads to a high glass transition, high viscosity and reduced relaxation.[23,24,98]

The azo-containing complexes are supramolecular photoresponsive materials with various applications in photonics and optoelectronics industries due to the photoactivity of the azo moiety and the high stability of the complex. For instance, the azobenzene-containing polymer of poly[4-[2-(methacryloyloxy)ethyl]-azobenzene] (PMEA) as well as its copolymer with Disperse Red 1 methacrylate (DR1M), poly(MEA-co-DR1M) were used for fabricating grating waveguide couplers.[99,100] Moreover, volume holographic optical storage devices (Figure 1.20) can be designed using different azobenzene-containing polymers and copolymers, such as poly(methyl methacrylate) (PMMA) doped with Disperse Red 1 (DR1) and diblock copolymers of PMMAs of different molecular weights with cyanoazobenzene containing methacrylate polymers.[101]

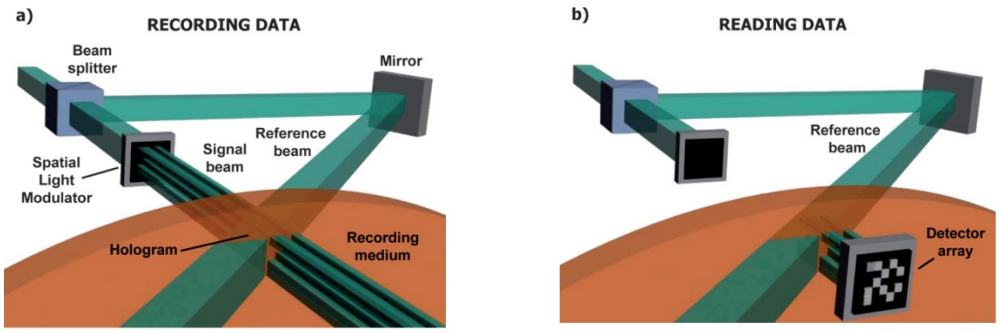

Figure 1.20. Schematic image of holographic optical storage set-ups (a) recording and (b) reading. Reproduced with permission from Ref. 101, Copyright 2009 Royal Society of Chemistry.

1.4. Light-induced motion in azocomplexes

Supramolecular azobenzene-P4VP complexes, in addition to their covalent counterparts, have received much research attention for their versatile and fascinating response to light. As will be described in this section, these photosensitive complexes undergo reversible photocontrolled deformation due to the molecular-level and higher-level movements upon irradiation of UV-visible light. In fact, as it was mentioned earlier, azobenzenes undergo reversible *trans-cis* photoisomerization at the azo bond that can translate the energy of incident light into significant micron-scale and even macroscopic motion.[102] These motions lead to photoinduced orientation and surface relief gratings (SRGs), which will be described in the Sections 1.5 and 1.6.

Natansohn and Rochon[102] reviewed the subject of photoinduced motion in azobenzene-containing polymers. They pointed out that photoisomerization under polarized light results in a series of motions that can be generally divided into three categories according to their characteristic length scale: (1) molecular-scale motions, (2) domain-scale motions, and (3) macroscopic motions, which are closely interrelated (Figure 1.21).[7]

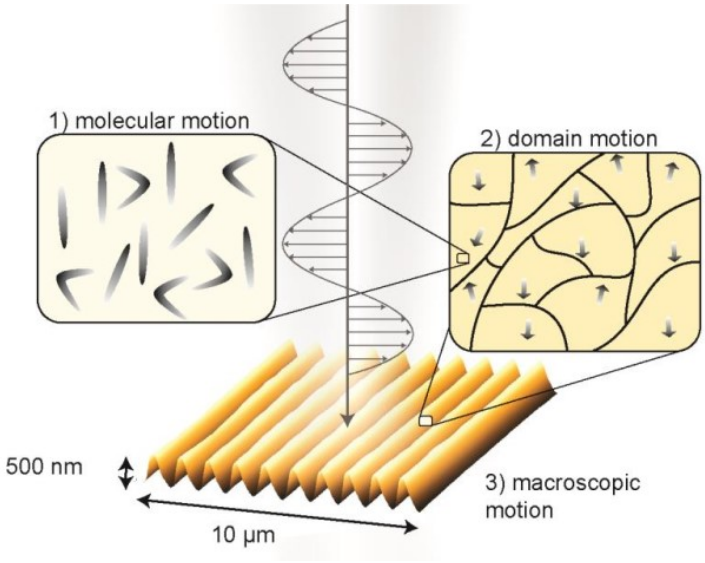

Figure 1.21. Illustration of the three levels of linearly polarized light-induced motions in azobenzene-containing polymers. At the molecular level, light generates *trans-cis-trans* isomerization, which depletes the chromophore concentration in the direction of polarization. At the domain level, the polar chromophore movement reorients polar domains. At the mass level, the light produces macroscopic movement of the polymer that can be used to inscribe surface or bulk patterns. Reproduced with permission from Ref. 7, Copyright 2014 Aalto University.

1.4.1. Molecular-level motion

The first level is the chromophore motion that is triggered by the polarized light. The resulting photoisomerization is induced by linearly polarized light due to the fact that the molecules having their transition dipole moments perpendicular to the light polarization direction are excluded from optical activation. Indeed, since the transition dipole moment vectors of the trans azobenzene typically coincides with an axis connecting the midpoints of the two benzenes,

the molecules that are perpendicular to the polarization plane of the light are inert to the incident beam.[103] On the other hand, this selectivity also originates from the fact that the absorption probability is proportional to the cosine square of the angle between the polarization direction and the chromophore transition dipole moment axis (Figure 1.22).

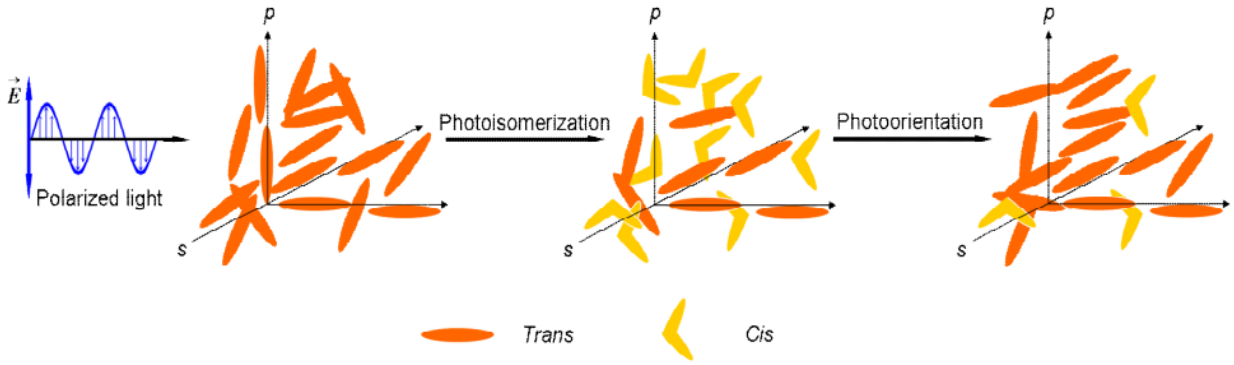

Figure 1.22. Schematic representation of the photoisomerization and photo-orientation of azobenzenes with linearly polarized light. The symbols, *p* and *s*, refer to the directions parallel and perpendicular to the electric field polarization of the incident light, respectively. Adapted from Ref. 104 with permission from author, Copyright 2014.

The selective photon absorption combined with the highly anisotropic structure of *trans* azobenzenes causes the concentration of the chromophores whose axis is aligned perpendicular to the incident light polarization direction to gradually increase under illumination by linearly polarized light, until reaching a saturation level. This results in the anisotropic alignment of the chromophores and, consequently, material birefringence. More specifically, two distinct processes are involved, as indicated in Figure 1.23. One is angular hole burning (AHB) or orientational hole burning. This is the rapid selective depletion of the *trans* isomers following *trans-cis* isomerization that induces an initial anisotropy in the distribution of *trans* and *cis* isomers. The other is angular redistribution (AR). This is a slower photoinduced alignment of the azobenzene molecules perpendicular to the light polarization direction that results from repetitive *trans-cis-trans* isomerization cycles. The original isotropic distribution of azobenzenes can be restored by unpolarized or circularly polarized light. Thus, the overall photoalignment process simultaneously

involves a fast mode (AHB) and a slow mode (AR), and this process can be modelled by a biexponential function of orientation as a function of irradiation time.[3,7,48,57,102,104,105]

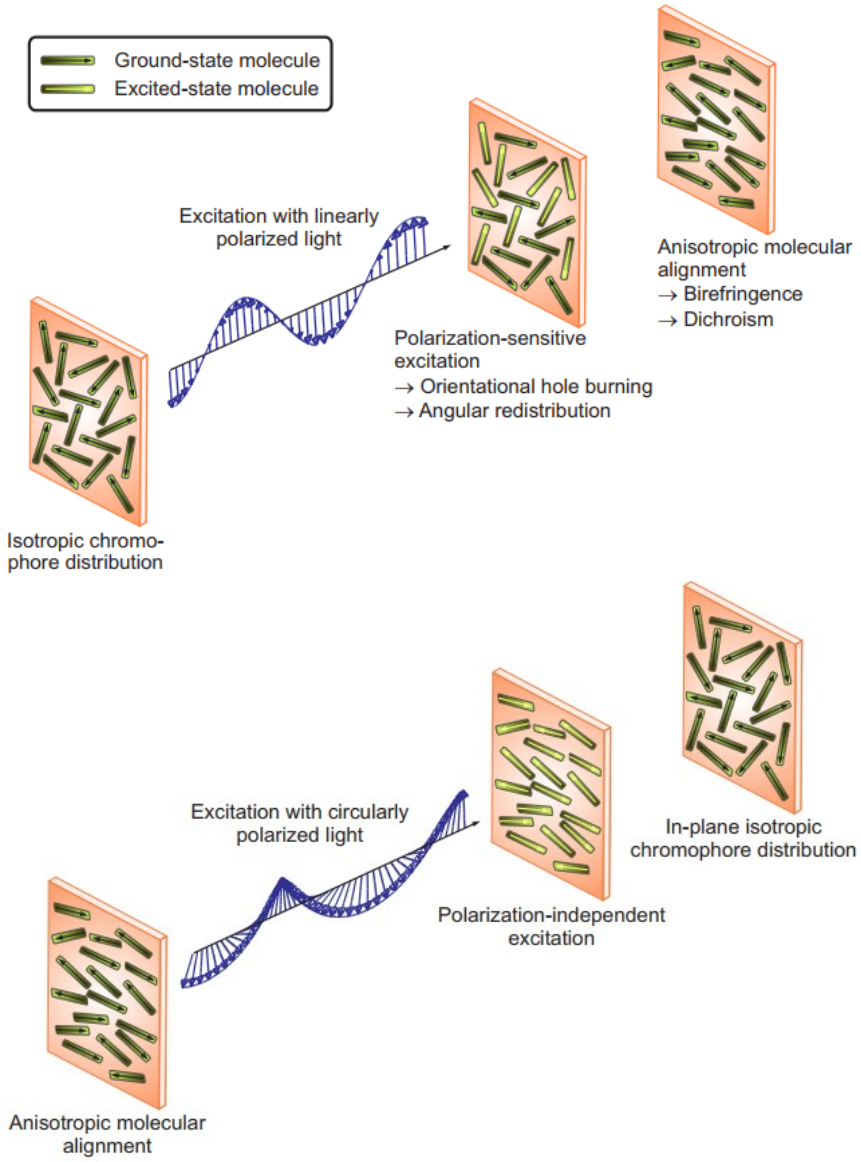

Figure 1.23. (top) Schematic presentation of the photoinduced in-plane alignment of azobenzenes upon excitation with linearly polarized light (bottom), Restoration of the initial isotropic state with unpolarized or circularly polarized light. Reprinted with permission from Ref. 48, Copyright 2009 Helsinki University of Technology.

1.4.2. Domain-level motion

The second level of motion takes place approximately on the nanometer scale. This occurs when the material displays some degree of intrinsic order, such as liquid crystalline or semi-crystalline structures. When the chromophores are aligned in an ordered structure, molecular-level

motion and photoisomerization are opposed by the forces sustaining the intrinsic order. Nonetheless, the molecular-level photo-orientation can lead to the reorientation of whole liquid crystalline or crystalline domains in the direction perpendicular to the light polarization. This collective movement of the chromophores in a domain is known as cooperative motion. This photodriven reorientation of entire liquid crystalline or crystalline domains results in a high degree of overall orientation in the ordered domains that is much higher than that in the amorphous domains.[102,106,107]

1.4.3. Macroscopic-level motion

The third level of motion is considered macroscopic because it takes place at a scale much larger than the size of the azobenzene units and it is capable of producing structural changes that are visible with the naked eye. Similar to the domain-level motion, this motion requires binding of the chromophore to the polymer matrix to induce massive motion in the polymer backbone. For instance, Yu et al.[108] showed that the intrinsic anisotropy of liquid crystalline azopolymers enables macroscopic motions, leading to repeated and precise bending of a free-standing polymer film along any chosen direction, while irradiated by linearly polarized light with different angles of polarization. They ascribed this photomechanical effect to the photoselective volume contraction that occurs in the material (Figure 1.24).

Moreover, Barrett and colleagues[109,110] found that amorphous azopolymers can undergo a crossover from photoexpansion to photocontraction depending on the temperature. They attributed the material photoexpansion to the internal pressure created by the isomerization and the material photocontraction to the denser packing of the dipolar molecules due to the molecular mobility in the material at higher temperatures. Although these interesting photomechanical effects can be employed in different applications ranging from actuators and sensors to photo-driven micromechanical devices,[49] the most complicated type of macroscopic motion is the light-induced surface patterning. This is an interference pattern of two laser beams that leads to periodic patterns on the film surface on the micrometer size.[111-113] These patterns are often called surface relief gratings (SRGs) and the mechanism of their formation is still debated in the literatures.

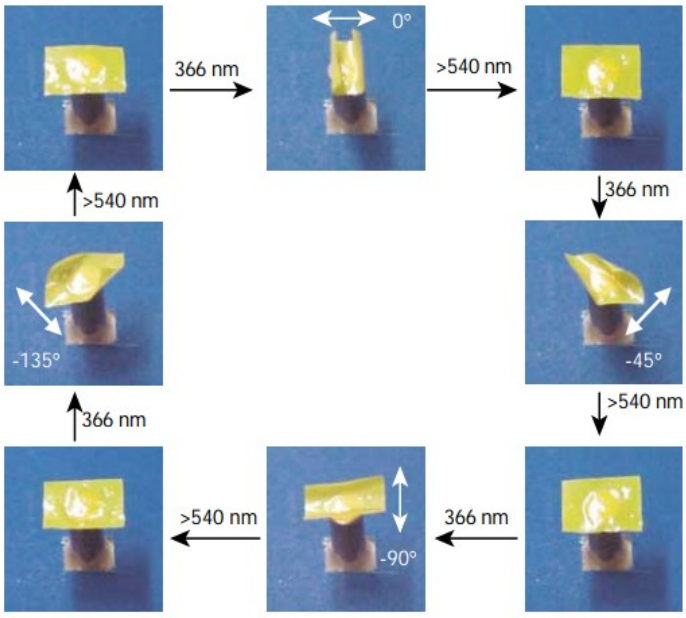

Figure 1.24. Photographic frames of the film bending in different directions in response to irradiation by linearly polarized light of different angles of polarization (white arrows) at 366 nm and being flattened again by visible light longer than 540 nm. The bending time for the four different bending directions was within 10 s, and the bent film reverted to the flat state in about 10 s. Adapted with permission from Ref. 108, Copyright 2003 Springer Nature.

1.5. Photoinduced orientation or photoalignment

As was mentioned earlier, the molecular-level motion of azobenzenes caused by linearly polarized light brings about a unique motion called photo-orientation or photoalignment. Indeed, linearly polarized light causing the molecules to reorient perpendicularly to the polarization plane leads to an anisotropic angular distribution compared to the initial uniform isotropic distribution.

The first observation of photoinduced anisotropy in azobenzene-containing material systems dates back to 1929, in work by Weigert, and was termed the "Weigert effect".[114] The developments done in this field were then summarized in the reviews by Kumar et al.[115] and Xie and colleagues.[116] They were inspired by the groups of Natansohn and Rochon to continue investigation in this field and to summarize more developments in their review.[102]

Most azobenzenes can isomerize and undergo photo-orientation; however, the efficiency of photoalignment is influenced by many parameters, such as the chromophore structure, inter- and intra-molecular interactions, cooperative motions, the interaction type between the chromophore and the polymer matrix in the case of supramolecular systems, the nature of the polymer backbone or matrix, the sample preparation process (type of solvent, film-casting method, heat-treatment), and the laser wavelength and intensity.[7,102] For instance, regarding the

chromophore structure, Ho and colleagues[117] found that pseudostilbene-type molecules show highly efficient photo-orientation due to their strongly asymmetric electron distribution and large dipole moment, which allows using the same wavelength for inducing both *trans-cis* and *cis-trans* isomerization and leads to an increase in the *trans-cis-trans* cycles per time unit to improve efficiency. The chromophore bulkiness, which can hinder molecular motion and thus slow the photo-orientation kinetics, and the strength of the dipole moment also play important roles in photoinduced orientation efficiency.[102,118]

It was also found that the length of the spacer, which is the structural unit (usually a linear alkyl chain) between the polymer backbone and the chromophore, can affect the photoinduced motion. The shorter the spacer length, the more restricted the chromophore motion, and the slower the growth rate of birefringence, but the greater its stability.[119] Or, vice versa, the longer the spacer length, the greater the chromophore mobility due to the flexibility of the spacer, and therefore the faster the kinetics of photo-orientation and relaxation. In addition, longer spacers can favour liquid crystalline structures in the system that tend to improve both the degree and stability of photoinduced birefringence,[120] due to strong cooperative movement and intermolecular interactions of the photochromic units and the mesogens.[106]

Moreover, although covalent attachment of the chromophores to polymer backbones as side chains improves the stability of photo-orientation in comparison with simple guest-host systems by reducing aggregation problems, the non-covalent supramolecular systems can also give rise to high photo-orientation and stable anisotropy. This effect was reported for ionically attached azobenzene-polymer complexes (Figures 1.16 - 1.18) by Xiao et al.[95] and Zhang et al.[23] Their results are all the more remarkable in that their materials involve the absence of a flexible spacer, yet are liquid crystalline and show high photo-orientation.

The anisotropy induced by photo-orientation is generally quantified in one of two ways: by measuring either the birefringence (anisotropy in refractive index) or dichroism (anisotropy in absorption spectrum). These are described in the following two subsections.

1.5.1. Photoinduced birefringence

Figure 1.25a presents a schematic illustration of a typical photoinduced birefringence (PIB) set-up where the orientation is induced in the chromophore system by a linearly polarized pump

beam of moderate power and with a wavelength in the absorption range of the chromophores.[7] Photoinduced orientational anisotropy is monitored by measuring the transmittance of a low-power probe beam through a polarizer/sample/analyzer configuration. The transmission direction of the polarizer/analyzer is set to ±45° relative to the polarization direction of the writing beam, to maximize the transmitted signal (*I*). Then the absolute birefringence (|Δn|), which is the difference between the refractive indices in the parallel (*p*) and perpendicular (*s*) directions can be calculated by equation 1.1:

$$I = I_0 \sin^2\left(\frac{\pi|\Delta n|d}{\lambda}\right) \quad 1.1$$

where *I* is the intensity of the transmitted light through the sample when the polarizer and the analyzer are positioned perpendicular to each other, I_0 is the intensity of the incident light in the absence of the sample (polarizer and analyzer parallel), *d* is the film thickness, and λ is the probe wavelength.[7,104]

Figure 1.25b illustrates a typical PIB curve for two inscription-relaxation-erasure cycles. In this case, photoalignment was first induced in a spin-coated film of the complex between P4VP and a polar bisazobenzene dye ([(2,5-dimethoxy-4-((4-nitrophenyl)diazenyl)-phenyl)diazinyl]-phenol; 2NHA) by a vertically polarized light beam.[7,121] The film was exposed to the polarized light for a given time to reach the saturation level of birefringence. After the writing beam was extinguished, this optically induced macroscopic birefringence decreased partially due to some relaxation caused by thermal randomization, reaching a plateau termed remnant birefringence. The remnant birefringence was subsequently erased with a circularly polarized writing laser. This randomizes the chromophore orientation in the plane of the sample film. The sequence was repeated a second time with the same result.[121,122]

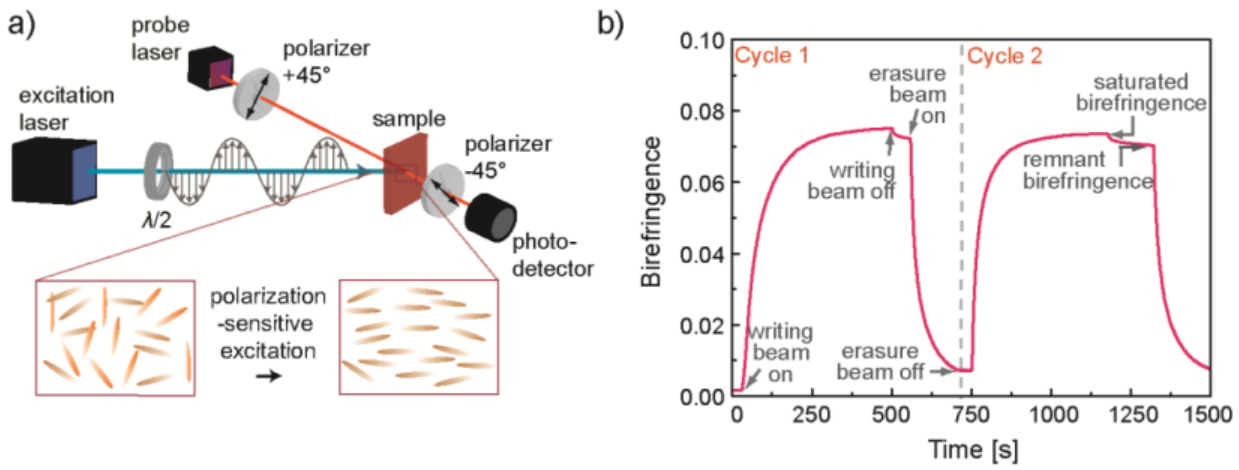

Figure 1.25. (a) Schematic representation of the experimental set-up for photoinduced birefringence (PIB) and the corresponding light-induced in-plane distribution of the azobenzene molecules upon excitation with linearly polarized light. (b) Typical birefringence measurement as a function of writing time. Adapted with permission from Ref. 7, Copyright 2014 Aalto University.

1.5.2. Photoinduced dichroism

While photoinduced birefringence is an optical method to quantify photoinduced anisotropy, spectral methods for measuring electronic dichroism using UV-visible[123] and Fourier transform IR (FT-IR)[102] spectroscopies are alternative tools to quantitatively investigate photo-orientation. Of these two, according to Natansohn and Rochon,[102] *"By far the most popular and informative spectral method to analyze the photoinduced motion is FT-IR."* Polarized FT-IR where the intensity of the absorbance bands changes with respect to the directions parallel or perpendicular to the polarization of the pump light is a practical and informative method to follow photoinduced orientation. Compared to polarized UV-visible spectroscopy, which measures the orientation of only the chromophores, and photoinduced birefringence, which measures only the overall orientation of all components, polarized FT-IR can distinguish between the specific orientation of different chemical groups, as determined by the choice of the bands analyzed.[102,104] Thus, polarized FT-IR spectroscopy is a practical tool for studying the photoinduced orientation of azocomplexes in this thesis.

In particular, infrared linear dichroism (IRLD) is useful for characterizing the molecular orientation in azopolymers with optical anisotropy. This technique can be used on samples that were irradiated prior to the measurement,[124] as well as in situ with irradiation.[125] The orientation information is obtained by measuring either the dichroic difference, $\Delta A = A_p - A_s$, or the dichroic ratio, $R = A_p/A_s$, of a given absorption band, where A_p and A_s are the absorbances of the investigated band for infrared radiation polarized parallel and perpendicular to the pump beam polarization, respectively.[126] Although IRLD is well suited for providing information on the dynamics of the photoinduced reorientation process, the time required for measuring A_p and A_s with a high signal-to-noise ratio severely limits the time resolution of the technique to several minutes. In 1984, Marcott[127] reported that the sensitivity of IRLD measurements can be improved by coupling infrared spectroscopy with the polarization modulation technique (PM-IRLD). The advantage of this method is the capacity to measure the dichroic difference spectrum directly by modulating the polarization of the infrared beam at high frequency (74 or 100 kHz) with a photoelastic modulator, so that the normalized linear dichroism ($<T_2>$) can be obtained by equation 1.2:[128]

$$\langle T_2 \rangle = \frac{A_p - A_s}{A_p + 2A_s} = \frac{\Delta A}{3A_0} \qquad 1.2$$

where ΔA is the dichroic difference and A_0 the structural absorbance.

PM-IRLD is applicable to determine quantitatively the segmental orientation in polymers, especially for samples showing a low level of orientation.[129] However, it is unable to measure separately the parallel and perpendicular spectra, and it is necessary to assume that A_0 does not evolve during the process, so the structural absorbance information is lost. A more advanced technique called PM-IRSAS, or polarization modulation infrared structural absorbance spectroscopy, was introduced by Liang and colleagues[130] to overcome this limitation. This new method is capable of measuring both the dichroic difference (ΔA) and the structural absorbance (A_0) simultaneously with a 200-ms time resolution.

There is a growing body of literature investigating photo-orientation of different azocomplexes. For instance, Hvilsted and co-workers[131-134] have used birefringence and spectral methods to study the photoinduced orientational behavior of a series of side-chain liquid crystalline polyesters having a different numbers of methylene units in the main chain between two ester

groups, and in the spacer linking the main chain with a cyano-functionalized azobenzene. The photoinduced orientation of azobenzene-doped polymers[135,136] and azopolymers with covalently bonded azobenzene side chains[137,138] was studied by Tawa et al. using polarized UV-vis spectroscopy and polarized FT-IR spectroscopy. Moreover, the dynamics of optically induced orientation in azopolymers has been studied by Pézolet and Buffeteau[126] as well as Labarthet et al.[139] using the PM-IRLD technique. Recently, Priimagi and colleagues[11,78,83] investigated the photoinduced anisotropy in different polymeric hydrogen-bonded azobenzene-containing complexes, including P4VP-azobenzene, by measuring birefringence. Besides, Wang et al.[140] investigated the photo-orientation of both the azobenzene molecules and the polymer host in hydrogen-bonded supramolecular azobenzene complexes with P4VP using the PM-IRSAS technique. They were able to show that replacing the H-tail with a cyano group induces both greater AR of the chromophores and measurable orientation of P4VP pyridine.

1.6. Photoinduced surface patterning

As mentioned earlier, one of the most remarkable consequences of photoinduced motion in azobenzene-containing polymers is the micron-scale mass migration.[49,111] It was first reported in 1995 by Rochon et al.[112] and Kim et al.[141] who independently, but concurrently discovered that illumination of a glassy azopolymer film [poly(Disperse Red 1 acrylate), PDR1A; Figure 1.26] with an interference pattern of light forms temporally stable surface patterns with modulation depths of hundreds of nanometers. They concluded that the gratings were inscribed due to mass migration of the polymer since the laser intensity (70 mW/cm^2) was not high enough to damage the film surface. The discovery of surface gratings has opened a new approach to fabricate diffracting elements and photonic components for use in waveguide coupling,[99] resonance optical filters,[142] liquid crystal alignment,[143,144] colloidal crystals,[145] replica molding,[146,147] photochemical imaging,[148,149] and micro/nanoarchitectures.[150,151]

As shown in Figure 1.27, when a thin film of an azobenzene-containing polymer is exposed to an interference pattern of light with spatial variation of the intensity and/or polarization, the polymer surface of the film deforms in response to the incident light. It also adopts the form of a replica of the incident interference pattern, resulting in a surface relief structure. The inscription

wavelength should be in the range of the absorption band of the material to induce both *trans-cis* and *cis-trans* isomerization. Indeed, the repetitive photoisomerization of azobenzene initiates mass transport of the polymer over distances of several micrometers, producing high-modulation-depth sinusoidal surface relief gratings (SRGs) at the polymer-air interface.[7,16,48] The width of this inscribed pattern can be up to a centimeter in size and the modulation depth of the grating can be hundreds of nanometers.[42] SRGs with an average modulation depth of a few hundreds of nanometers can be inscribed within minutes; however, depending on the material nature and the illumination intensity, it can sometimes take hours to saturate the diffraction signal.[7]

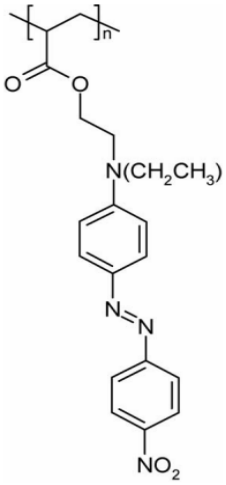

Figure 1.26. Chemical structure of poly(Disperse Red 1) acrylate, a pseudostilbene side-chain azopolymer. Reproduced with permission from Ref. 57, Copyright 2006 Elsevier.

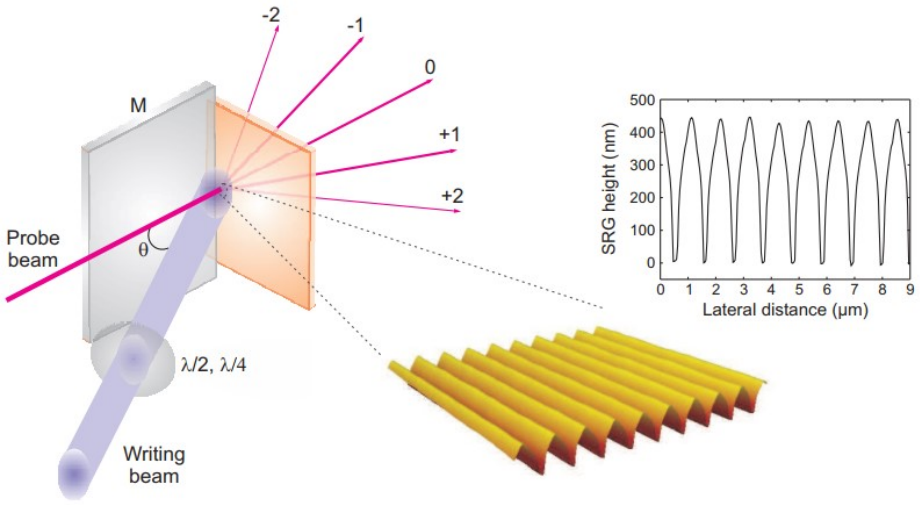

Figure 1.27. An example of a surface relief grating (SRG) (bottom center: atomic force micrograph (AFM)) in an azobenzene-containing film after illumination with a polarization/ intensity interference pattern (schematic at left) and the AFM 2D surface profile of an actual grating inscribed on a thin polymer film (right). The terms λ/2 and λ/4 denote waveplates that are

used to control the polarization of the irradiation beam, and M refers to a mirror that reflects half of the incident beam onto the sample to form the interference pattern. Reprinted with permission from Ref. 48, Copyright 2009 Helsinki University of Technology.

The mass migration of the azopolymers, which typically occurs from illuminated areas towards the dark fringes of the interference pattern, can be detected either in situ or ex situ. The *in situ* detection can be done by directing a low-power non-isomerizing laser beam (probe laser) through the area of the interference pattern and then monitoring the diffraction of the probe beam from the emerging grating structures. The *ex situ* recognition can be performed by using different nanomicroscopic techniques, most frequently atomic force microscopy (AFM).[16] The inscribed gratings can be subsequently erased either thermally (above the glass transition temperature) or radiatively.[56]

This fascinating phenomenon has received considerable attention both experimentally and theoretically during the past two decades. The photoinduced surface-patterning phenomenon can occur in a wide range of azobenzene-containing materials at irradiation intensities as low as 5 mW/cm^2.[152] In spite of all the research in this field, the fundamentals behind this complicated photomechanical process are still not comprehensively understood. For instance, it is known that very different mechanisms underlie the mass transport phenomenon in amorphous and liquid crystalline systems.[7] Holme and co-workers[153] had reported that the appearance of large peaks or trenches in the SRG pattern depends on the architecture of the polymer. They found that, in amorphous oligomers, the molecules migrate from the light and the maxima of the surface pattern coincide with the dark regions. This results in the deep trenches (more than a μm). In liquid crystalline polyesters, the molecules tend to migrate to the irradiated regions to produce significant topographic maxima (up to several hundred nanometers). Besides, Seki et al.[154-157] have concluded that, for SRG formation in LC polymers, it is essential to predrive the azobenzenes into a *cis*-rich state, e.g. by exposing with UV light, while SRG inscription in amorphous materials requires efficient *trans-cis-trans* continuous cycling of azobenzenes.

In 2009, Toshchevikov and colleagues[158] proposed a microscopic theory to understand the underlying mechanism of SRG formation in amorphous side-chain azobenzene polymers. Their theory was based on the interaction of chromophores in side chains with the polarized light that

leads to the orientation anisotropy of azobenzene-containing material systems. This perpendicular reorientation with respect to the electric vector of the light gives rise to mechanical stress in the system under polarized illumination. Their approach is based on dividing the surface of the film into individual microscopic parts where the light intensity or the direction of light polarization is constant, so the local deformation of each part is a consequence of two factors: (I) the interaction of the molecules with the homogeneous light in each infinitesimal part and (II) a balance between stresses appearing in the neighbouring parts. Therefore, the orientation of molecules in each part leads to the deformation of the local part, so the molecules can move to another part whose light intensity or polarization differs. Then the deformation of each local part results in the translational movement of molecules. Thus, the whole phenomenon can be considered as a combination of two approaches: "orientational approach" and "mass transport approach".[159] Saphiannikova et al.[160] analyzed selected experiments done by other researchers to provide convincing evidence that the recent microscopic theory can satisfy all main criteria - light- induced softening and diffusion, molecular architecture (rigidity of the main chain and the length of the spacer in side chains), and temperature - required for the light-induced phenomenon.

However, Hurduc et al.[161] believed that the athermal photo-fluidization of azopolymers due to repetitive isomerization of azobenzenes upon illumination is the key factor in SRG formation where the deformation process can be considered as an anisotropic flow of the polymer material. They proposed a mechanism relying on three simultaneous processes, as illustrated in Figure 1.28: (1) polymer photo-fluidization in illuminated regions, (2) mass movement from illuminated to dark regions, and (3) inverse mass displacement from dark to illuminated regions. Although these processes occur simultaneously, depending on the polymer chemical structure and experimental conditions, one or the other process can be dominant. They claimed that the inverse migration from dark to illuminated regions, an erasure process, only occurs when the laser source is on and this erasure process stops once the laser is switched off.

The debate between these two different views (reorientational and photo-fluidization) was addressed by Yadavalli et al.[162] through investigating the response of three photosensitive polymer films to irradiation with interference patterns and homogeneous light and studying the evolution of the film deformation in situ under continuous irradiation. They chose three polymers Azo-Psi, Azo-PCMS, and PAZO (Figure 1.29) having glass transition temperatures of 32 °C, 87 °C, and

95 °C, respectively, to represent extreme cases of flexible and rigid materials. Their experiments supported the reorientation mechanism proposed by Toshchevikov and colleagues.[158] However, the comprehensive mechanism of SRG formation is still unknown, and as Ambrosio and co-workers[163] point out, this photoinduced phenomenon might be controlled by a combination of several microscopic mechanisms.

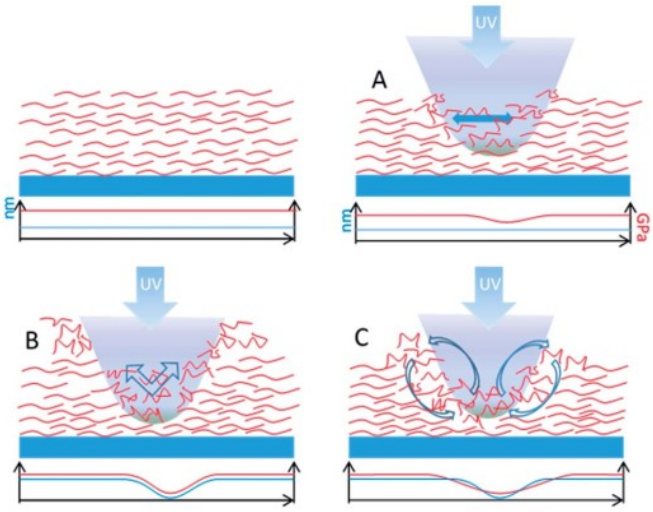

Figure 1.28. The mechanism proposed by Hurduc and co-workers for SRG formation during laser irradiation, involving at least three simultaneous processes: (A) polymer photo-fluidization in illuminated regions, (B) mass displacement from illuminated to dark regions, and (C) inverse mass transport from dark to illuminated regions. Reproduced with permission from Ref. 161, Copyright 2014 Royal Society of Chemistry.

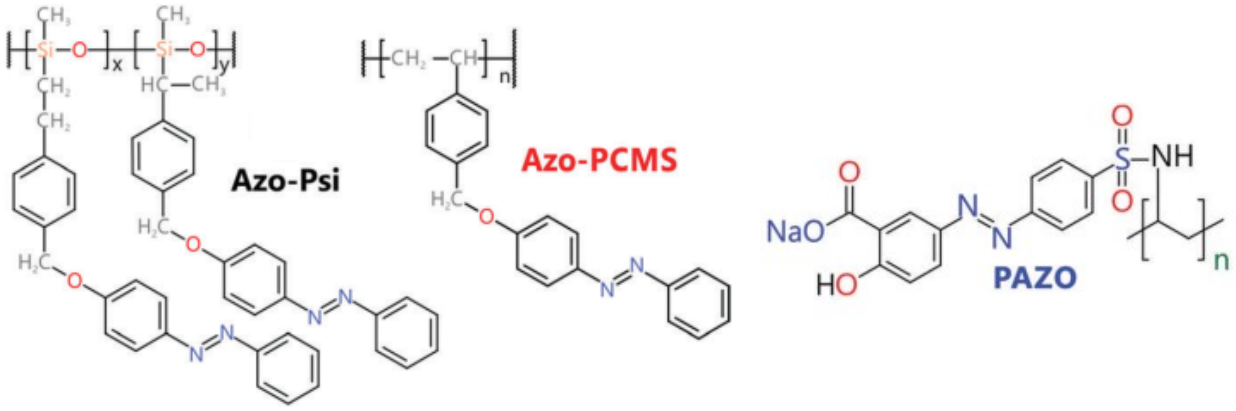

Figure 1.29. Chemical structures of Azo-Psi, Azo-PCMS, and PAZO. Adapted with permission from Ref. 162, Copyright 2016 Royal Society of Chemistry.

Efficient photoinduced mass transport in azobenzene-containing polymers requires strong bonding between the chromophores and the polymer backbone, so conventional guest-host azopolymers produce very weak SRGs in comparison with the supramolecular azocomplexes.[48] In

general, the efficiency of SRG inscription strongly depends on the nature of the material system, such as the degree of azo functionalization, the molecular weight of the migrating units, the initial film thickness, as well as, for supramolecular systems the interaction type.[79,86,91] In addition the experimental procedures, like the polarization of the writing beams and the irradiating light intensity are also important.[164,165]

Figure 1.30 indicates the dependency between laser polarization and the diffraction efficiency (DE) of a DR1-containing side-chain polymer (PDR1M). For instance, a p-polarized or circularly polarized writing beam gives rise to a diffraction efficiency of around 40%, whereas for an s-polarized laser, the diffraction efficiency is <1%.[48] Priimagi and co-workers[82] have studied the efficiency of grating inscription on films of hydrogen-bonded complexes of 4-(2-pyridylazo)-*N,N*-dimethylaniline (PADA) and poly(4-vinyl phenol) (PVPh) as a function of chromophore concentration and the molecular weight of the polymer host. They concluded that stable gratings with modulation depths as high as 440 nm and with diffraction efficiency exceeding 40% can be inscribed in the equimolar complexes under illumination with a p-polarized beam. They also found that the modulation depth increases with increasing chromophore content as well as with decreasing molecular weight of the polymer host, as shown in Figure 1.31. On the other hand, Sobolewska and Bartkiewicz[166] showed that surface relief gratings can be successfully inscribed in azopolymers with short-chain polymer backbones, obtaining from a long-chain polymer by ultrasonic treatment, using the s-polarization configuration. They found that the efficiency of SRGs strongly depends on the length of the main polymer chains in the case of the s-s configuration due to the different motion capcacity of the main chain, which is strictly related to its length. The shorter the length of the main chain, the higher the amplitude gratings.

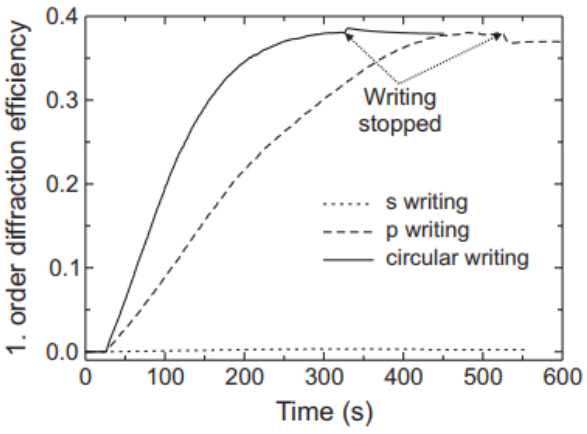

Figure 1.30. Diffraction efficiency of thin films of PDR1M illuminated by a 488-nm laser (100 mW/cm^2) with different polarizations. Reprinted with permission from Ref. 48, Copyright 2009 Helsinki University of Technology.

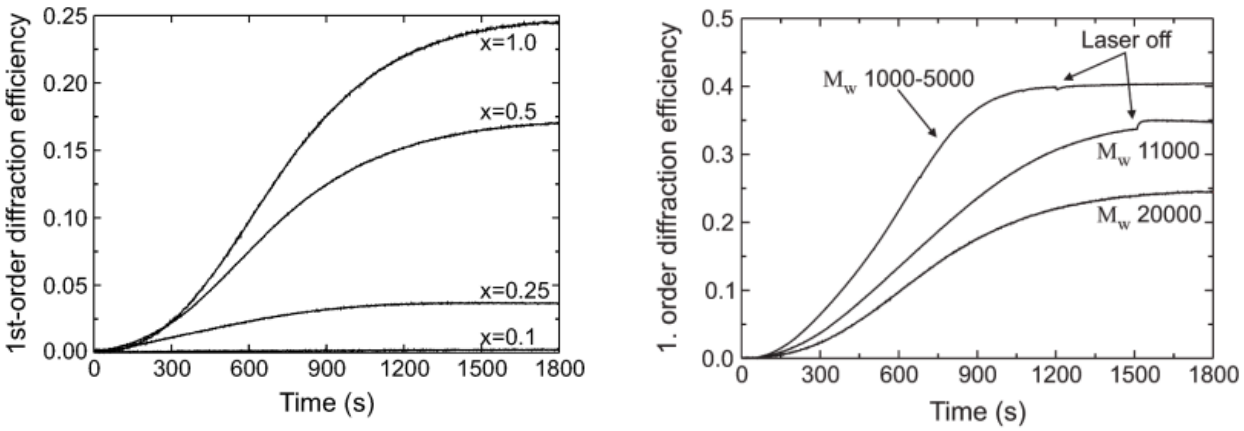

Figure 1.31. Growth of the first-order diffraction efficiency of the PVPh(PADA)$_x$ complexes as a function of chromophore content (left) and of the PVPh(PADA)$_{1.0}$ as a function of PVPh molecular weights (right). Adapted with permission from Ref. 82, Copyright 2009 American Chemical Society.

Efficient SRG patterns can also be inscribed in ionically bonded polyelectrolyte-azobenzene complexes and sol-gel materials.[23,24,34,70,86] In fact, Kulikovska and colleagues were the first to report an example of efficient SRG formation in an ionically bonded complex, as indicated in Figure 1.32a, with a modulation depth of 1.65 μm.[34] They also demonstrated that polysiloxane sol-gel networks that are ionically complexed to an azobenzene, as shown in Figure 1.32b, can lead to efficient SRG formation.[70] On the other hand, the formation of SRG gratings with a modulation depth of 360 nm, exceeding the original film thickness of 305 nm, in a timescale of 5 minutes and with relatively low irradiance (65 mW/cm^2), was also reported for ionic complexes between methyl orange and methylated P4VP of relatively high molecular weight (viscosity MW = 200 kg/mol).[23,24]

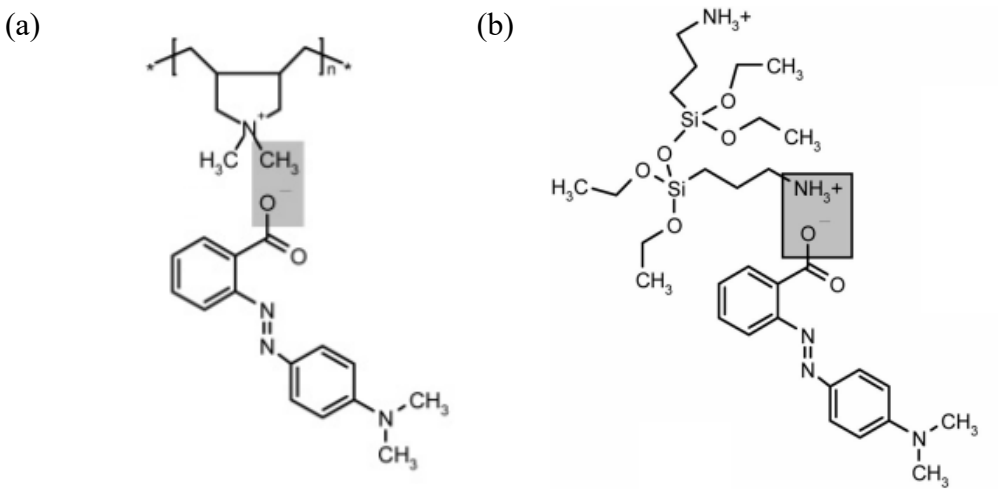

Figure 1.32. Ionic interaction in an azobenzene-based supramolecular (a) complex and (b) sol-gel material. Adapted with permission from (a) Ref. 34, Copyright 2007 American Chemical Society and (b) Ref. 70, Copyright 2008 American Chemical Society.

Following some reports of inscribing SRGs in H-bonded complexes,[12,167] Priimagi and co-workers[91] compared halogen-bonded complexes to previously investigated hydrogen-bonded materials. They concluded that complexes containing halogen-bonded azo molecules exhibit higher patterning efficiency than their hydrogen-bonded counterparts, which was attributed to the higher directionality of the halogen bonds compared to hydrogen bonds (Figure 1.33). Likewise, a comparison between ionically-bonded complexes and hydrogen-bonded complexes was made by Wang and colleagues[86] in our group. They studied the effect of pure hydrogen bonding using azoOH and poly(dimethylaminoethyl methacrylate) (PDM) vs. mixed ionic and hydrogen bonding through proton transfer using azoCOOH and PDM, and pure ionic bonding via ion exchange using azoSO_3 and quaternized PDM (PDMQ) on SRG formation efficiency, as indicated in Figure 1.34. They found that the efficiency of SRG inscription on spin-coated films of purely ionic-bonded complexes (azoSO_3/PDMQ) is highest while the proton transfer systems (azoCOOH/PDM) show somewhat more efficient SRG formation than that of the purely hydrogen-bonded materials (azoOH/PDM). The comparison was, however, somewhat compromised by the tendency for the azoCOOH in the proton transfer complex to phase separate and crystallize.

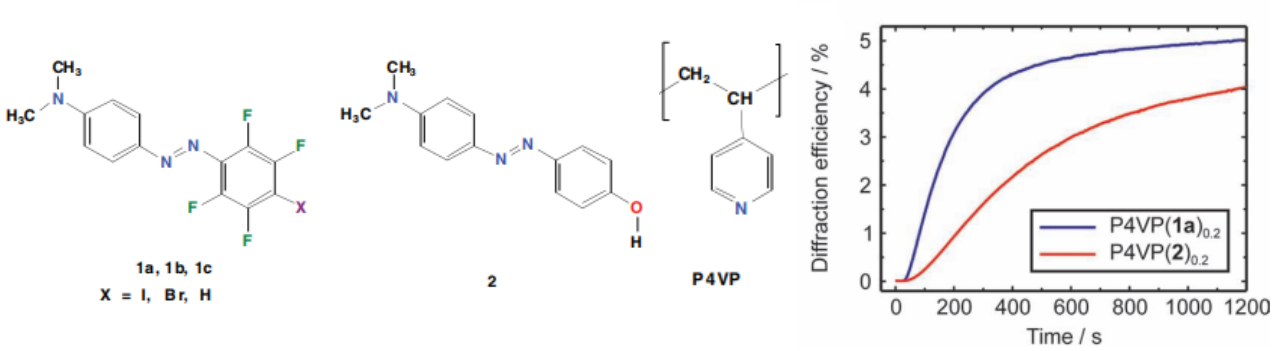

Figure 1.33. Chemical structures of the azobenzene derivatives and polymer host used to make halogen-bonded complexes and their hydrogen-bonded counterparts (left) and the time evolution of the first-order diffraction efficiency of spin-cast thin films of X-bonded ($P4VP(1a)_{0.2}$) and H-bonded ($P4VP(2)_{0.2}$) complexes during SRG formation (right). Adapted with permission from Ref. 91, Copyright 2012 John Wiley and Sons.

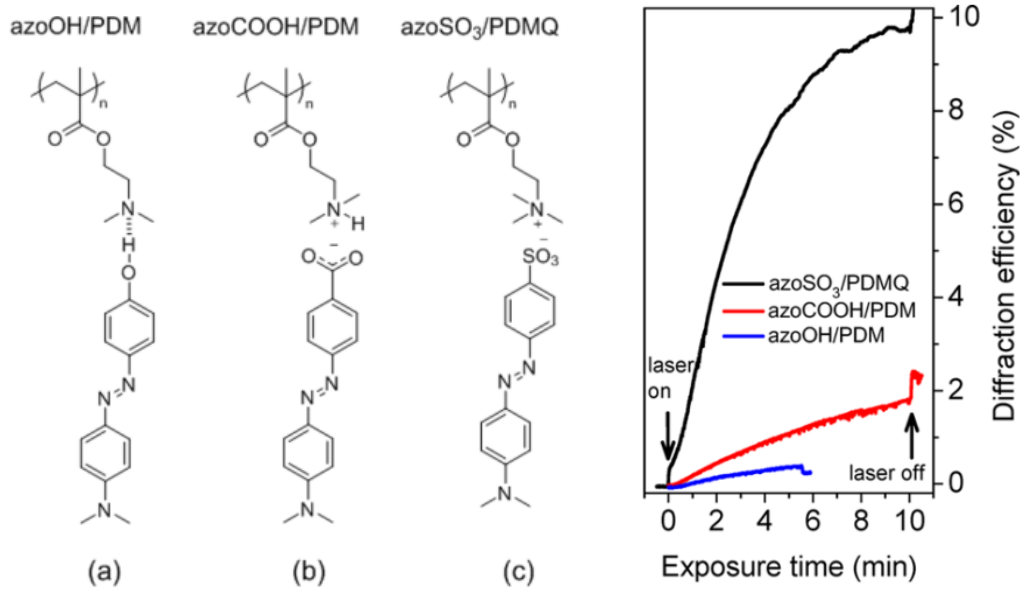

Figure 1.34. Chemical structures of analogous (a) hydrogen-bonded, (b) proton transfer, (c) ion exchange complexes, and the first-order diffraction efficiency upon SRG inscription (laser irradiance 190 mW/cm^2). Adapted with permission from Ref. 86, Copyright 2016 American Chemical Society.

1.7. Objectives and content of the thesis

On the one hand, light can be considered as an attractive means to trigger changes in the physciochemical and mechanical properties of materials from remote distances. On the other hand, a simple way to fabricate light-responsive materials is to use photoactive molecules that undergo either configurational or conformational modifications upon photon absorption. Despite extensive azopolymer research, understanding the complicated relationship between the light-triggered effects and the molecular architecture still remains a challenge for researchers in different fields, such as chemistry, physics, and biology. Most of the fundamental understanding on azobenzene-based light-induced motions is based on traditional, covalently functionalized polymers. To address the current shortcoming and enrich the fields, we were motivated to study photo-triggered effects both at the molecular and the macroscopic levels in supramolecular azobenzene materials.

Azopolymers prepared through non-covalent interactions in the form of supramolecularly bonded azobenzene-polymer complexes are alternatives to address the challenges of traditional all-covalent synthesis of azomaterials. As indicated earlier, this approach simplifies investigations for comparing different molecular parameters and for determining how they affect light-induced phenomena. This is important to better understand these phenomena.

The two light-induced phenomena that are often most investigated are photo-orientation (usually through birefringence or dichroism measurements) and the macroscale mass transport with polarized light leading to SRG inscription. The most informative method to study photo-orientation, as described above, is by infrared spectroscopy, especially PM-IRSAS developed in our group.[130] This method has been used less often than birefringence, although it is a more powerful technique for providing molecular-level information.

To date, comparisons of selected photoinduced phenomena in analogous azo derivatives with different tails have been made both for an H-bonding series[78,83,168] and an ionic bonding series.[23,24,95] Different bonding types have also been compared for a small number of systems, particularly the effect of H- vs. X-bonding on light-induced surface patterning.[79,91] The effect of ionic bonding (both by ion exchange and by proton transfer) vs. H-bonding on SRG formation were compared by Wang et al.,[86] but, as mentioned above, the system suffered from crystallization of the azo molecules in the case of the proton transfer system. As already discussed, the effect of

molecular weight of the polymer host on the photoinduced SRG inscription efficiency has been investigated to a limited extent.[82,111,152,169] However, the findings are contradictory and thus the impact of the molecular weight on the molecular photo-orientation remains controversial.

In this context, we chose to compare (a) the effect of the hydrogen bond (H-bonded) vs. ionic bond (i-bonded) and (b) the effect of the polymer molecular weight (MW = 5.2, 50, and 200 kg/mol) for both types of bonding. Our investigations focus on two photoinduced properties, namely (i) molecular-level photo-orientation and (ii) SRG formation in spin-coated films of the complexes. The azocomplexes employed, shown in Scheme 1.1, are based on P4VP as the polymer host. The azo derivatives used for the two types of bonding are identical except for the functional group involved in the supramolecular bond. The H-bonded complexes are formed by simple mixing of the components and the i-bonded complexes are formed by ion-exchange procedures, following methylation of P4VP. Although this study is fundamental in nature, the knowledge acquired from the study will benefit the design of efficient photoresponsive materials and improved optical devices.

(a)

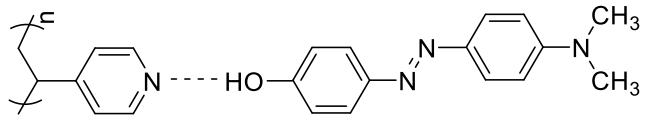

(b)

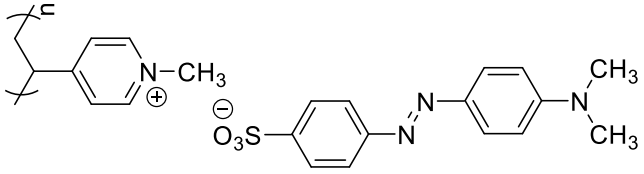

Scheme 1.1. Supramolecular complexes of (a) poly(4-vinylpyridine) (P4VP) with 4-hydroxy-4′-dimethylaminoazobenzene (azoOH) and (b) methylated poly(4-vinylpyridine) (P4VPMe) with methyl orange (MO).

The thesis is presented in 4 chapters:

Chapter 1 contains general information about the principles of supramolecular binding strategies and an overview of the most relevant studies of state-of-the-art supramolecular azobenzene-containing complexes as well as the light-induced movements in these systems.

Chapter 2 presents the experimental section including the materials used for this project and the preparation of supramolecular hydrogen-bonded and ionically-bonded azopolymers as well as the instrumentation and sample preparation.

Chapter 3 gives the main results regarding this research. These will be submitted to Macromolecules as a full paper for publication. The experimental work was mainly conducted by the author of the thesis, under the supervision of Profs. Bazuin and Pellerin and postdoctoral fellow, Dr. Jaana Vapaavuori. The SRG experiments presented here were conducted in the laboratory of Prof. R. Georges Sabat at the Royal Military College of Canada. They were done in part by Prof. Sabat. Dr. Xiaoxiao Wang determined the method of quaternization of the low molecular weight P4VP. All will be coauthors of the publication.

Chapter 4 summarizes the conclusions obtained from the thesis work and proposes ideas for future research.

Chapter 2: Experimental Details

2.1. Materials

Poly(4-vinylpyridine) (P4VP), having a weight-average molecular weight (M_w) of 5.2 kg/mol and a polydispersity index (M_w/M_n) of 1.20, was purchased from Polymer Source. P4VP with viscosity average molecular weights of 50 kg/mol and 200 kg/mol were obtained from Scientific Polymer Products. For simplicity, these polymers will be called 5k, 50k, and 200k. 4-Hydroxy-4′-dimethylaminoazobenzene (azoOH, >98%) was obtained from Tokyo Chemical Industry and 4-[(4-dimethylamino)phenylazo]benzene sulfonate (MO) from Riedel-de Haën. *N,N*-dimethylformamide (DMF, 99.8%), iodomethane (99.5%), and nitromethane (≥95%) were bought from Sigma-Aldrich and dimethyl sulfoxide (DMSO, 99.9%) from American Chemicals. Chloroform (99.8%) was bought from EMD Chemicals and tetrahydrofuran (THF, 99.9%) from Fisher Scientific. P4VP was dried in a vacuum oven at 60 °C overnight before use. The other chemicals were used as received. Milli-Q water was obtained from a Millipore Gradient A10 with resistivity 18.2 MΩ.cm at 25 °C.

2.2. Synthesis

The H-bonded complexes were prepared by dry mixing the appropriate amounts of azoOH and P4VP for a 1:1 azoOH:VP molar ratio, followed by dissolution in DMF at the desired concentration. This solution was directly used to prepare spin-coated films. The extent of complexation between the azoOH and the P4VP was verified by ^{1}H NMR (Bruker Ultrashield 400 MHz spectrometer) in DMSO-d_6 (99.96%, Sigma-Aldrich) and by IR spectroscopy.

To synthesize the i-bonded complexes (Scheme 2.1), approximately 10 g (164 mmol) of nitromethane were gradually added to 500 mg of the chosen P4VP (5 wt%) while stirring gently (300 rpm) at 46 °C in an oil bath until the polymer was fully dissolved. Then, 1000 µL (approximately 3 equivalents relative to the pyridine units) of CH_3I were added all at once to the solution to fully quaternize the P4VP. The solution was left to stir for 5 days at 46 °C. The quaternized P4VP (P4VPMe) was precipitated by dropwise addition of the solution to about 150

mL of ethyl ether (99%, EMD Chemicals) under vigorous stirring. This precipitate was then filtered and left to dry in a fume hood overnight. The extent of quaternization was verified by ^{1}H NMR in deuterium oxide (D_2O, 99.9%, Sigma-Aldrich) and by IR spectroscopy.

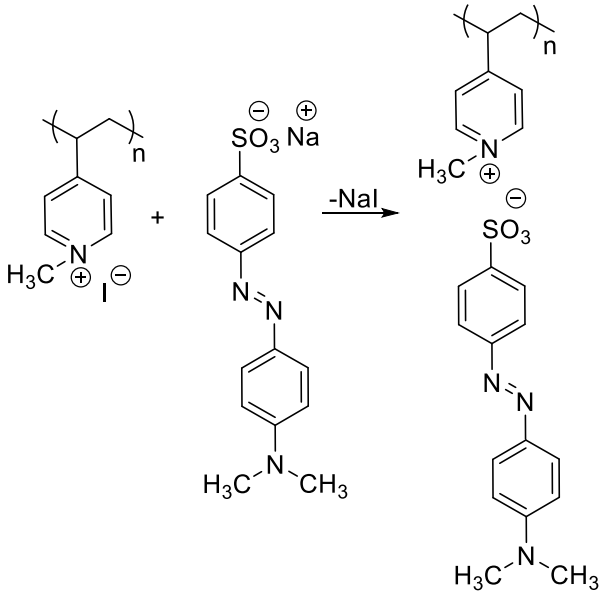

Scheme 2.1. Synthesis of the supramolecular ionic complex of methylated P4VP (P4VPMe) and methyl orange (MO).

To complex MO with P4VPMe (50k and 200k), 1.14 equivalent (1777 mg) of MO was dissolved in warm DMSO (about 45 °C) and heated at 45 ˚C for at least one hour and 1 equivalent of P4VPMe was dissolved in Milli-Q H_2O (25 mg/mL concentration). Then, the MO solution was gradually added to the P4VPMe solution, causing precipitation after stirring at 45 °C for 1 hour. The precipitate was redissolved by adding a sufficient amount of DMSO to the solution. Then, the solution was dialyzed (Spectra/Por molecular porous membrane tubing, M.W. cutoff 3500 Da; Spectrum Laboratories) for almost 3 weeks against Milli-Q water. The P4VPMe/MO solution was added drop-by-drop to the dialysis bag and the Milli-Q water was refreshed regularly over the dialysis period to eliminate the counterions (Na^+ and I^-), DMSO, and excess MO.

The procedure to synthesize the MO/P4VPMe 5k complex was slightly modified. In the quaternization step, 5 instead of 3 equivalents of CH_3I (1500 μL) was used. In the complexation step, the molar ratio of P4VPMe to MO was 1:1.5 instead of 1:1.14. Moreover, instead of preparing the P4VPMe solution in Milli-Q water, we dissolved the methylated polymer in DMSO and added

just 2 mL of Milli-Q water into solution. Besides, after a few days, we lessened the volume of solution in the dialysis bag by transferring part of it into a beaker, subjecting it to freeze-drying, redissolving the precipitate in DMSO and then re-adding it to the dialysis bag. We repeated this cycle several times and each time the solution was added to the bag slowly using a pipettor. After some weeks of dialyzing, since the colour of the water was still orange, we used an additional method of purification in which we redissolved the precipitate in DMSO and reprecipitated it by drop by drop addition into Milli-Q water under vigorous stirring. The suspension obtained was then centrifuged at 13,000 rpm for 5 min in a centrifuge (Sorvall, RC 5C Plus) and the precipitate was collected. This method took a considerable amount of time and caused loss of part of the material.

The resulting precipitates of the three MWs were freeze-dried for 5 days at -90 °C, and then dried in a vacuum oven at 60 °C for 3 days followed by 100 °C for 1 day. Equimolar complexation between MO and P4VPMe was verified by ^{1}H NMR in DMSO-d_6.

2.3. Instrumentation and sample preparation

Differential scanning calorimetry (DSC) was conducted with a PerklinElmer DSC 8500 calorimeter calibrated with indium to obtain the T_g for the original uncomplexed P4VP's. The DSC analysis was performed on evaporated and vacuum-dried samples (overnight at 70 °C). All T_g's were determined, after an initial cycle of heating and cooling, as the average half-height of the heat capacity jump in the second and third heating scans using a heating rate of 10 °C/min from 50 °C to 180 °C was followed by a ballistic cooling where each cycle followed by an isotherm of 3 min. The sample amount was between 2 and 3 mg.

Spin-coated films of each complex were prepared with a spin-coater model G3P8 from Specialty Coating Systems, using a spin-coating time of 60 s and different spin speeds depending on the desired film thickness for either series of complexes. The film thickness was measured with a Bruker DektakXT profilometer.

For UV-vis measurements, thin films of the 50k complex were spin-coated from 7 wt% DMF solutions on BaF_2 substrates at speeds of 1100 rpm and 1400 rpm for H-bonded and

i-bonded complexes, respectively. The films had a similar optical density at 488 nm (OD = 0.32 and 0.40 for H-bonded and i-bonded complexes, respectively). The UV-vis spectra of the thin films were recorded with a fiber-coupled spectrometer (Ocean Optics USB2000+) equipped with a DH-mini light source. A linearly polarized 488-nm diode laser (JDSU FCD488-020) of intensity around 20 mW/cm^2 was coupled to the UV-vis spectrometer (Scheme 2.2)[42] to induce photoisomerization in the sample during 5 min. This set-up allows determining the minimum content of the *cis* isomer (P_{cis}) according to Equation 3.1.

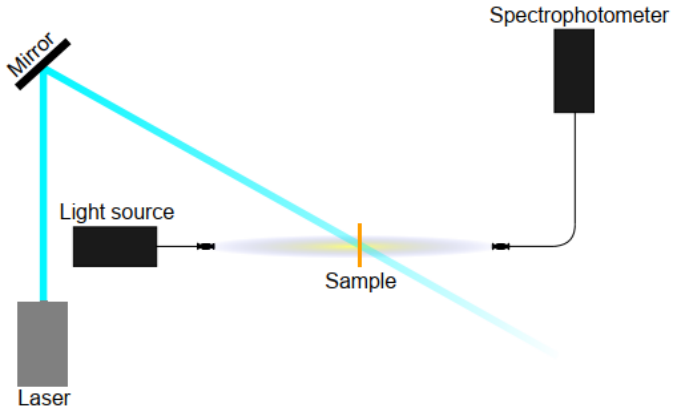

Scheme 2.2. Schematic representation of the experimental set-up for the UV-vis spectroscopy measurements. Reproduced from Ref. 42, Copyright 2014.

For IR measurements, films with a thickness of 500 - 600 nm were prepared by spin-coating 13 wt% DMF solutions onto BaF_2 windows. Spin speeds varying from 300 to 1100 rpm were used for the H-bonded complexes and from 300 to 2100 rpm for the i-bonded complexes, depending on the MW of the polymer host. Five samples of each complex were prepared and analyzed for reproducibility. Prior to spin-coating, the solution of the 5k ionic complex was filtered through a 0.45 µm pore-size syringe filter for homogenization. The optical density at 488 nm of the H-bonded and the i-bonded complexes films for IR spectroscopy was comparable (between 1.5 to 2). After spin-coating, the H-bonded and i-bonded films were dried in a vacuum oven at 70 °C and 90 °C, respectively, for 1 day to evaporate the residual DMF, which was confirmed by the absence of the intense DMF band around 1660 cm^{-1} in the IR spectra. The drying temperature of 70 °C was used for H-bonded to avoid losing a perceptible amount of azoOH by sublimation during the drying period.

Static IR measurements of the complex films were done on a Bruker Optics Vertex 70 Fourier transform IR spectrometer with a deuterated L-alanine triglycine sulfate (DLATGS) detector. The absorbance spectra were recorded with a resolution of 4 cm^{-1} by averaging 150 scans. For comparison, spectra of the pure components were obtained in the attenuated total reflection (ATR) mode using a Bruker Optics Tensor 27 FT-IR spectrometer equipped with a liquid-nitrogen-cooled mercury cadmium telluride (MCT) detector and a MIRacle (Pike Technologies) accessory with a silicon ATR element. The ATR spectra were recorded with a resolution of 4 cm^{-1} by averaging 256 scans on samples evaporated from solutions of pure P4VP 50k in chloroform (5% wt), pure P4VPMe 50k in MilliQ water (5% wt), pure MO in DMSO (5% wt), and pure azoOH in THF (5% wt).

To compare the spectroscopic glass transition temperatures of the various H-bonded complexes, 1% DMF solution of each complex was cast on the single reflection diamond element of a Heated Golden Gate (Specac) ATR accessory of the same Tensor 27 FT-IR spectrometer. At first, the samples were heated to a maximum temperature depending on the polymer MW (110, 125, and 135 ℃ for 5k, 50k, and 200k complexes, respectively). Next, an isotherm of 3 min was used to erase the thermal history. The ATR spectra were recorded by averaging 100 scans with a 4 cm^{-1} resolution during a cooling cycle with a ramp of 2 °C/min. Background scans were recorded for each sample applying the same temperature cycles. The spectroscopic T_g of H-bonded samples were obtained upon cooling by plotting the absorbance of the 1008 cm^{-1} band of the azocomplex as a function of temperature.

The polarization modulation infrared structural absorbance spectroscopy (PM-IRSAS) technique,[130] as illustrated in Scheme 2.3, was used to probe the time-resolved photo-orientation of both series of complexes.[140] This is a more powerful quantitative technique, capable of recording the structural absorbance information with 200 ms time resolution, in comparison with polarization modulation infrared linear dichroism (PM-IRLD)[170] to analyze the molecular orientation and conformation. This method allows measuring the dichroic difference (ΔA) and the structural absorbance spectra (A_0) simultaneously to calculate the orientation function ($<P_2>$).[130]

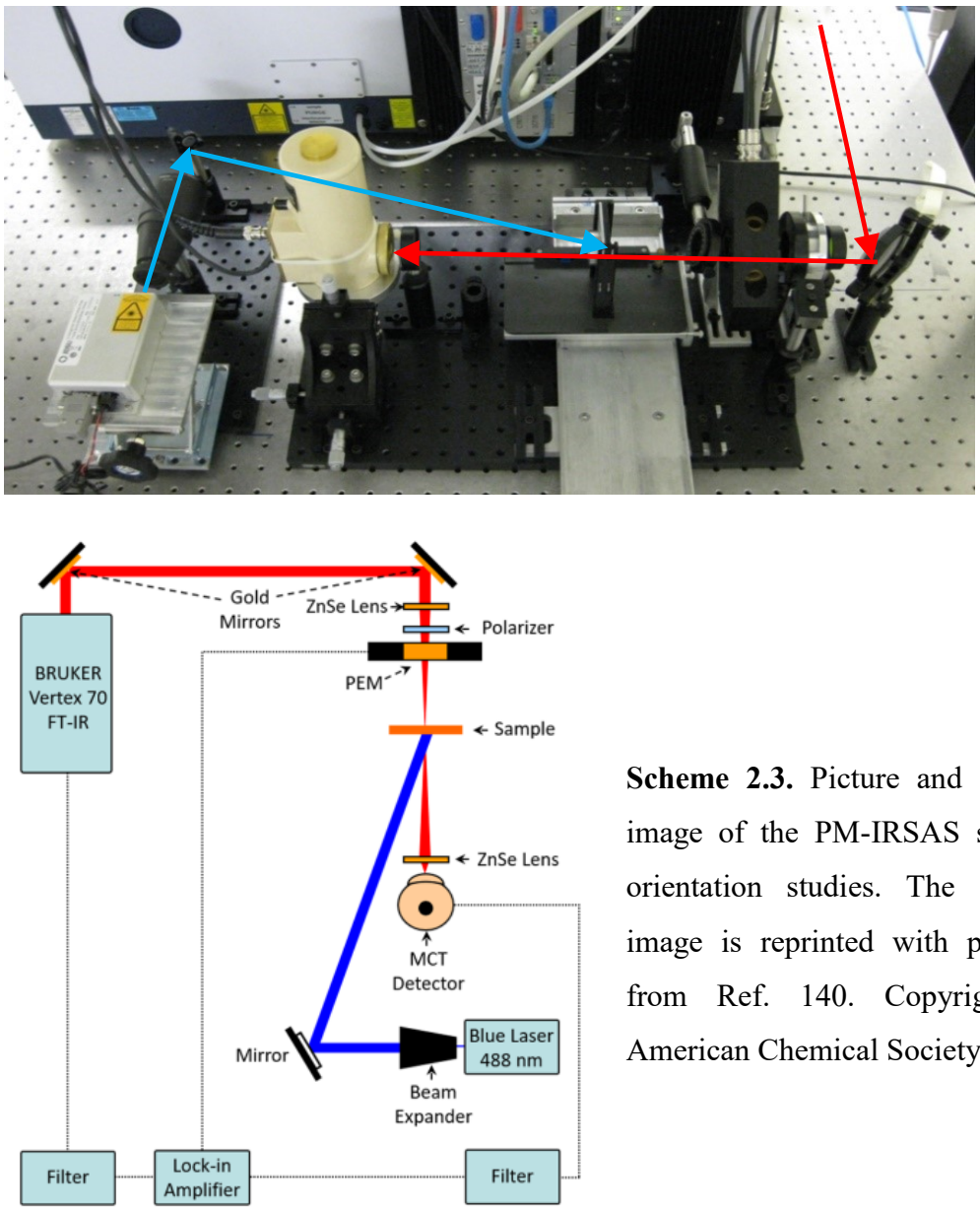

Scheme 2.3. Picture and schematic image of the PM-IRSAS set-up for orientation studies. The schematic image is reprinted with permission from Ref. 140. Copyright 2018 American Chemical Society.

PM-IRSAS measurements were performed on IR samples prepared as described above. A Vertex 70 spectrometer with an external optical set-up consisting of a vertically polarized 488-nm diode laser (JDSU FCD488-020) with a beam diameter of 0.7 mm expanded to 7 mm (using a 10X Thorlabs BE10M beam expander) to cover a cross-sectional area of the IR probe beam with an irradiance of approximately 20 mW/cm^2 was used. The external set-up contains two ZnSe lenses, a KRS-5 wire-grid polarizer (Optometrics), a photoelastic modulator (PEM-90 type II/ZS50, Hinds Instruments) to switch the polarization of the IR beam from parallel (*p*) to perpendicular (*s*) at 100

kHz, a liquid nitrogen-cooled mercury cadmium telluride (MCT) photovoltaic detector (Kolmar Technologies), a lock-in amplifier (Stanford Research Systems, SR830 DSP) with a 30-μs time constant, and two dual-channel electronic filters (Frequency Devices, 90TP/90IPB) to generate the dichroic difference (ΔA) and the individual polarized spectra (A_p and A_s).[130] The PM-IRSAS spectra were recorded with a resolution of 4 cm^{-1} during 1700 s of laser irradiation (photo-orientation) and 1700 s of subsequent thermal relaxation (laser off). Spectra were obtained by averaging 20 scans per spectrum (~4 s/spectrum) and 100 scans (~19 s/spectrum) during the first 1 min of the illumination (laser on) and relaxation (laser off), respectively, to follow the fast changes in orientation. Spectra were then recorded with a variable number of coadded scans (up to 320 scans per spectrum or ~61 s/spectrum) to increase the signal-to-noise ratio when following the slower orientation and relaxation processes.

To estimate the angle α between the transition dipole moment of the specific vibrational modes and the main axis of the molecule of interest (Equation 3.2) density functional theory (DFT) calculations were performed on Compute Canada's supercomputer Graham using the Gaussian 16 software. Results were analysed using GaussView 6. All molecules were optimized with the B3LYP functional and the 6-311+G(d,p) basis set before simulating their infrared spectra. No imaginary frequencies were obtained.

Surface relief gratings (SRG) were photochemically inscribed to study the macroscopic motion of azocomplexes under illumination. SRGs were inscribed on films of average thickness of 500-600 nm that were spin-coated on glass slides from 13% DMF solutions at ambient temperature. Grating formation was realized using a Lexel model 95L argon-ion laser (7 W) at 488 nm with a range of irradiation intensities (measured by Coherent Powerwand) including 100, 200 and 400 mW/cm^2. The inscribing laser beam was spatially filtered, collimated, and circularly polarized by a quarter-wave plate, to have the two oppositely rotating interfering beams impinge on the sample. To produce SRG patterns, the incident laser beam was directed so that half passed directly through the sample and the other half was reflected from a Lloyd's mirror interferometer that was installed perpendicular to the sample to produce an interference pattern. A mechanically chopped 633-nm He-Ne laser was employed as the probe laser. The inscription of the SRGs was tracked during 1000 s of laser illumination by measuring the first-order diffraction of the probe beam using a photodiode as a function of time. The transmitted first-order diffracted signal was

attenuated with a 0.4 % neutral density filter before reaching the silicon photodiode to avoid detector saturation. The photodiode signal was then captured using a SRS model 830 lock-in amplifier and recorded on a computer (Scheme 2.4).[7] The diffraction efficiency (DE) was calculated by dividing the power of the first-order diffracted signal (pump laser on) by the power of the zeroth order diffracted signal (pump laser off) after completion of the SRG. To have the same sensitivity in the lock-in for zeroth order as for the first order, a 6.6 % neutral density filter was used in addition to the 0.4% filter.

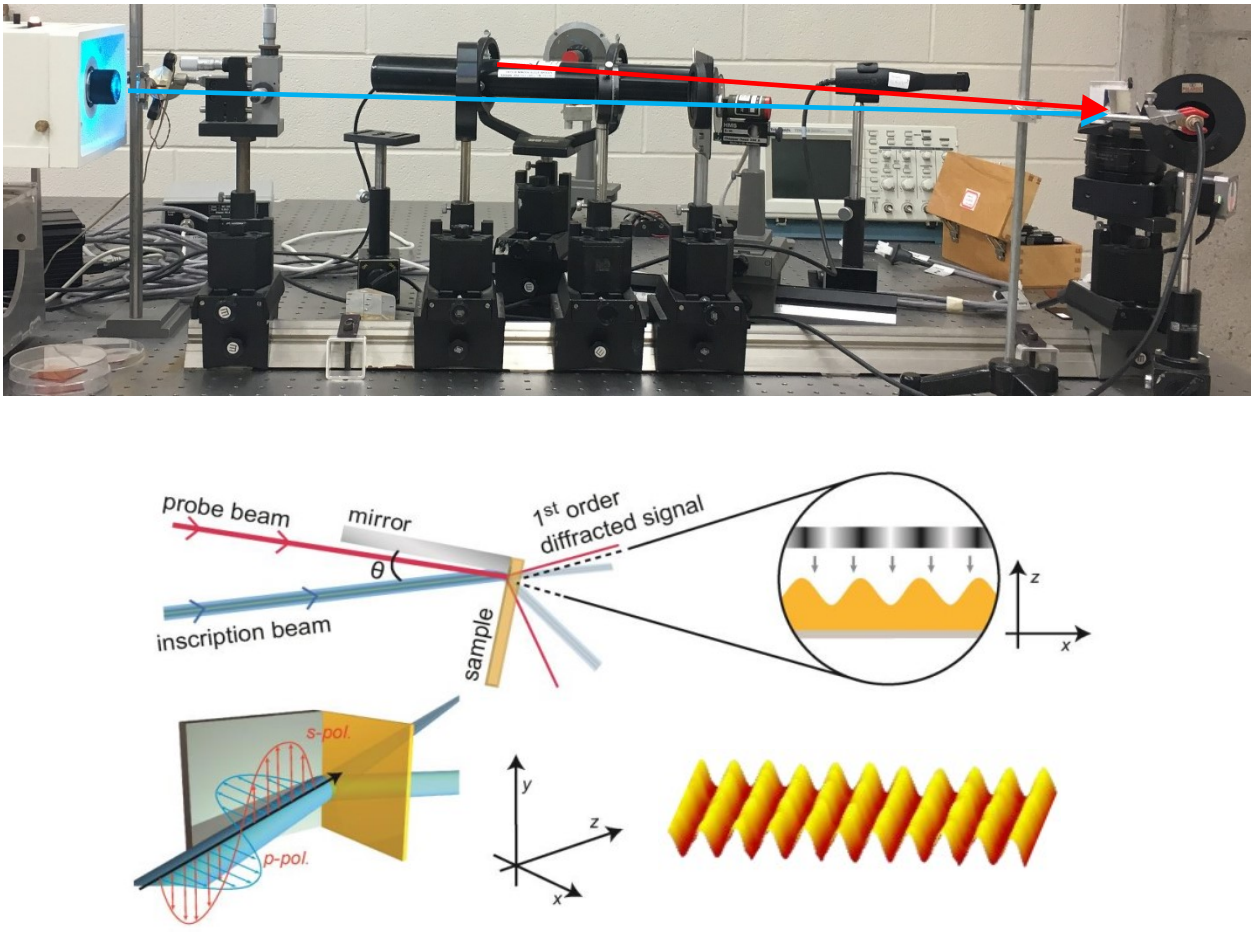

Scheme 2.4. Picture and schematic image of the SRG inscription set-up. The schematic image is adapted with permission from Ref. 7. Copyright 2014 Aalto University.

Chapter 3: Results and Discussion

The objective of this work is to understand the impact of polymer molecular weight on the photoinduced orientation and SRG diffraction efficiency (DE), of two types of photoactive supramolecular azopolymer complexes. Before presenting these results, we should verify the nature and the extent of complexation between the polymer and the azobenzenes. Visually, the films of all strongly coloured complexes are uniform and they show no visible evidence of phase separation or crystallization. The azoOH complex films are transparent, in keeping with their amorphous non-liquid crystalline character.[171] The MO complex films are slightly cloudy, in keeping with their smectic A liquid crystalline character.[23]

3.1. Spectroscopic analysis of the complexes

3.1.1. UV-visible analysis

Figure 3.1 shows the UV-visible spectra of thin films of azoOH/P4VP and MO/P4VPMe 50k complexes on BaF_2 substrates before (initial state) and after 5 min of irradiation with 488 nm polarized light. For comparison, the spectra of the pure azos in dilute DMF solutions (8.5 µg/mL) are also shown. The complex with a molecular weight of 50k was selected because it served as an intermediate between the 5k (unentangled) and 200k (entangled) samples.

The similarity between the UV-vis spectra of the azoOH/P4VP complex thin film and the corresponding azoOH dilute solution in DMF, in particular the maximum wavelength (λ_{max}) of the main absorption, reinforces the visual observation that the azoOH/P4VP complex is amorphous and that the azo is well dispersed in the polymer matrix, which is an indirect indication of complexation between the two moieties (Figure 3.1a).[172] The main band at 410 nm is assigned to $\pi-\pi^*$ absorption of the *trans* configuration, while the $n-\pi^*$ absorption appears as a small shoulder at around 467 nm for the spin-coated film.[86,173-177] When the azoOH/P4VP thin films are illuminated with linearly polarized 488-nm light, a decrease in the intensity of the main band is observed. This indicates *trans-cis* photoisomerization. The formation of *cis* isomers is confirmed by the increase of absorbance around 540 nm due to the $n-\pi^*$ absorption band of the *cis*

conformers. This decrease in the band intensity can be used to estimate the conversion extent of the *trans* isomer and the minimal *cis* isomer value. According to Equation 3.1, the value is approximately 14% after 5 min of laser illumination. In addition, the absence of changes in the λ_{max} of *trans* absorption upon illumination suggests that the chromophore-chromophore interactions of azo molecules are not affected by the isomerization.[140] Moreover, since the 488-nm irradiation can excite both the *trans* π-π* and the *cis* n-π* bands of azobenzene molecules, fast *trans-cis-trans* photoisomerization cycles are produced and these prevent accumulation of the *cis* isomers during irradiation. This behavior is required for efficient photo-orientation and SRG inscription.

$$P_{cis} = 1 - \frac{A_{irr}}{A_{ini}} \quad 3.1$$

P_{cis} is the minimum content of *cis* isomer, A_{irr} is the maximum absorbance under irradiation, and A_{ini} is the initial absorbance before irradiation.

In contrast with the H-bonded complex, the blue shift in the absorption maximum of the UV-vis spectrum of i-bonded complex from 428 nm for pure MO in DMF solution to 394 nm for a spin-coated film indicates significant differences in the chromophore-chromophore interactions in dilute solutions and in thin films (Figure 3.1b). This 34-nm shift in λ_{max} of the main absorption ($\pi-\pi^*$ transition) of the *trans* state to a shorter wavelength, which is accompanied by differences in the spectral shape between MO in solution and in the complex thin film, can be ascribed to the changes of the polarity of the local environment of the chromophore in different matrices (DMF vs. polymer).[95,178,179] and to the excitonic coupling of the azos in the smectic A liquid crystalline packing in the thin film.[23,86,173] Also, the distinct shoulder near 450 nm for the thin films may originate from a *trans* $n-\pi^*$ transition, a typical characteristic of azobenzene molecules.[173,176,180] Similar to hydrogen-bonded complexes, ionically-bonded complexes show a decrease in the absorption of the main *trans* absorption band due to the photoisomerization from *trans* to *cis* state with no change in the λ_{max} after irradiation. This decrease in the band intensity is an indirect indicator of the minimal *cis* isomer content (20%) immediately after 5 min of laser illumination. This value is close to the 14% value obtained for the H-bonded complex.

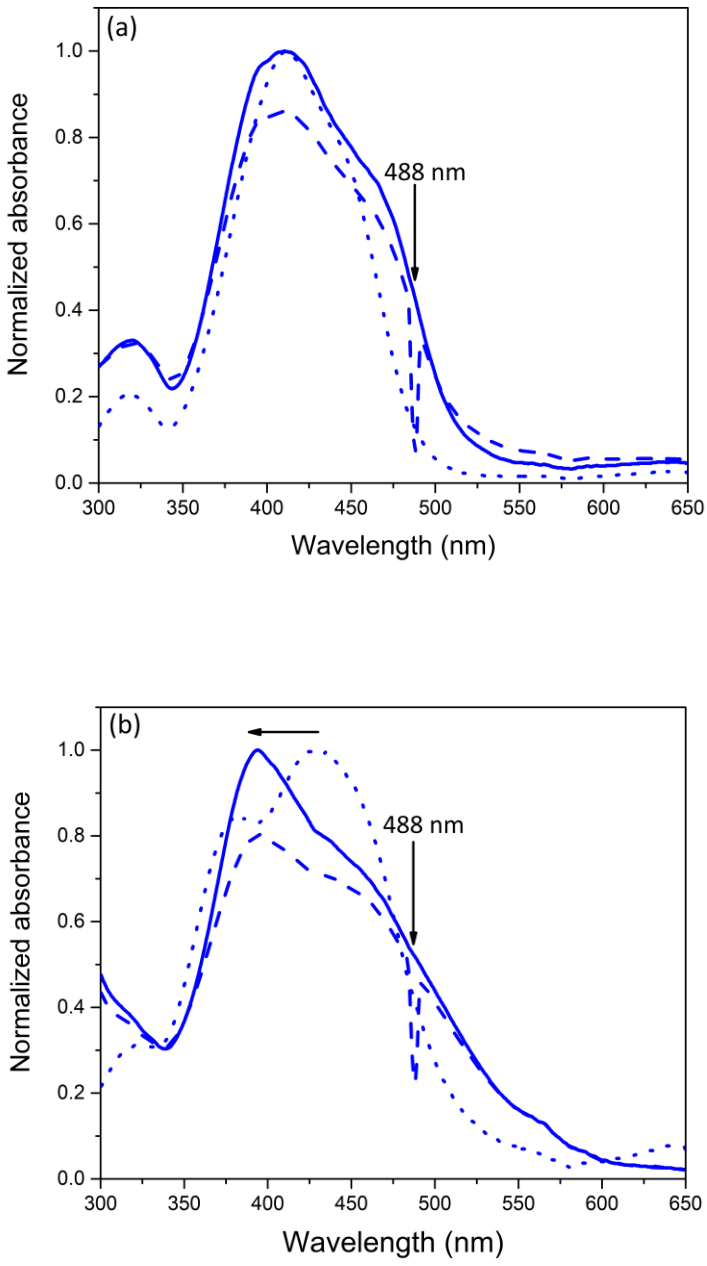

Figure 3.1. Normalized UV-vis absorption spectra of spin-coated thin films of (a) azoOH/P4VP and (b) MO/P4VPMe 50k complexes at equimolar ratio before (initial state, solid lines) and after 5 min of irradiation (dashed lines) compared to the spectra of the pure azos in dilute DMF solution (8.5 μg/mL; dotted lines). The minimum in absorbance at 488 nm in the spectra under irradiation is due to the scattering of the laser to the detector from the sample surface.

3.1.2. Infrared analysis

Since the position, the width, and the shape of IR bands depend on the molecular environment of the absorbing chemical groups of the complexes, we used static infrared spectroscopy (IR) to verify the formation of hydrogen bond between P4VP and azoOH.[181] A comparison between the second derivatives of the transmission IR spectrum of spin-coated film of H-bonded azoOH/P4VP 50k complex and the ATR spectra of the pure components between 960 and 1030 cm^{-1} is made in the Figure 3.2a. The 993 cm^{-1} band in the spectrum of pure P4VP, which is related to a vibrational stretching mode of the free pyridine, shifts to 1008 cm^{-1} in the spectrum of the azoOH/P4VP complex. This band shift confirms the formation of a hydrogen bond between the pyridine and the hydroxyl group of azoOH. The complexation is not complete based on the small residual band at 993 cm^{-1} (which could be also partially due to the contribution of the azoOH band at around 996 cm^{-1}).[89,90,182] The amplitude of the shift is consistent with previous observations for P4VP complexes with various hydroxyl-terminated small molecules. It also indicates a hydrogen bond of moderate strength.

Quaternization (methylation) of P4VP can be confirmed by comparing the ATR spectra of samples evaporated from solutions of pure P4VP 50k in chloroform (5% wt) and pure P4VPMe 50k in MilliQ water (5% wt) in Figure 3.2b. The disappearance of the stretching mode bands of the pyridine ring at 993 cm^{-1}, 1415 cm^{-1}, and 1557 cm^{-1} are proofs of transformation of the pure P4VP to P4VPMe. Additional qualitative evidence of the formation of methylated vinylpyridine is the appearance of a strong band at 1641 cm^{-1} in the ATR spectrum of P4VPMe. This is the pyridinium ion equivalent of the pyridine stretching mode at 1596 cm^{-1}.[93,94,183,184] While IR spectra of the i-bonded complexes confirm the presence of MO and P4VPMe, they do not provide direct information about their specific interaction. However, ionic complexation between MO and P4VPMe can be confirmed using other techniques, such as energy-dispersive analysis, ^{1}H NMR, and elemental analysis, as shown in our previous work.[23,173]

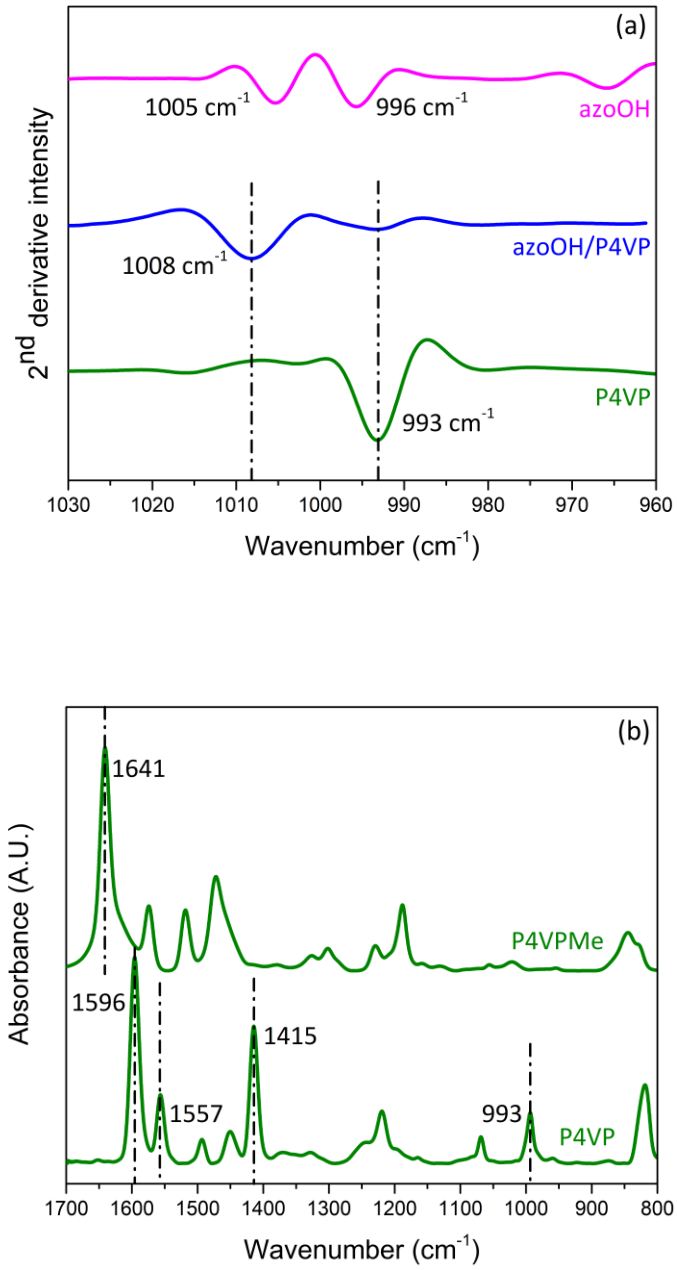

Figure 3.2. (a) Second derivative ATR spectra of pure P4VP, pure azoOH, and azoOH/P4VP 50k complex, and (b) ATR spectra of pure P4VP 50k vs. P4VPMe 50k. All bands appear as negative in second derivative spectra.

3.1.3. ^{1}H NMR analysis

^{1}H NMR spectra can verify both the quaternization of P4VP in ionic complexes and the equimolar content of azo and polymer repeat units in both series of complexes. The ^{1}H NMR spectrum in Figure 3.3a, which shows that the ratio of the d/c signals is very close to 1, indicates that P4VP has been quaternized (i.e. methylated) to P4VPMe by essentially 100%. The absence of the pyridine signals at 6.59 and 8.26 ppm in the spectrum is additional confirmation of complete methylation.

Figure 3.3b shows the equimolar ratio of MO to P4VPMe in ionic 50k complexes by comparing the integrated intensity of MO peaks (signals e or i) to P4VPMe peaks (signals c or d).[23,173] The ionic complexation, even in DMSO solution, can be also confirmed by considering the broader shape of all MO peaks in the ionic complex spectrum in comparison with the sharp peaks at the same chemical shifts for pure MO (Figure 3.3c). We can ascribe this difference in the band shape to the decreased mobility of the small molecules (MO) due their attachment to P4VPMe through ionic bonds.

Likewise, for H-bonded 50k complexes (Figure 3.3d), the 1:1 azoOH/P4VP molar ratio can be confirmed using the integrated intensities of either signals e, h or signals g, f (azoOH) and either signal c or signal b (P4VP). The results show that the H-bonded complexation is equimolar; Signal d, which is ascribed to the proton of the azo OH group, is found at 10.0 ppm but cannot be considered as a sign of H-bonding in the complexes since it's chemical shift is the same in the spectrum of pure azoOH due to the hydrogen bond between azoOH and DMSO-d_6. In fact, the high resolution of the azoOH peaks compared to those of P4VP indicates that complexation does not occur in solution. Nevertheless, the combined NMR and IR results validate the equimolar composition and high degree of complexation in the H-bonded system.

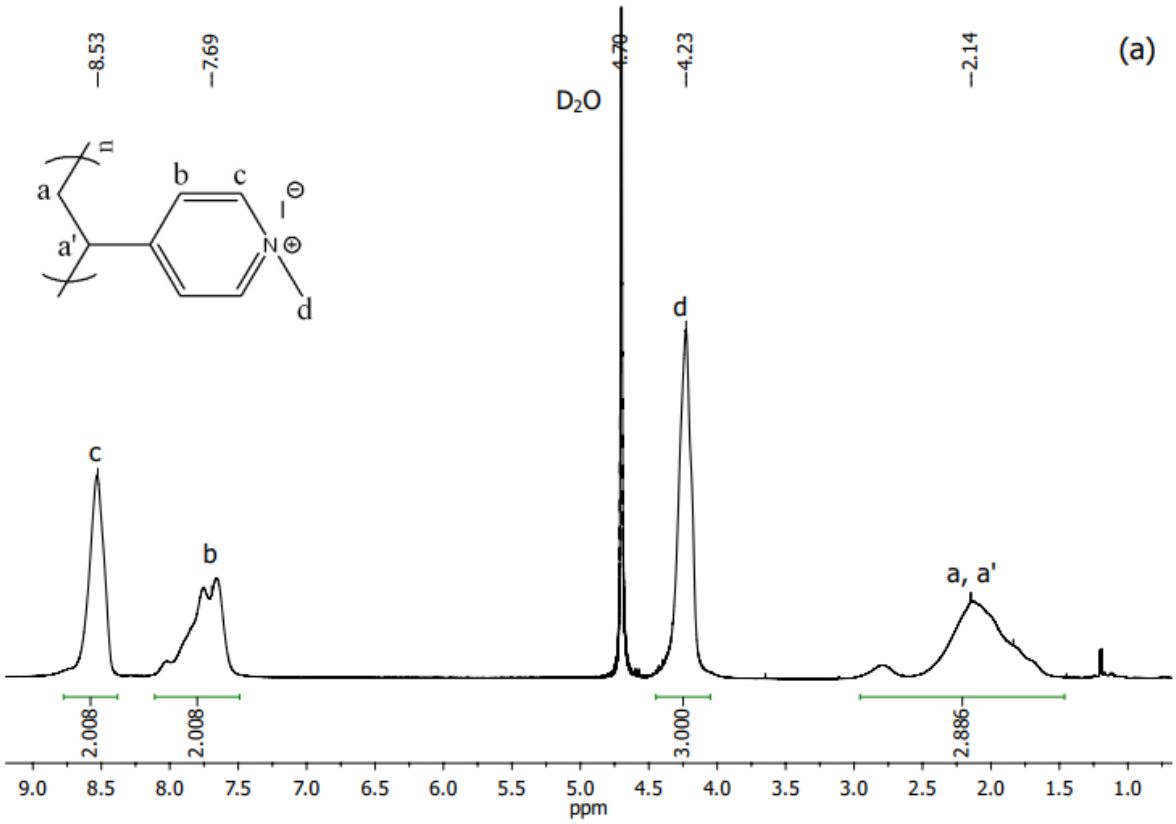
(a)
8.53
7.69
4.70
4.23
2.14
D2O
a
a'
b
c
d
n
c
b
d
a, a'
2.008
2.008
3.000
2.886
9.0 8.5 8.0 7.5 7.0 6.5 6.0 5.5 5.0 4.5 4.0 3.5 3.0 2.5 2.0 1.5 1.0
ppm

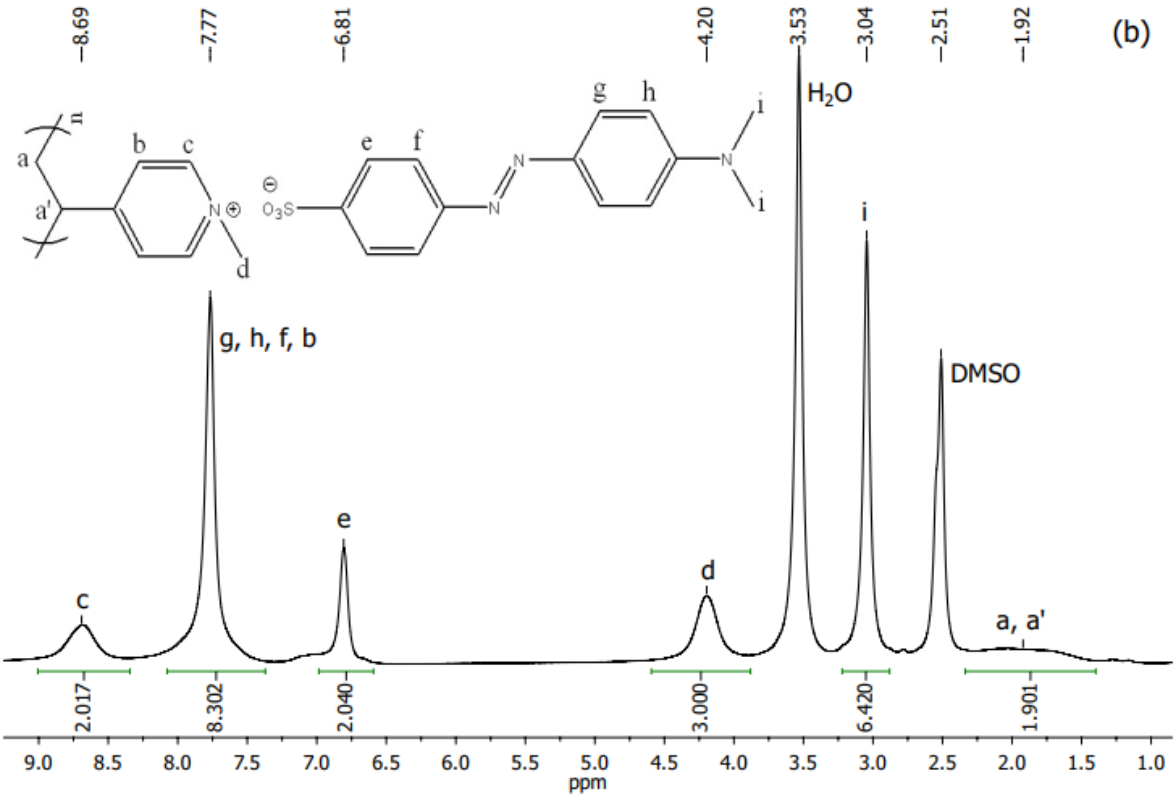
(b)
8.69
7.77
6.81
4.20
3.53
3.04
2.51
1.92
H2O
g, h, f, b
e
d
c
i
DMSO
a, a'
2.017
8.302
2.040
3.000
6.420
1.901
9.0 8.5 8.0 7.5 7.0 6.5 6.0 5.5 5.0 4.5 4.0 3.5 3.0 2.5 2.0 1.5 1.0
ppm

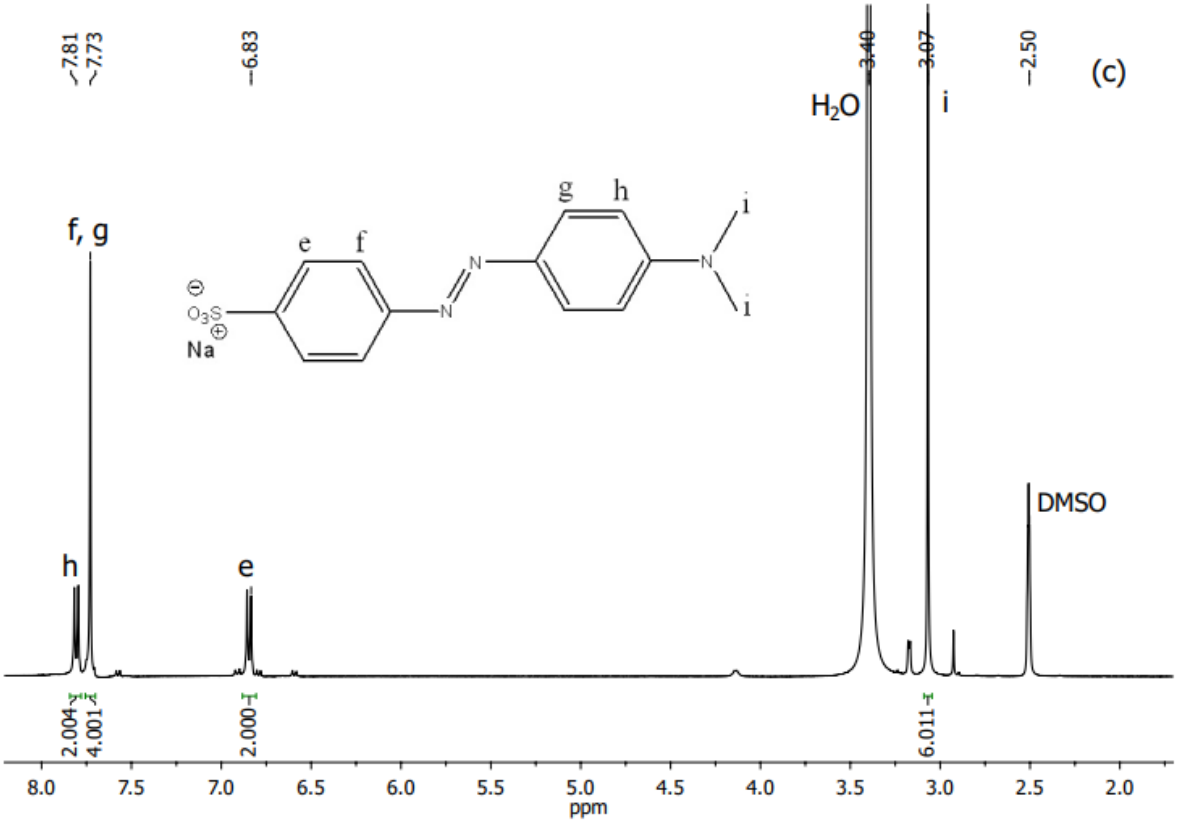
(c)
H2O
DMSO
f, g
h
e
i
g
h
e
f
i
i
O3S
Na
2.004
4.001
2.000
6.011
ppm

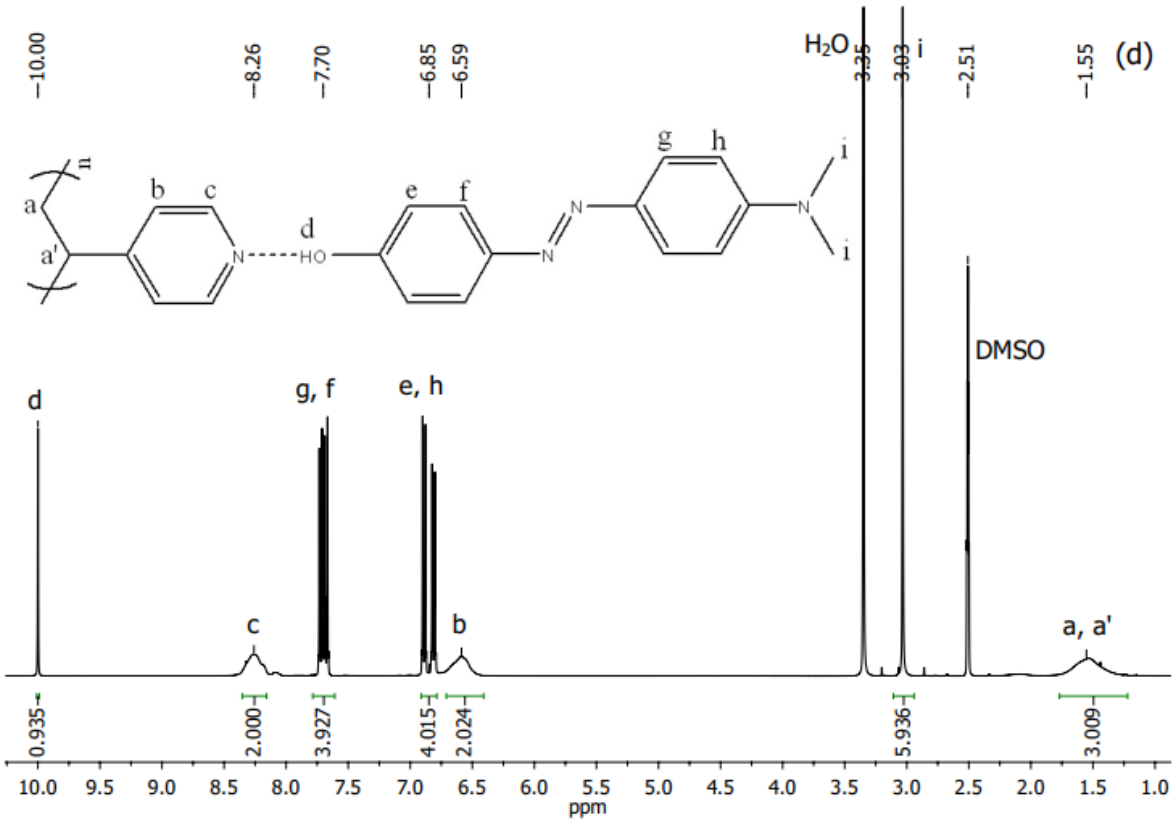
(d)
H2O
DMSO
d
g, f
e, h
c
b
a, a'
a
a'
n
b
c
d
HO
e
f
g
h
i
i
0.935
2.000
3.927
4.015
2.024
5.936
3.009
ppm

Figure 3.3. ^{1}H NMR spectra of (a) P4VPMe 50k in D_2O, (b) MO/P4VPMe 50k complex in DMSO-d_6, (c) pure MO in DMSO-d_6, and (d) azoOH/P4VP 50k complex in DMSO-d_6. The numbers associated with signals indicate the integration values. The spectra were normalized based on the signals d, d, e, and c for panels (a), (b), (c), and (d), respectively. The small peaks around 3 ppm in panel (c) are due to impurities.

3.2. Photoinduced orientation and thermal relaxation

The principal technique employed to track photo-orientation of azocomplexes under consideration is PM-IRSAS. For photo-orientation studies, the orientation parameters, or $\langle P_2 \rangle$ values, should be calculated using well-isolated bands to avoid contribution from the other component and with bands of sufficient intensity to provide an acceptable signal to noise ratio. Figure 3.4a shows a comparison between the transmission IR spectrum of a spin-coated film of azoOH/P4VP 50k complex and the ATR spectra of pure components (the bands of interest are indicated). For this complex, we selected the intense 1148 cm^{-1} and 1363 cm^{-1} azoOH bands as well as the reasonably well isolated 1008 cm^{-1} and 1418 cm^{-1} P4VP bands. Although the 1600 cm^{-1} band is even more intense than the two other above-mentioned bands, it is not well-isolated. According to DFT calculations, the band around 1363 cm^{-1}, which is common to both azo compounds, is due to a complex mode involving in plane C–H deformation and ring stretching of the phenyl near the dimethylamino group, bending of the dimethylamino group, and C–N stretching. The 1148 cm^{-1} band is ascribed mainly to aromatic C–H deformation of both of the phenyl. The 1008 cm^{-1} and 1418 cm^{-1} bands can be assigned to a symmetric ring deformation and antisymmetric C–H deformation of the pyridine, respectively.

Likewise, Figure 3.4b shows the spectra for the ionic complex and its pure components where the intense 1113 cm^{-1} and 1365 cm^{-1} MO bands, as well as the 1643 cm^{-1} P4VPMe band, were chosen for orientation quantification. The 1113 cm^{-1} band has been attributed previously to S=O stretching mode,[22,95] but DFT suggests it is due to complex vibration of the complete molecule. The 1643 cm^{-1} band of P4VPMe is assigned to a symmetric stretching mode of the pyridinium group.

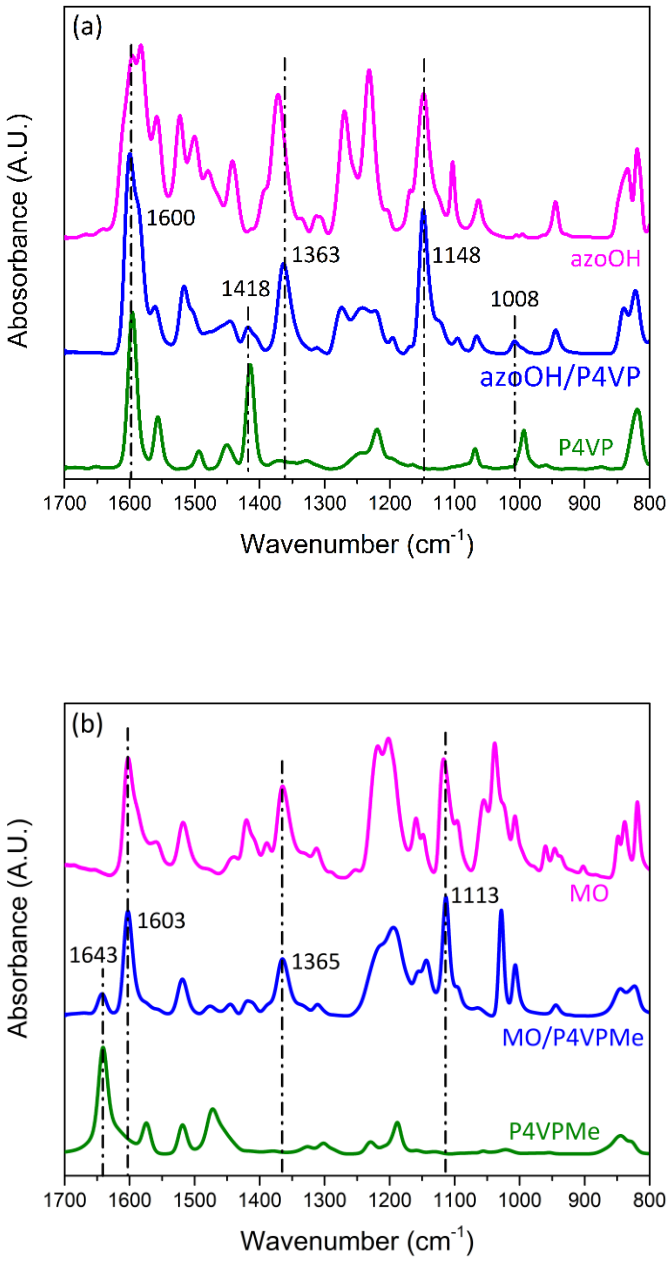

Figure 3.4. Infrared spectra of spin-coated films of (a) H-bonded azoOH/P4VP and (b) i-bonded MO/P4VPMe 50k complexes compared to ATR spectra of the pure components. The azo-containing spectra are normalized with respect to the 1148 cm^{-1} azoOH and the 1113 cm^{-1} MO bands in (a) and (b), respectively.

The $<P_2>$ values were calculated by Equation 3.2, considering the appropriate α angle for the selected bands. Based on DFT calculations (in vacuo), the transition dipole moment of the vibrational mode of the various azoOH (1148 and 1363 cm^{-1}) and MO (1113 and 1365 cm^{-1}) bands is along the azo long axis, so $\alpha = 0°$ was used in all cases. For P4VP, the transition dipole moment of the 1008 cm^{-1} band lies along the N-C4 axis of the pyridine, so $\alpha = 0°$ was used. Since the 1418 cm^{-1} band is perpendicular to the N-C4 axis, $\alpha = 90°$ was used. Finally, the 1643 cm^{-1} P4VPMe band is parallel to the N-C4 axis and $\alpha = 0°$.

$$\langle P_2 \rangle = \left(\frac{2}{3cos^2\,\alpha - 1}\right)\left(\frac{\Delta A}{3A_0}\right) \quad 3.2$$

where

$$\Delta A = A_p - A_s \quad 3.3$$

and

$$A_0 = \frac{A_p + 2A_s}{3} \quad 3.4$$

In Equations 3.2 - 3.4, A_p and A_s are the spectra polarized parallel and perpendicular to the pump laser polarization, respectively, and α is the angle between the transition dipole moment of the specific vibrational mode and the main axis of the molecule of interest.

The $<P_2>$ values of the selected azo bands are studied as a function of time during irradiation at 488 nm (laser on) and thermal relaxation (laser off), as indicated in Figures 3.5a and 3.5b for the H-bonded and i-bonded complexes, respectively. In both cases, the $<P_2>$ values are negative since the perpendicular absorption is higher than the parallel absorption, resulting in negative dichroism. Therefore, the absolute $<P_2>$ values were considered to study the photoinduced orientation in both series of azocomplexes. In addition, the orientation is highly repeatable for the pairs of azo bands both in terms of the shape of the curves and the amplitude of the orientation parameters.

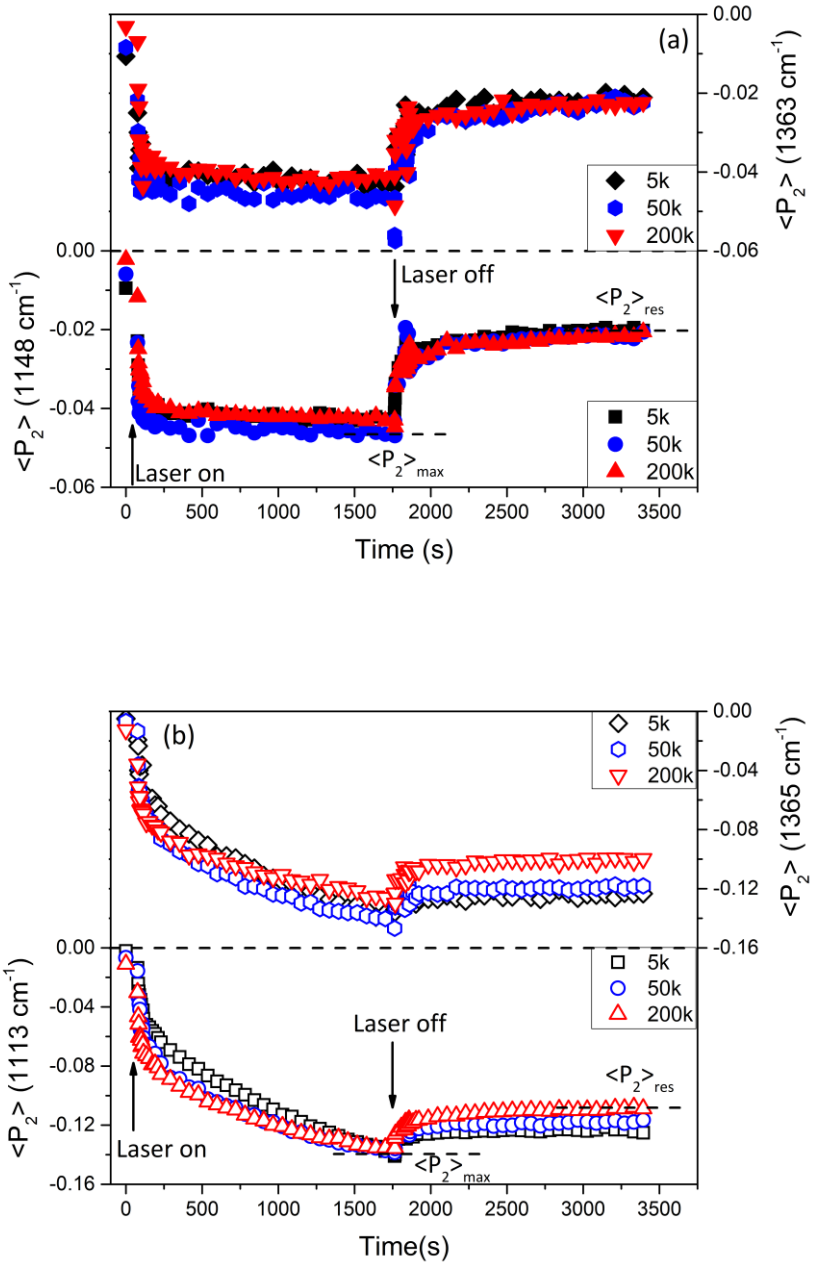

Figure 3.5. Photoinduced orientation (<P_2>) as a function of time during orientation (laser on) and thermal relaxation (laser off) for (a) 1148 and 1363 cm^{-1} azoOH bands of three azoOH/P4VP complexes (5k, 50k, and 200k) (b) 1113 and 1365 cm^{-1} MO bands of analogous MO/P4VPMe complexes.

Figure 3.6 compares the time-dependent behavior of azoOH band and MO during the 1700 s of both orientation (laser on) and relaxation (laser off) periods. For simplicity, only the 1363 cm^{-1} azoOH band and 1365 cm^{-1} MO band are shown. Before illumination, the initial $\langle P_2 \rangle$ value is around zero because of the random orientation in the fresh spin-coated films. Upon irradiation, the $\langle P_2 \rangle$ values first grow rapidly towards negative values, indicating photo-orientation of the azo molecules perpendicularly to the polarized light direction. For longer irradiation times, the photo-orientation of azoOH reaches a quasi-plateau that represents saturation and $\langle P_2 \rangle_{max}$. On the other hand, for i-bonded complexes, the photo-orientation of MO continues to grow at a slower rate after the initial period and it does not reach a plateau during the timescale of the experiment. This is a clear indication of lack of the saturation of the orientation. Therefore, the $\langle P_2 \rangle$ values are similar for both series of complexes during the fast process; however, the i-bonded complexes reach larger absolute $\langle P_2 \rangle$ values, on the order of 0.14 vs. 0.047 after 1700 s of irradiation, as a consequence of the slower process. Moreover, the kinetics to reach maximum orientation appear to be different for the 5k complex compared to the i-bonded complex of higher molecular weight. This effect will be studied later when analyzing quantitatively the photo-orientation kinetics.

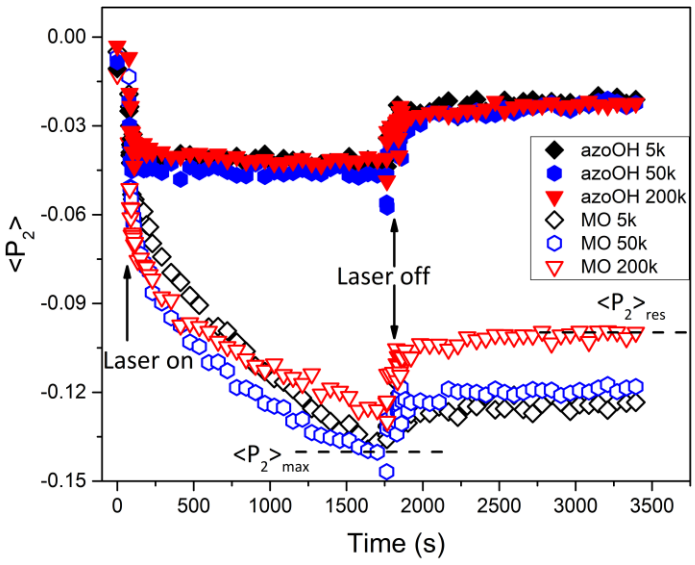

Figure 3.6. Photoinduced orientation and thermal relaxation processes of three hydrogen bonded and ionically bonded complexes (5k, 50k, and 200k).

Figure 3.6 also indicates that the orientation reached by each given azo is essentially independent of the polymer host molecular weight. This is in contrary to our initial expectations. The quantitative $<P_2>_{max}$ values are collected in Table 3.1. They confirm that there is no significant correlation between the $<P_2>_{max}$ values and the molecular weight of the polymer backbone.

Table 3.1. The maximum orientation ($<P_2>_{max}$) and the percentage of the residual orientation ($<P_2>_{res}$) after relaxation for selected bands of H-bonded and i-bonded complexes.

	$<P_2>_{max}$		$<P_2>_{res}$ (%)	
azoOH/P4VP	1148 cm^{-1}	1363 cm^{-1}	1148 cm^{-1}	1363 cm^{-1}
5k	-0.043 ± 0.004	-0.043 ± 0.004	47 ± 2	50 ± 3
50k	-0.046 ± 0.004	-0.047 ± 0.005	47 ± 7	48 ± 9
200k	-0.043 ± 0.003	-0.041 ± 0.002	50 ± 5	54 ± 5
MO/P4VPMe	1113 cm^{-1}	1365 cm^{-1}	1113 cm^{-1}	1365 cm^{-1}
5k	-0.14 ± 0.01	-0.14 ± 0.01	92 ± 2	90 ± 3
50k	-0.14 ± 0.01	-0.14 ± 0.01	87 ± 3	85 ± 2
200k	-0.13 ± 0.01	-0.13 ± 0.01	80 ± 2	80 ± 2

The fast orientation can be related to a phenomenon called angular hole burning (AHB). This is a rapid depletion of the *trans* isomers whose molecular main axis is parallel to the laser polarization direction as they are selectively photoisomerized.[185-188] Indeed, this fast photoconversion is dependent on the probability of the laser absorption by the *trans* conformers. This is proportional to the cosine squared of the angle between the direction of the polarized laser light and the azo electronic transition dipole moment vector. Thus, there is a greater absorption possibility for the molecules parallel to the direction of the incident polarized laser, leading to an apparent orientation by angular selective depletion. Therefore, the steep drop in the $<P_2>$ values of azoOH band during the first few seconds of irradiation followed by a quasi-plateau strongly suggests that the photo-orientation of azoOH/P4VP is dominated by the fast AHB process. On the other hand, the slow orientation process that follows the rapid AHB is governed by a mechanism

named angular redistribution (AR). This is associated with multiple *trans-cis-trans* isomerization cycles that statistically reorients the main axis of the chromophore and culminates in the accumulation of the *trans* azo molecules in the direction perpendicular to the laser polarization.[140,185,188-190] In fact, at first, the *cis* states become populated during the rapid AHB until a photostationary state is reached, then they isomerize back to the stable *trans* forms at the same rate as the *trans-cis* reaction. This is indicative of efficient *trans-cis-trans* isomerization cycling. Contrary to the azoOH/P4VP complexes, the behavior of MO/P4VPMe complexes at long irradiation times implies that the slow AR process of *trans* isomers towards the perpendicular direction to the polarized light is important in the photo-orientation of i-bonded complexes.

In addition to the considerable differences in the shape of the photo-orientation curve of the two types of azo complexes, the absolute value of $<P_2>_{max}$ for i-bonded complexes is about three times larger than that of H-bonded complexes (0.14 ± 0.01 vs. 0.047 ± 0.005). This difference, which appears to be a consequence of the presence or absence of the AR process, respectively, can be attributed not only to the difference in the nature of the supramolecular bonds giving rise to the relatively different material properties but more importantly to the different azo-azo interactions. On the one hand, an ionic bond is the strongest non-covalent supramolecular interaction whose strength reaches that of a covalent bond.[16] On the other hand, the interactions between MO–MO are much stronger than those between azoOH–azoOH. Besides, Xiao et al.[95] and Zhang et al.[23,173] demonstrated that ionic bonding between MO and alkylated (ethylated or methylated) P4VP results in the formation of a liquid crystalline smectic A mesophase. They reported high photoinduced birefringence values up to 0.2 for the ionic complexes between MO and P4VPMe. This property was attributed to the ionic nature of the interaction and liquid crystalline order of these ionically bonded azocomplexes. However, hydrogen bonding between the phenol group of azoOH and P4VP results in an amorphous structure.[168,171] Vapaavuori et al.[171] have studied the birefringence of the azocomplex of P4VP with azoOH at different chromophore concentrations and concluded that with an equimolar ratio, as for the complexes prepared here, the azoOH/P4VP complex reaches a lower birefringence value than similar azocomplexes in which the dimethyl amino tail group is replaced by a cyano group. This was attributed to liquid-crystalline order at high degrees of complexation with CN-tailed azo. Moreover, this different behavior for complexes with different tail groups can be also ascribed to differences in the dipole moment, where the higher dipole azo (cyano-tailed azo with a dipole moment of 6.8 D)[140] is capable of

undergoing AR, while the lower dipole azo (dimethyl amino-tailed azo with a dipole moment of 3.8 D) essentially orients only by AHB at 100% complexation. These results are consistent with our observations of lower $<P_2>$ values for the amorphous H-bonded complexes in comparison with the liquid crystalline structure and mesomorphic behavior of i-bonded complexes. On the other hand, this difference can be also partially explained by ionic polymers having a tendency to adopt a more extended main-chain conformation than their corresponding neutral polymers due to the repulsion between similarly charged repeat units of the polymer.[16]

After irradiation, orientation relaxation begins rapidly during the first few seconds until reaching a quasi-plateau for both azopolymers. However, the full recovery of $<P_2>$ to pre-irradiated initial values is not obtained after 1700 s relaxation time. This shows that the photoinduced anisotropy can be preserved in both complexes after turning off the laser but not completely. Thus, at the end of the measurement, the residual orientation ($<P_2>_{res}$) observed is evidence of the resistance of the materials to thermally induced motion.[42,140,170,191] The percentage of residual orientation, that is the percentage ratio of residual orientation $<P_2>_{res}$ after 1700 s of thermal relaxation to the $<P_2>_{max}$, listed in Table 3.1, is significantly higher for MO/P4VPMe than for azoOH/P4VP for any given molecular weight. This indicates that i-bonded complexes are more efficient in preserving the photoinduced orientation than the H-bonded complexes. This result is in line with the earlier conclusion about the predominance of AHB in the photo-orientation stage of azoOH/P4VP and balanced contributions of AHB and AR to the $<P_2>_{max}$ of MO/P4VPMe. Vapaavuori and colleagues[171] reported that around 50% of the photoinduced birefringence disappeared after illumination for their amorphous complexes, while their liquid crystalline complexes did not show birefringence relaxation. The percentages of residual orientation ($<P_2>_{res}$) of the complexes under consideration here are in a good agreement with their findings.

Although there is no effect of polymer molecular weight on $<P_2>_{res}$ for H-bonded complexes, as shown in Figure 3.6 and Table 3.1, there is a decrease in the residual orientation for i-bonded complexes of higher molecular weight. This behavior is counterintuitive based on the higher T_g and viscosity of high MW polymers. It is nonetheless, consistent with the difference that appears in the photo-orientation process, where the orientation of the 5k i-bonded sample continues to grow at long irradiation times without saturating. We attribute this difference to AR that is more

efficient for the ionic 5k complex, which in turn, leads to a higher proportion of the orientation that resists relaxation and culminates in higher residual orientation.

Furthermore, comparing the percentage of $\langle P_2 \rangle_{res}$ of azoOH/P4VP 200k (dimethyl amino-tailed azo) with H-bonded complexes of the same MW and with different azo tail groups that were studied previously in our group[140] shows that changing the tail group from hydrogen to either dimethyl amino or cyano promotes stronger interactions as well as higher photo-orientation. The increase in dipole moment also induces a greater proportion of angular redistribution (AR vs. AHB) of the chromophores. This in turn leads to greater residual orientation of 10, 54 and 80%, respectively. This comparison can be expanded to the H-bonded and i-bonded complexes under study where stronger MO–MO interactions in MO/P4VPMe complexes than azoOH–azoOH interactions in azoOH/P4VP complexes lead to higher photo-orientation, higher contribution of AR, and finally higher percentage of $\langle P_2 \rangle_{res}$.

Since the kinetics of the photo-orientation and thermal relaxation processes of the H-bonded and i-bonded complexes are different, they were fitted with biexponential functions involving fast and slow modes. These are shown in Equations 3.5 and 3.6, respectively:[118,140,192,193]

$$\langle P_2 \rangle = A\left[1 - e^{\left(-\frac{t}{\tau_a}\right)}\right] + B\left[1 - e^{\left(-\frac{t}{\tau_b}\right)}\right] \quad 3.5$$

In Equation 3.5, the parameters A and B represent the contributions of the fast (AHB) and slow (AR) modes in the photo-orientation process with time constants τ_a and τ_b, respectively. Indeed, AHB can be analyzed by A and τ_a (or 1/ k_a) in Equation 3.5, where k_a depends on the *trans-cis-trans* isomerization rates, the quantum yield for photoinduced *trans-cis* and *cis-trans*, and the local mobility of the azo moiety.[118,186] The azo mobility is controlled by the azo size, the local free volume around the azo, the glass transition temperature of the matrix, and the strength of the bonding interaction between the azo molecules and the polymer host.[118,186] Quantifying AR can be done by B and τ_b (or 1/ k_b) in Equation 3.5, where k_b depends on the interaction type between the azo and the polymer backbone and the mobility of the polymer segments.[118]

$$\langle P_2 \rangle = Ce^{\left(-\frac{t}{\tau_c}\right)} + De^{\left(-\frac{t}{\tau_d}\right)} + E \quad 3.6$$

In Equation 3.6, τ_c and τ_d are the time constants of the fast and slow modes of thermal relaxation, respectively, *C* and *D* are the contributions to the thermal relaxation process, and *E* represents the residual orientation remaining after infinite time. For convenience, the fits were performed, using OriginPro 2015, on the absolute values of the orientation parameters ($<P_2>$ values were multiplied by -1).

Examples of the curve fitting for the growth and loss of orientation of selected azo bands for both complexes are illustrated in Figure 3.7. Figures 3.7a and 3.7b show an acceptable agreement (Adj. R^2 = 89 and 99.5% for photo-orientation and 89 and 79% for thermal relaxation of H-bonded and i-bonded complexes, respectively) between the experimental data and fitted data for both processes. The relative contributions of AHB and AR processes in the photo-orientation of the azo band in either series of complexes are shown in Table 3.2.

Table 3.2 supports our previous scenario, based on qualitative observations, about the predominance of AHB process in the photo-orientation stage of azoOH/P4VP. Approximately 12% weighted contribution is from the slow AR component in the orientation of H-bonded complexes, and it is independent of the molecular weight of the host polymer. The AHB process occurs on a timescale on the order of a few seconds (from 2 to 8 s) for all molecular weights. The characteristic time for AR could not be determined with confidence because of its very small contribution to photo-orientation of the H-bonded complexes. These results are consistent with previous observations for another amorphous H-bonded complex.[140] In strong contrast, the important contribution of AR in the orientation process of MO/P4VPMe is supported by an almost 58% weighted contribution of the slow process. In contrast to the H-bonded complexes, the importance of AR is raised by decreasing the molecular weight of the polymer with B becoming more important for 5k > 50k > 200k. These results are consistent with the difference observed in residual orientation where orientation stability was found to decrease with higher molecular weight. The characteristic times for AHB are very similar to those found for azoOH.

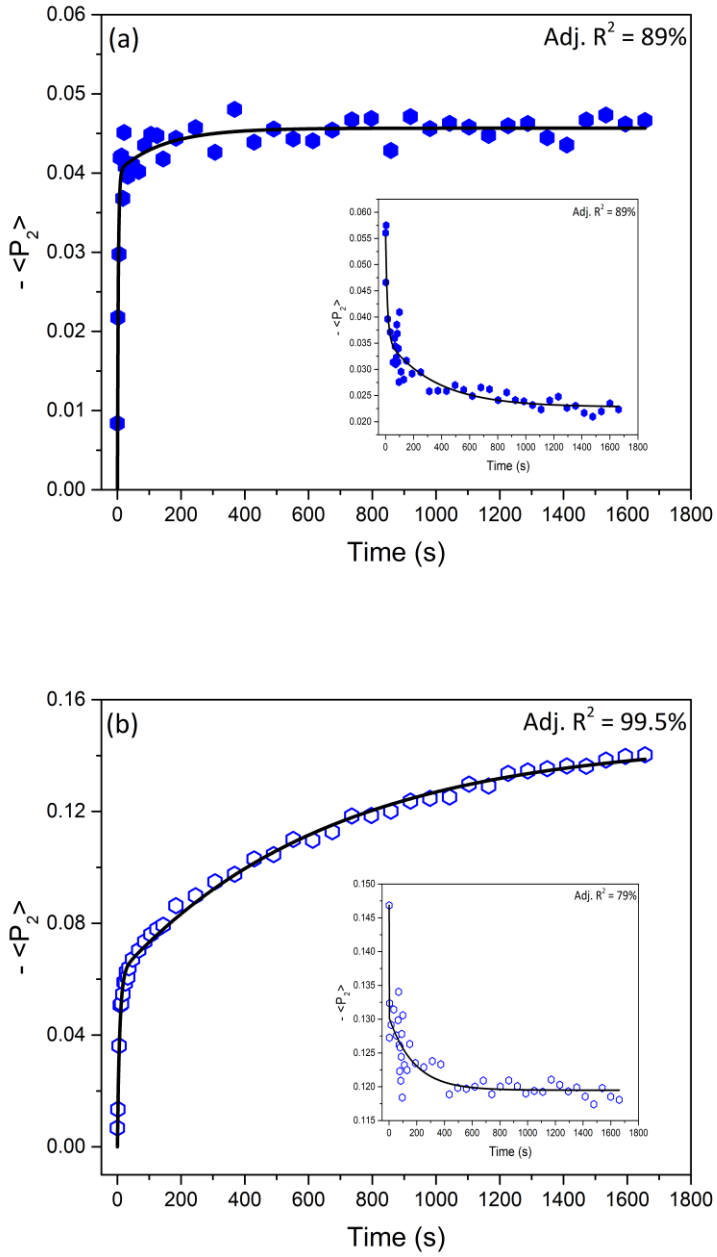

Figure 3.7. Growth of orientation of (a) 1363 cm^{-1} azoOH band of H-bonded 50k complex and (b) 1365 cm^{-1} MO band of i-bonded 50k complex during 1700 s photo-orientation. The insets show the loss of orientation during 1700 s of thermal relaxation. Solid lines are fits to the biexponential functions (Equations 3.5 and 3.6). The $<P_2>$ values were multiplied by -1.

Table 3.2. Parameters obtained by fitting the photo-orientation growth of selected azo bands of H-bonded and i-bonded complexes in Equation 3.5.

	MW (g/mol)	τ_a (s)	τ_b (s)	A_n (%)*	B_n (%)*
azoOH/P4VP	5k	2	167	87	13
	50k	3	145	88	12
	200k	8	472	88	12
MO/P4VPMe	5k	8	1097	31	69
	50k	7	664	42	58
	200k	3	618	51	49

* $A_n = \frac{A}{A+B} \times 100$ and $B_n = \frac{B}{A+B} \times 100$

In addition to the two above-mentioned phenomena, a third mechanism labeled rotational diffusion (RD) has also an effect on the reorientation of azo moieties. RD is a mechanism due to thermal diffusion of the ground state molecules that tends to order and restore the isotropic thermodynamic equilibrium.[185,186] On the other hand, the azo molecules can undergo rotational diffusion because of the local free volume provided around the chromophores by each light-induced isomerization step.[194,195] These diffusion motions are due to, at least partly, the lateral azo-azo interactions as well as the internal molecular motions, such as rotation, bending, and bond torsion of both trans and cis isomers.[140,196-198]

Similar to the photo-orientation process, the kinetics of the thermal relaxation involves an initial fast decay mode followed by a slower decay. The fast decay, with contribution C and rate constant τ_c (or $1/k_c$), is associated to thermal cis to trans back isomerization and thermally activated dipole reorientation in order to randomize the anisotropy. The slow decay having contribution D and rate constant τ_d (or $1/k_d$) has been ascribed to slower dipole reorientation involving motions of the polymer matrix as well as rotational diffusion of *trans* isomers.[118,192] Thus, the decrease in the orientation is most likely associated with both thermal relaxation and angular reorientation of some azobenzene groups.[170]

To investigate the orientation of polymer host in the H-bonded complexes, we followed the behavior of the well-isolated 1418 and 1008 cm^{-1} P4VP bands. No clear orientation could be measured in the PM-IRSAS spectra. To validate this, static polarized FT-IR spectra were measured in situ with azoOH/P4VP 50k complex irradiated for 1000 s. No significant orientation is observable for the P4VP side chain in Figure 3.8a. This behavior means that the orientation of the azoOH cannot be translated to orientation of the large passive polymer backbone through supramolecular interaction.[89,172] This result can be ascribed to the predominance of AHB in the orientation of azoOH. This observation is in line with our previous study,[140] which showed that efficient AR is a prerequisite for efficient orientation of the photopassive polymer.

Likewise, the 1643 cm^{-1} P4VPMe band was used to study the polymer orientation in the i-bonded complexes. Again, there is no indication of polymer orientation in the PM-IRSAS spectra (not shown) and in the ΔA spectrum of the MO/P4VPMe 50k complex measured by static polarized FT-IR under irradiation (Figure 3.8b). This is in spite of the occurrence of AR for this complex. This discrepancy can be understood by keeping in mind that ionic bonds are non-directional in nature. Therefore, they probably cannot transfer the orientation of MO to the photopassive pyridinium. As a conclusion, the azobenzene photoisomerization is neither capable of inducing orientation of the polymer main chain nor reorienting the pyridines in any of the azocomplexes. In fact, the polymer IR bands are contaminated by azo bands. Since the azo orientation is much larger than the polymer orientation, it creates an apparent polymer orientation.

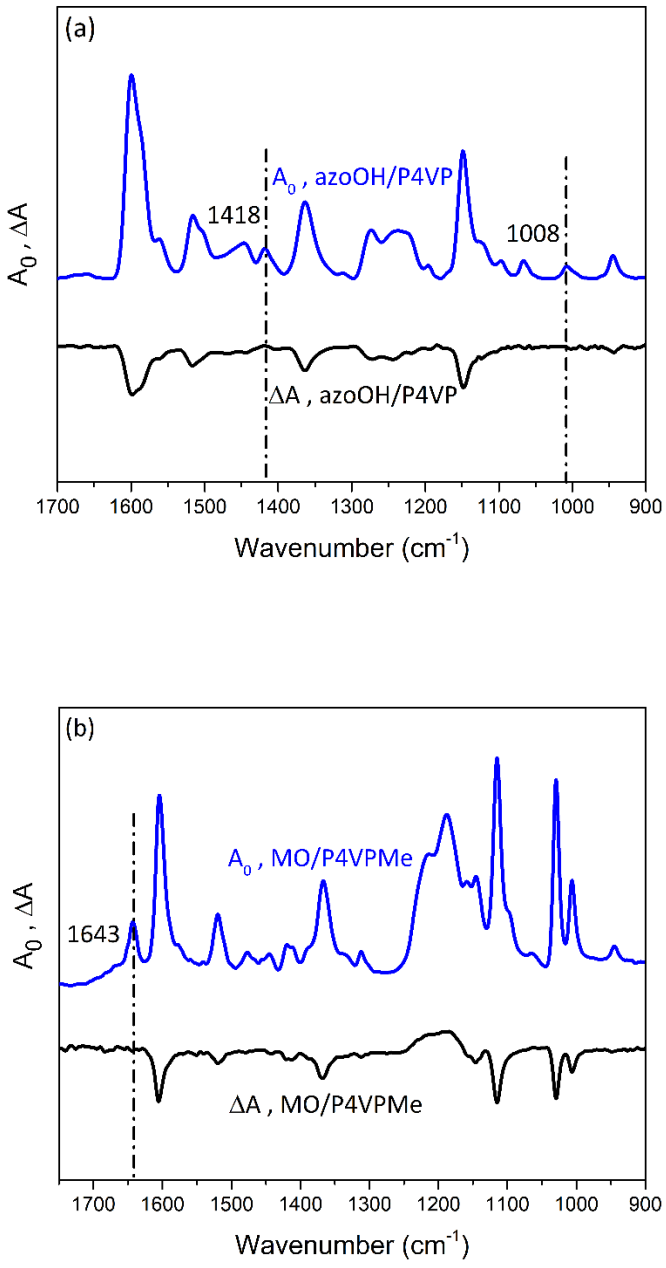

Figure 3.8. Static IR structural absorbance spectra (A_0) and dichroic difference spectra (ΔA) under irradiation of (a) azoOH/P4VP 50k complex and (b) MO/P4VPMe 50k complex. The dichroic difference spectrum in panel (a) is multiplied by 2 for clarity.

3.3. Surface relief grating formation

SRG inscription was conducted to study the photoinduced macroscopic-scale mass transport upon illumination by a sufficiently intense interference pattern of polarized beams. From the literature,[49,171,191] we know that molecular-scale photo-orientation, as probed by PM-IRSAS, and SRG diffraction efficiency (DE) are interconnected. However, they are not directly proportional because they involve different mechanisms. Experimental[199] and computational[200] studies shed some light on the massive mass transport mechanism underlying SRG formation below the glass transition temperature. Nevertheless, as discussed in Section 1.6 of Chapter 1, the fundamental mechanism controlling this complex phenomenon is not completely understood.

In this study, an interference pattern of circularly polarized 488-nm light with different intensities (100, 200, and 400 mW/cm^2) is used for SRG inscription. A direct comparison between the SRG inscription efficiency of the azocomplexes can be obtained from the first-order diffraction efficiency (DE). This is expressed as the percentage of the power of the first-order diffracted signal that is measured during 1000 s SRG inscription (laser on) relative to the power of the zeroth order signal during 60 s after SRG formation (laser off). Figure 3.9a presents the DE values as a function of time, while the samples are illuminated with a light of intensity of 200 mW/cm^2 for both H-bonded and i-bonded complexes (5k, 50k and 200k). The DE plots show that not only is there a difference between the SRG formation efficiency and inscription kinetics for the H-bonded and i-bonded complexes, but also that the SRG inscription is highly dependent on the polymer molecular weight. The ionically bonded complexes have much greater DE values after 1000 s of illumination than the H-bonded complexes. This is especially the case for lower molecular weight polymer. This demonstrates their higher performance to inscribe SRG patterns. Moreover, the DE values of three H-bonded complexes increase almost linearly during 1000 s laser irradiation without tending towards saturation up to the end of the measurement timescale. Meanwhile, there is an approximately linear growth in DE values of the i-bonded complexes during the first half of the irradiation time followed by a plateau indicating saturation. This difference can be related to the different interaction type and bond strength in the H-bonded and the i-bonded complexes as well as to the amorphous[168,171] and the liquid crystalline structures[23,173] of the hydrogen bonded and the ionically bonded complexes, respectively.

The results are all consistent with the results reported by Zhang et al.,[23,173] and Vapaavuori and colleagues[171] who independently studied the efficiency of SRG inscription on a library of i-bonded and H-bonded complexes of only one MW polymer using lower laser irradiance (65 mW/cm^2) and higher laser irradiance (300 mW/cm^2), respectively. They concluded that in the H-bonded series, the amorphous complexes are superior in SRG inscription efficiency, while in i-bonded series, the more rigid the complex, the more efficient the SRG formation. Following their studies, Wang and colleagues[86] compared the SRG formation efficiency, using a 488-nm laser with an irradiance of 190 mW/cm^2, between the analogous H-bonded and i-bonded complexes of azoOH and MO with poly(dimethylaminoethyl methacrylate) (PDM) and quaternized PDM (PDMQ), respectively. They found that the ionically bonded complexes lead to greater SRG formation efficiency than their H-bonded counterparts.

Figure 3.9a indicates that irradiation of the spin-coated azocomplex films with high intensity circularly polarized 488-nm light produces initial and rapid reversible volume birefringence gratings, reaching maximum efficiency about ~0.2% and ~1% in a few seconds for H-bonded and i-bonded complexes, respectively. These volume gratings resemble the photo-orientation produced by low intensity linearly polarized 488-nm beam used in PM-IRSAS. Consequently, the diffraction efficiency emerging from a volume grating is higher for i-bonded complex than for H-bonded complex. After the initial step, the growth of the birefringence volume gratings is overshadowed by mass transport of the polymer chains, resulting in surface relief gratings. This leads to a decrease in the rate of DE increase, suggesting that the transient and permanent gratings do not diffract in phase. This is consistent with the rise in DE after illumination. The different kinetics of SRG inscription for H-bonded and i-bonded complexes could be ascribed to different contributions of AHB and AR processes in this photoinduced phenomenon. Although AHB contributes greater than AR to the photoresponse of the H-bonded complexes, angular redistribution is not completely nil. The latter leads to very slow kinetics of DE inscription and it does not saturate over the 1000 s experiment. It seems that the DE of the H-bonded complexes could potentially match the i-bonded complexes with extended illumination. However, the AR culminates in greater DE and faster inscription kinetics for the ionic 5k complex compared to the higher MW complexes. This can be assigned to its more efficient AR process that is observed by PM-IRSAS. We thus conclude the rate of DE inscription is related to the AR efficiency.

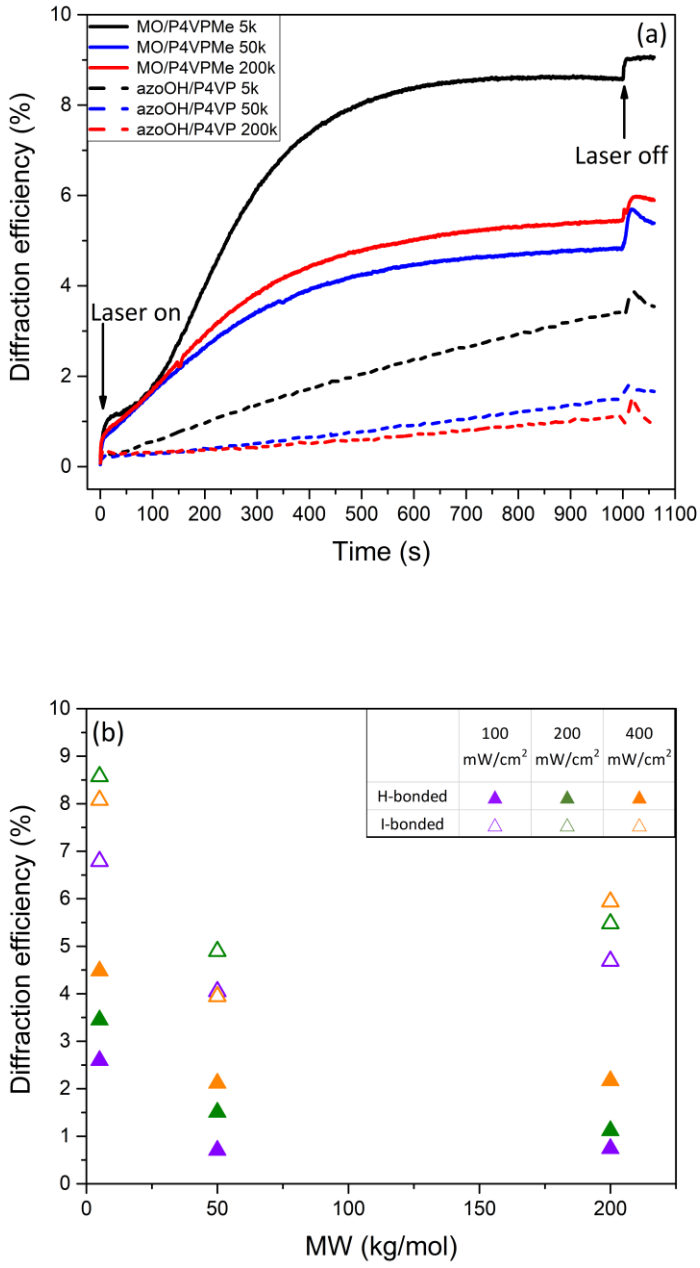

Figure 3.9. (a) Evolution of surface relief gratings formation as a function of illumination time for H-bonded and i-bonded complexes of different molecular weights (irradiance of 200 mW/cm^2), (b) DE of the azocomplexes at t =1,000 s as a function of polymer MW and laser irradiance.

Upon turning the laser off after 1000 s of irradiation, the DE value can either increase or decrease for either series of complexes (Figure 3.9a). This abrupt change in DE could be explained

by a phase difference between the transient volume gratings and the surface relief gratings, an increase in DE being observed when the two types of gratings are out of phase.[201] Thus, for quantitative comparison of the temporal stability of the gratings, the residual diffraction efficiency (DE_{res}), expressed as the percentage of the DE value recorded 60 s after irradiation with respect to maximum of DE at 1000 s, was calculated. This value can be used as an indication of the relative importance of the transient and permanent gratings.[202] Indeed, the transient gratings disappear as soon as the laser is turned off. DE_{res} is therefore indicative of the permanent relief grating. Interestingly, all azocomplexes show an increase in DE after illumination with a residual DE_{res} of 106% - 111% (Table 3.3). We attribute this increase to changes in the refractive index caused by thermal *cis-trans* isomerization. Then we can conclude that all the gratings are stable.

Table 3.3. The percentage of the residual diffraction efficiency of all azocomplexes.

	DE_{res} (%)	
	azoOH/P4VP	**MO/P4VPMe**
5k	109 ± 1	106 ± 2
50k	111 ± 2	111 ± 6
200k	108 ± 1	108 ± 4

Since the efficiency of SRG inscription is dependent on the bulk properties of polymer matrix and the laser irradiance, we also studied the role of the polymer molecular weight and the laser irradiance on the grating inscription process. Figure 3.9b, shows the DE values for all complexes after irradiation (1000 s) as a function of polymer MW for different laser intensities (100, 200, and 400 mW/cm^2). The plot confirms that the mass migration decreases sharply with increasing the polymer MW, in particular when comparing the 5k complexes with either the 50k or 200k complexes (the differences between the two high MW complexes are not statistically significant). This effect could be due either to the increase in T_g with MW of the polymer host or to the increase in polymer chain entanglements that hinders polymer motion.[49,86,203] Although the evaluated polymers cover a large MW range from unentangled (5k) to highly entangled (200k), the T_g's of the pure P4VP samples measured by DSC only vary from 130 °C to 150 °C between low and high MW polymers. While we could not determine the T_g of the complexes by DSC, it was possible to use temperature-controlled infrared spectroscopy to determine the spectroscopic

glass transition temperatures for the three H-bonded azocomplexes. Consistent with the small difference observed for the pure P4VP samples, the H-bonded complexes under study do not show large differences in T_g between the complexes of low and high MW (from 69 ℃ to 81 ℃ for complexes of low to high MW). We can therefore conclude that polymer entanglement density plays a more important role in SRG inscription efficiency than the T_g of azopolymers. This phenomenon involves in the large-scale material motion and it can be hindered by a high polymer entanglement density. Thus, the highest-efficiency grating is inscribed on a film with the lowest polymer MW. This result is in line with the previous studies done by Barrett et al.,[203] Börger et al.,[169] and Priimagi et al.[82] They studied complexes made from different chromophores and polymer hosts and they showed that increasing the MW of the polymer host reduces the inscription rate and culminates in a lower modulation depth of the gratings.[204] In contrast, it appears that molecular-level orientation, a local motion studied by IR spectroscopy, is much less affected by the entanglement density (see Figure 3.6). Our group previously showed with a series of well-controlled mixtures of photoactive molecular glasses that the maximum orientation under irradiation rises strongly with T_g. But it decreases when it becomes too high because of excessive viscosity of the surrounding matrix. The saturated level of orientation was correlated with the rate at which SRG could be inscribed, but not their saturated DE. The results obtained suggest that the AHB process is weakly affected by either the T_g or entanglement density, while the AR process is more sensitive to molecular weight. This is possibly because it involves larger scale motions (although at still much smaller scale than the macroscopic transport during SRG writing), making it susceptible to the degree of entanglement. This reinforces the conclusion that optimizing the AR process is required for efficient kinetics of photoinduced mass transport.

Finally, Figure 3.10a shows that increasing the light irradiance increases DE values for all H-bonded complexes, while a similar rise can only be seen for i-bonded when going from 100 to 200 mW/cm^2. This is due to the fact that the H-bonded complexes never reach saturated DE within 1000 s of illumination for this range of irradiance. The increase in SRG inscription speed converts into larger DE values. In contrast, the DE curves of the i-bonded complexes are saturated at 200 mW/cm^2. A further increase does not increase the saturated DE. In fact, a small decrease at 400 mW/cm^2 could be the consequence of sample heating. We also determined the DE of ionic complexes at t = 300 s (Figure 3.10b), which is the time immediately before reaching saturation at 200 mW/cm^2. This was to correlate the speed at which complexes reach saturation with different

laser irradiance. The results show that increasing irradiance allows reaching saturation faster but not to further improve saturated DE. Then, we can conclude that the 2-fold increase in the laser intensity brings about a higher DE for both azocomplexes. This is consistent with the results obtained by Wang et al.[86]

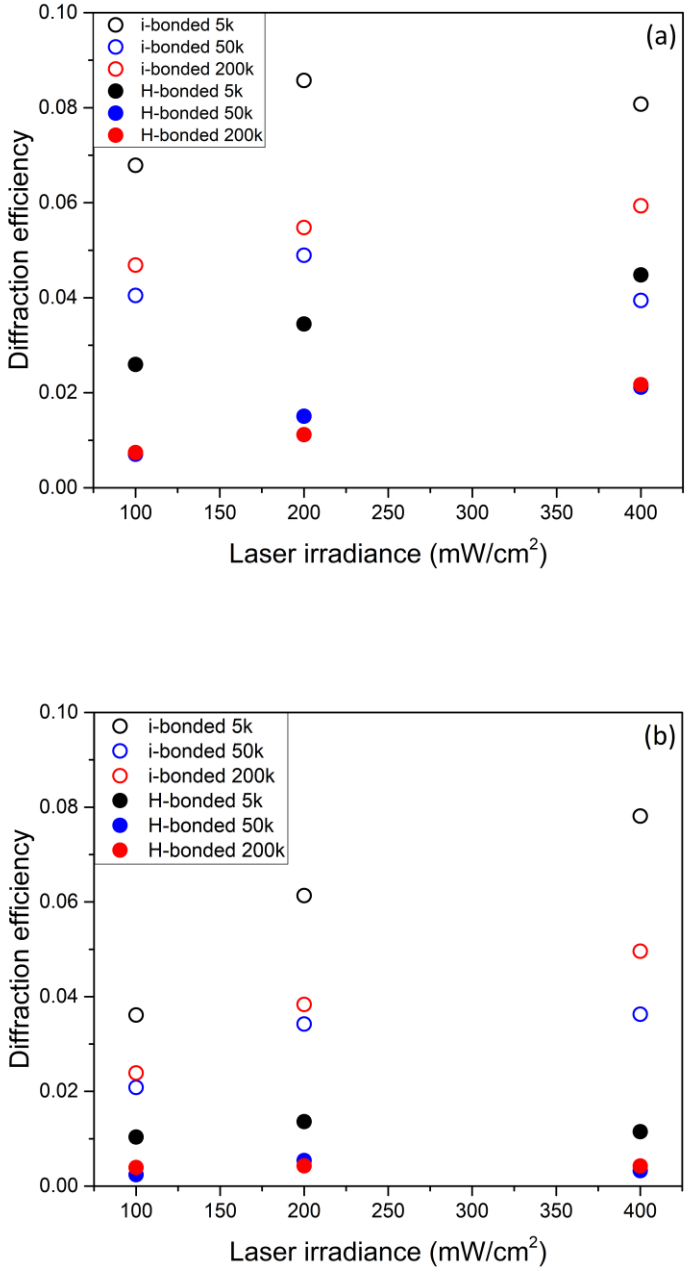

Figure 3.10. The DE of all azocomplexes (a) at t =1,000 s and (b) at t = 300 s as a function of laser irradiance.

These results suggest that a compromise between polymer MW and light irradiance, regardless of the T_g of the azocomplex, enables optimizing the SRG inscription efficiency. Although the compounds that cannot orient do not show a good SRG efficiency, the materials capable of orientation, such as the H-bonded complexes studied, do not necessarily lead to high DE values. This may be because of the inefficiency of the polymer matrix to take advantage of the *trans-cis-trans* isomerization cycles.

Chapter 4: Conclusions and Future Work

3.1. Conclusions

The work presented in this thesis dealt with supramolecular azobenzene-containing complexes and their important light-induced properties. We conducted a comparative study of molecular photoalignment and macroscopic motion as a function of both supramolecular interaction type and polymer molecular weight for two different series of supramolecular azopolymers. In our study, the small-molecule azo derivative binds non-covalently to the polymer, poly(4-vinylpyridine) (P4VP). On the one hand, the photo-orientation and orientation relaxation of hydrogen-bonded (H-bonded) complexes, prepared through complexation between the hydroxyl group of the small molecule and the P4VP, and ionically-bonded (i-bonded) complexes, obtained by an ionic interaction between quaternized P4VP (P4VPMe) and the sulfonate group of the azo molecule, illuminated with linearly polarized 488-nm laser, were investigated using polarization modulation structural absorbance spectroscopy (PM-IRSAS), in order to study the effect of the targeted variables on the photoinduced molecular orientation ($<P_2>$). On the other hand, the formation of surface relief gratings (SRG) of H-bonded and i-bonded azocomplexes with an interference pattern of circularly polarized 488-nm light was investigated to determine the diffraction efficiency (DE) during SRG inscription, to assess the extent of macroscopic mass transport.

We used the H-bonded complexes to extend our knowledge regarding the effect of the tail group on the photoinduced properties of equimolar H-bonded complexes by comparing our results with those obtained by Wang et al.[140] and Vapaavuori et al.[78] who used different tail groups (CN and H) with different azo content. Vapaavuori et al.[78] found that the saturated birefringence per azobenzene unit differs by increasing azobenzene content. It increases with increasing the content of CN-tailed azobenzene, while it decreases with increasing the content of H-tailed azobenzene. However, their studies were based on birefringence measurements, which reflect the overall orientation of all components in the system. Wang and co-workers[140] used PM-IRSAS for the same systems to investigate the orientation of each individual component. They found that the photo-orientation of both azocomplexes containing CN and H tails decreases with increasing the mole

percent of azobenzene molecules relative to the pyridine of P4VP with a higher photo-orientation for CN-tailed azocomplexes. They ascribed this behavior to the effect of lower free volume when the mole percent of azobenzene is high and concluded that this effect of free volume is present in both complexes, regardless of the structural difference between azobenzenes. On the other hand, the i-bonded complexes selected here to investigate the photosensitivity of azocomplexes is one of the spacer-free dye-polyelectrolyte ionic complexes used by Zhang et al.[23,24] to study the photoinduced birefringence. Our findings complement our knowledge about the impact of the ionic bond on the different photoinduced properties. Moreover, the selected photoactive azo molecules (azoOH vs. MO) for azocomplex formation in this thesis differed only in the head group that interacted non-covalently with the P4VP. Notably the neutral (hydroxyl) and charged (sulfonate) head group bonded to the polymer host through hydrogen and ionic interactions, respectively. These molecules were selected for their efficient *trans-cis-trans* photoisomerization with polarized light.

The photoisomerization of azo molecules in the spin-coated thin films of either series was confirmed using UV-visible spectroscopy coupled to the linearly polarized 488-nm light. Studying the UV-vis spectra under illumination showed that all the samples undergo reversible *trans-cis* isomerization at this wavelength with slightly different minimum *cis* content (14% vs. 20% for azoOH/P4VP and MO/P4VPMe, respectively). This emphasizes the fact that using light with a wavelength of 488 nm to orient the molecules is justified since the photoresponse and the absorbance of both azo molecules (azoOH vs. MO) before and immediately after 5-min illumination are relatively similar. Moreover, since the 488-nm laser can excite both *trans* and *cis* states of azobenzene derivatives, it can be used to inscribe SRGs on azo-containing polymer films. The absence of a shift in the absorption peak of thin films before irradiation and under irradiation means that no chromophore aggregation occurred in these equimolar complexes when irradiated.

FT-IR analyses proved the formation of hydrogen bonds between the pyridine of P4VP and the hydroxyl of the azoOH molecules, according to the shift of the free pyridine band from 993 cm^{-1} to 1008 cm^{-1}. Clear evidence of ionic bonding is difficult to obtain by FT-IR analysis, since the starting compounds are themselves ionic. However, the formation of ionic bonds between the MO molecules and P4VPMe was consistent with the ^{1}H NMR analysis of the complexes in DMSO-d_6 and the difference in their solvent solubility compared to the starting compounds.

Besides, the same preparation procedure was used as in previous work, where the absence of the starting counterions was confirmed by energy dispersive spectroscopic analysis along with confirmation of the stoichiometry by elemental analysis.[23]

The PM-IRSAS data showed that the azobenzene molecules orient more in i-bonded complexes than in H-bonded complexes; notably, the orientation function achieved during the photo-orientation stage ($<P_2>_{max}$) is about three times greater for the i-bonded complexes than for the H-bonded complexes. This difference can be accounted for by the different interaction type and the bond strength in two series of azocomplexes. In particular, the sulfonate-pyridinium ionic bond is significantly stronger than the OH-pyridine hydrogen bond. Moreover, the i-bonded complexes have smectic A liquid crystalline character, while the H-bonded complexes have amorphous non-liquid crystalline character. This implies that the MO–MO lateral interactions among the complexed side chains in the i-bonded complexes are much stronger than the azoOH–azoOH lateral interactions in the H-bonded complexes. This favors cooperative reorientation of the chromophores.

In addition to the different $<P_2>_{max}$ values, the photo-orientation and thermal relaxation kinetics in the two series of azocomplexes are different. In both cases, there is a rapid increase in orientation during the first few seconds of irradiation. This fast process is followed by a quasi-plateau for the H-bonded complexes, while the orientation continues to develop for the i-bonded complexes. This difference can be explained by the angular hole burning (AHB) and angular redistribution (AR) phenomena. The photo-orientation in the H-bonded complexes is dominated by the AHB of the *trans* isomers due to *trans-cis* photoisomerization. This is assigned to the fast orientation component of the biexponential model. The slow orientation mode is assigned to AR. This is associated with multiple *trans-cis-trans* isomerization cycles, and it contributes more to the photo-orientation of the i-bonded complexes. Furthermore, after illumination and initiation of orientation relaxation, the optical anisotropy decreases to different extents in the two series without reaching the initial pre-irradiation $<P_2>$ values for either. Notably, at the end of the measurement, the percent residual orientation ($<P_2>_{res}$) is higher for MO/P4VPMe than for azoOH/P4VP, at 86% vs. 49% on average, respectively.

The results also indicate that while both azo molecules orient under polarized illumination, the P4VP does not, contrary to what was observed by Wang et al.[140] This is based on the bands of

the polymer side chain that show no clear evidence of orientation. The movements causing orientation of the azo molecules are therefore not transmitted to the polymer backbone by supramolecular interactions in the systems studied here. However, changing the tail group from dimethyl amino to cyano in analogous H-bonded complexes induces P4VP pyridine orientation.[140] This can be ascribed to the different dipole moment of the azos. A high dipole azo capable of undergoing AR appears to be a prerequisite for the efficient orientation of the photopassive polymer. Conversely, lower dipole azos (dimethyl amino-tailed azo or H-tailed azo) essentially only show AHB.[140]

The deformation of the film surface due to macroscopic mass transport of the polymer chains was tracked by the first-order diffraction efficiency (DE) during 1000 s of SRG inscription (laser on). This was to compare the surface relief grating formation efficiency in the two series of the azobenzene-polymer complexes. We found that the i-bonded complexes have higher SRG performance than the H-bonded complexes, especially for lower molecular weight hosts. This higher SRG performance of the i-bonded complexes is in line with their greater molecular photo-orientation ($<P_2>$), measured by PM-IRSAS. Moreover, the kinetics controlling the SRG inscription are different for the two series. I-bonded complexes reach a plateau as an indication of saturation after an initial increase in DE values during the measurement timescale. In H-bonded complexes, the DE values increase monotonically during the 1000-s laser irradiation without tending towards saturation. Irradiation of the spin-coated azocomplex films with circularly polarized 488-nm light produces the rapid inscription of a reversible volume birefringence grating. This resembles the photo-orientation process in PM-IRSAS that reaches an efficiency of about ~0.2% and ~1% in a few seconds for H-bonded and i-bonded complexes, respectively. The phase grating can be connected to the AHB process. After that, the growth of the diffraction efficiency is dominated by mass transport of the polymer chains resulting in surface relief gratings, which is assigned to the AR phenomenon.

The residual DE depends on the relative importance and phase relationship between the transient volume phase grating and the permanent surface relief grating. Despite different $<P_2>_{res}$ for both series of complexes, the percentage of DE_{res} for both series is similar. In fact, all azocomplexes show an increase in DE and a residual DE of around 110% after irradiation. This is

a sign of temporal stability of the SRG and out-of-phase diffraction by the different types of gratings.

In addition to the effect of the interaction type on the SRG efficiency of these complexes, the laser power also plays a role. We studied this effect by exposing the azopolymer films to circularly polarized light with different irradiances ranging from 100 to 400 mW/cm^2. The results indicate that although there is a linear correlation between the laser irradiance and the DE values in H-bonded complexes, the DE values decrease above a threshold of around 200 mW/cm^2 for the i-bonded complexes. This can be ascribed to the fact that the DE reaches a saturated level that decreases at higher irradiance due to sample heating.

Another objective of this project was to investigate the impact of the molecular weight of the polymer host on the photosensitivity of the H-bonded and i-bonded complexes. We found that although polymer molecular weight does not have a significant impact on molecular photo-orientation in terms of $<P_2>_{max}$, which was contrary to our initial expectations, there is a decrease in residual orientation ($<P_2>_{res}$) of only the i-bonded complexes for higher molecular weight. However, the molecular weight has a substantial effect on the SRG inscription efficiency, it decreases with molecular weight in both azocomplexes. This indicates that mass migration during SRG formation decreases sharply with increase in the polymer molecular weight. This can be rationalized by polymer chain entanglement that hinders polymer motion. In spite of the large range of molecular weight from unentangled (5k) to highly entangled (200k) systems, small differences in the T_g's of the pure P4VP (130 ℃ - 150 ℃) were observed. This indicates that entanglement density is more important than the T_g in these complexes. In addition, the three H-bonded complexes do not show large differences in their glass transition temperatures (69, 73, and 81 ℃ for 5k, 50k and 200k, respectively). Polymer entanglement is therefore more important to SRG inscription efficiency by large-scale material motion than the T_g of the azocomplexes. Thus, the highest-efficiency grating is inscribed on a film with the lowest polymer molecular weight. This is valid within the range where the decrease in T_g is not detrimental to the SRG inscription process and temporal stability.

3.2. Future work

These fundamental findings contribute to understanding the effect of the nature and the strength of the supramolecular interaction as well as the effect of polymer molecular weight on the photoinduced motions (molecular and macroscopic) of azobenzene-containing polymers. This study has also contributed to finding the relationship between molecular-scale motions and the photoresponse of the material at larger scales as guidelines for designing efficient photoresponsive materials used in optical devices through supramolecular chemistry. This knowledge can be leveraged for developing more efficient materials for surface relief grating applications, such as designing grating waveguide couplers.

Since our study has found that the type and strength of the supramolecular interaction in the azobenzene-polymer complexes affect the photoinduced properties of these materials at both the molecular and macroscopic levels, it is of interest to extend these studies to other systems. These include other polymers (e.g. liquid crystalline-polymers with flexible spacers in the main chain or polymers with branched structures), azo molecules either with the same substituents at *ortho* positions or with other azo tails ($–NO_2$, $–NH_2$, –COOH, and –OR) at the *para* position, more complicated azos like bisazo instead of monoazo, and other bonding types like the halogen bond. Although there are a few publications regarding halogen-bonded complexes (X-bonded) between P4VP and halogenated azobenzene with the same tail group as used in our study,[79,91,172,205,206] these have uniquely dealt with the low-molecular-weight P4VP, ranging from 1000 to 5000. Thus, there is no comprehensive investigation, to the best of our knowledge, of the effect of high-molecular-weight P4VP on the photoresponsiveness of such X-bonded complexes for comparison with our results.

Moreover, a comparative study on the same systems with different degrees of complexation is of interest to investigate the impact of the azobenzene content on the light-induced properties and extend the understanding of different types of supramolecular interaction. Additionally, it is desirable to validate the effect of the rigidity of the backbone on the photoinduced properties of supramolecular complexes; for example, by choosing three different main-chain polymers with flexibilities ranging from very flexible to highly rigid, which is likely easiest to accomplish using H-bonds as the supramolecular bond. This is especially relevant since ionic bonding rigidifies the

polymer due to electrostatic repulsion. This may be the reason why the light response of ionically bonded complexes is stronger than hydrogen bonded complexes.

As mentioned in Chapter 3, the H-bonded systems used in our study are amorphous, while their analogous i-bonded materials have a liquid crystalline (LC) structure. Thus, it is not clear to what extent the differences between the two systems is a direct result of either the different supramolecular bond type/strength or the LC vs. non-LC character. Therefore, an important and direct follow-up must be to separate the LC effect from the type of supramolecular bond. This can be done by comparing two azos having the same tail, one that H-bonds and one that i-bonds, and that have the same LC/isotropic characters. For example, a CN-tailed azobenzene leads to a LC system for H-bonding at high degrees of complexation (greater than ~35%).[140] Synthesizing a MO analogue with a CN tail to obtain ionic complexes with the same LC structure (if possible) would allow determining more clearly the effect of the interaction type on the photoresponse of azocomplexes. Moreover, since the azocomplexes used in this study are spacer free, investigating the effect of the spacer on the photoinduced properties of these systems can be of interest.

In summary, supramolecular chemistry is a facile strategy to prepare a variety of azocomplexes for investigating the effect of different parameters, such as the role of chromophore-chromophore intermolecular interactions, flexible spacer groups, and the architecture of the host material on the photoinduced properties of such azobenzene-containing systems, and for a variety of applications in optics and photonics or even applications far beyond the scope seen up to now.

References

1. http://www.nobelprize.org/nobel_prizes/chemistry/laureates/1987/. (accessed August 2018).

2. Lehn, J.-M., Supramolecular Polymer Chemistry-Scope and Perspectives. *Polymer International* **2002,** *51*, 825.

3. Vapaavuori, J.; Bazuin, C. G.; Priimagi, A., Supramolecular Design Principles for Efficient Photoresponsive Polymer-Azobenzene Complexes. *Journal of Materials Chemistry C* **2018,** *6*, 2168.

4. Lehn, J. M., From Supramolecular Chemistry Towards Constitutional Dynamic Chemistry and Adaptive Chemistry. *Chemical Society Reviews* **2007,** *36*, 151.

5. Faul, C. F. J.; Antonietti, M., Ionic Self-Assembly: Facile Synthesis of Supramolecular Materials. *Advanced Materials* **2003,** *15*, 673.

6. Binder, W. H.; Zirbs, R., Supramolecular Polymers and Networks with Hydrogen Bonds in the Main- and Side-Chain. *Advances in Polymer Science* **2006,** *207*, 1.

7. Koskela, J. E. Light-Fuelled Motions in Azobenzene-Containing Materials. D*octoral Dissertation*, Aalto University, **2014**.

8. Pollino, J. M.; Weck, M., Non-Covalent Side-Chain Polymers: Design Principles, Functionalization Strategies, and Perspectives. *Chemical Society Reviews* **2005,** *34*, 193.

9. Weck, M., Side-Chain Functionalized Supramolecular Polymers. *Polymer International* **2007,** *56*, 453.

10. Priimagi, A.; Cattaneo, S.; Ras, R. H. A.; Valkama, S.; Ikkala, O.; Kauranen, M., Polymer-Dye Complexes: A Facile Method for High Doping Level and Aggregation Control of Dye Molecules. *Chemistry of Materials* **2005,** *17*, 5798.

11. Priimagi, A.; Kaivola, M.; Rodriguez, F. J.; Kauranen, M., Enhanced Photoinduced Birefringence in Polymer-Dye Complexes: Hydrogen Bonding Makes a Difference. *Applied Physics Letters* **2007,** *90*, 121103.

12. Zettsu, N.; Ogasawara, T.; Mizoshita, N.; Nagano, S.; Seki, T., Photo-Triggered Surface Relief Grating Formation in Supramolecular Liquid Crystalline Polymer Systems with Detachable Azobenzene Unit. *Advanced Materials* **2008,** *20*, 516.

13. Arunan, E.; Desiraju, G. R.; Klein, R. A.; Sadlej, J.; Scheiner, S.; Alkorta, I.; Clary, D. C.; Crabtree, R. H.; Dannenberg, J. J.; Hobza, P.; Kjaergaard, H. G.; Legon, A. C.; Mennucci, B.; Nesbitt, D. J., Defining the Hydrogen Bond: An Account (IUPAC Technical Report). *Pure and Applied Chemistry* **2011,** *83*, 1619.

14. Kato, T.; Mizoshita, N.; Kanie, K., Hydrogen-Bonded Liquid Crystalline Materials: Supramolecular Polymeric Assembly and the Induction of Dynamic Function. *Macromolecular Rapid Communications* **2001,** *22*, 797.

15. Kato, T.; Mizoshita, N.; Kishimoto, K., Functional Liquid-Crystalline Assemblies: Self-Organized Soft Materials. *Angewandte Chemie, International Edition in English* **2006,** *45*, 38.

16. Vapaavuori, J. Design of Efficient Photoresponsive Azobenzene Materials through Supramolecular Functionalization. D*octoral Dissertation*, Aalto University, **2013**.

17. Minkin, V. I., Glossary of Terms Used in Theoretical Organic Chemistry (IUPAC Recommendations 1999). *Pure and Applied Chemistry* **1999,** *71*, 1919.

18. Nieuwkerk, A. C.; Marcelis, A. T. M.; Koudijs, A.; Sudhölter, E. J. R., Ion Pair Amphiphiles from Sodium Dodecyl Sulfate and Ammonium Amphiphiles Carrying Functionalized Azobenzene Units. *Liebigs Annalen - Recueil* **1997,** *1997*, 1719.

19. Guan, Y.; Antonietti, M.; Faul, Ionic Self-Assembly of Dye-Surfactant Complexes: Influence of Tail Lengths and Dye Architecture on the Phase Morphology. *Langmuir* **2002,** *18*, 5939.

20. MacKnight, W. J.; Ponomarenko, E. A.; Tirrell, D. A., Self-Assembled Polyelectrolyte-Surfactant Complexes in Nonaqueous Solvents and in the Solid State. *Accounts of Chemical Research* **1998,** *31*, 781.

21. Zhou, S.; Chu, B., Assembled Materials: Polyelectrolyte-Surfactant Complexes. *Advanced Materials* **2000,** *12*, 545.

22. Lin, X.; Zhong, A.; Chen, D.; Zhou, Z.; He, B., Studies on Self-Assembly and Characterization of Polyelectrolytes and Organic Dyes. *Journal of Applied Polymer Science* **2003,** *87*, 369.

23. Zhang, Q.; Bazuin, C. G.; Barrett, C. J., Simple Spacer-Free Dye-Polyelectrolyte Ionic Complex: Side-Chain Liquid Crystal Order with High and Stable Photoinduced Birefringence. *Chemistry of Materials* **2008,** *20*, 29.

24. Zhang, Q.; Wang, X.; Barrett, C. J.; Bazuin, C. G., Spacer-Free Ionic Dye-Polyelectrolyte Complexes: Influence of Molecular Structure on Liquid Crystal Order and Photoinduced Motion. *Chemistry of Materials* **2009,** *21*, 3216.

25. Wang, G. J.; Engberts, J. B. F. N., Induction of Aggregate Formation of Cationic Polysoaps and Surfactants by Low Concentrations of Additives in Aqueous-Solution. *Langmuir* **1994,** *10*, 2583.

26. Abdallah, D.; Cully, M. J.; Li, Y.; Shipp, D. A., Stoichiometric Complexes of Polyelectrolyte and Azo-Functionalized Surfactant. *Colloid and Polymer Science* **2008,** *286*, 739.

27. Bazuin, C. G.; Tork, A., Generation of Liquid Crystalline Polymeric Materials from Non Liquid Crystalline Components Via Ionic Complexation. *Macromolecules* **1995,** *28*, 8877.

28. Tibirna, C. M.; Bazuin, C. G., Liquid Crystalline Complexes of an Azo-Containing Surfactomesogen with Oppositely Charged Polyelectrolytes. *Journal of Polymer Science Part B: Polymer Physics* **2005,** *43*, 3421.

29. Engelking, J.; Menzel, H., Monolayers of Complexes from Amphiphiles and Rigid Rod-Like Polyelectrolytes. *Thin Solid Films* **1998,** *327-329*, 90.

30. Panambur, G.; Robert, C.; Zhang, Y.; Bazuin, C. G.; Ritcey, A. M., Langmuir Monolayers of Polyion Complexes of Soluble Quaternary Ammonium-Functionalized Azobenzene Chromophores. *Langmuir* **2003,** *19*, 8859.

31. Panambur, G.; Zhang, Y.; Yesayan, A.; Galstian, T.; Bazuin, C. G.; Ritcey, A. M., Preparation and Characterization of Polyion-Complexed Langmuir-Blodgett Films Containing an NLO Chromophore. *Langmuir* **2004,** *20*, 3606.

32. Zucolotto, V.; Barbosa Neto, N. M.; Rodrigues, J. J.; Constantino, C. J. L.; Zílio, S. C.; Mendonça, C. R.; Aroca, R. F.; Oliveira, O. N., Photoinduced Phenomena in Layer-by-Layer Films of Poly(Allylamine Hydrochloride) and Brilliant Yellow Azodye. *Journal of Nanoscience and Nanotechnology* **2004,** *4*, 855.

33. Zucolotto, V.; He, J.-A.; Constantino, C. J. L.; Barbosa Neto, N. M.; Rodrigues, J. J.; Mendonça, C. R.; Zílio, S. C.; Li, L.; Aroca, R. F.; Oliveira, O. N.; Kumar, J., Mechanisms of Surface-Relief Gratings Formation in Layer-by-Layer Films from Azodyes. *Polymer* **2003,** *44*, 6129.

34. Kulikovska, O.; Goldenberg, L. M.; Stumpe, J., Supramolecular Azobenzene-Based Materials for Optical Generation of Microstructures. *Chemistry of Materials* **2007,** *19*, 3343.

35. Priimagi, A.; Cavallo, G.; Metrangolo, P.; Resnati, G., The Halogen Bond in the Design of Functional Supramolecular Materials: Recent Advances. *Accounts of Chemical Research* **2013,** *46*, 2686.

36. Metrangolo, P.; Meyer, F.; Pilati, T.; Resnati, G.; Terraneo, G., Halogen Bonding in Supramolecular Chemistry. *Angewandte Chemie, International Edition in English* **2008,** *47*, 6114.

37. Rissanen, K., Halogen Bonded Supramolecular Complexes and Networks. *CrystEngComm* **2008,** *10*, 1107.

38. Fourmigué, M., Halogen Bonding: Recent Advances. *Current Opinion in Solid State and Materials Science* **2009,** *13*, 36.

39. Politzer, P.; Murray, J. S., Halogen Bonding: An Interim Discussion. *ChemPhysChem* **2013,** *14*, 278.

40. Meyer, F.; Dubois, P., Halogen Bonding at Work: Recent Applications in Synthetic Chemistry and Materials Science. *CrystEngComm* **2013,** *15*, 3058.

41. Desiraju, G. R.; Ho, P. S.; Kloo, L.; Legon, A. C.; Marquardt, R.; Metrangolo, P.; Politzer, P.; Resnati, G.; Rissanen, K., Definition of the Halogen Bond (IUPAC Recommendations 2013). *Pure and Applied Chemistry* **2013,** *85*, 1711.

42. Heikkinen, I. The Impact of Supramolecular Bond Strength and Directionality in Orienting Passive Host Molecules. *Special Assignment Report*, Aalto University, **2014**.

43. Shields, Z. P.; Murray, J. S.; Politzer, P., Directional Tendencies of Halogen and Hydrogen Bonds. *International Journal of Quantum Chemistry* **2010,** *110*, 2823.

44. Politzer, P.; Murray, J. S.; Clark, T., Halogen Bonding: An Electrostatically-Driven Highly Directional Noncovalent Interaction. *Physical Chemistry Chemical Physics* **2010,** *12*, 7748.

45. Metrangolo, P.; Neukirch, H.; Pilati, T.; Resnati, G., Halogen Bonding Based Recognition Processes: A World Parallel to Hydrogen Bonding. *Accounts of Chemical Research* **2005,** *38*, 386.

46. Cavallo, G.; Metrangolo, P.; Milani, R.; Pilati, T.; Priimagi, A.; Resnati, G.; Terraneo, G., The Halogen Bond. *Chemical Reviews* **2016,** *116*, 2478.

47. Rau, H., Photoreactive Organic Thin Films. 1st ed.; *Elsevier Sci. Ltd.*: **2002**.

48. Priimagi, A. Polymer-Azobenzene Complexes: From Supramolecular Concepts to Efficient Photoresponsive Polymers. D*octoral Dissertation*, Helsinki University of Technology, **2009**.

49. Mahimwalla, Z.; Yager, K. G.; Mamiya, J.-i.; Shishido, A.; Priimagi, A.; Barrett, C. J., Azobenzene Photomechanics: Prospects and Potential Applications. *Polymer Bulletin* **2012,** *69*, 967.

50. Turansky, R.; Konopka, M.; Doltsinis, N. L.; Stich, I.; Marx, D., Switching of Functionalized Azobenzene Suspended between Gold Tips by Mechanochemical, Photochemical, and Opto-Mechanical Means. *Physical Chemistry Chemical Physics* **2010,** *12*, 13922.

51. Henzl, J.; Mehlhorn, M.; Gawronski, H.; Rieder, K. H.; Morgenstern, K., Reversible *Cis-Trans* Isomerization of a Single Azobenzene Molecule. *Angewandte Chemie, International Edition in English* **2006,** *45*, 603.

52. Rau, H.; Lueddecke, E., On the Rotation-Inversion Controversy on Photoisomerization of Azobenzenes. Experimental Proof of Inversion. *Journal of the American Chemical Society* **1982,** *104*, 1616.

53. Norikane, Y.; Tamaoki, N., Light-Driven Molecular Hinge: A New Molecular Machine Showing a Light-Intensity-Dependent Photoresponse That Utilizes the *Trans-Cis* Isomerization of Azobenzene. *Organic Letters* **2004,** *6*, 2595.

54. Muraoka, T.; Kinbara, K.; Aida, T., Mechanical Twisting of a Guest by a Photoresponsive Host. *Nature* **2006,** *440*, 512.

55. Varhegyi, P.; Kerekes, A.; Sajti, S.; Ujhelyi, F.; Koppa, P.; Szarvas, G.; Lorincz, E., Saturation Effect in Azobenzene Polymers Used for Polarization Holography. *Applied Physics B: Lasers and Optics* **2003,** *76*, 397.

56. Jiang, X. L.; Li, L.; Kumar, J.; Kim, D. Y.; Tripathy, S. K., Unusual Polarization Dependent Optical Erasure of Surface Relief Gratings on Azobenzene Polymer Films. *Applied Physics Letters* **1998,** *72*, 2502.

57. Yager, K. G.; Barrett, C. J., Novel Photo-Switching Using Azobenzene Functional Materials. *Journal of Photochemistry and Photobiology A: Chemistry* **2006,** *182*, 250.

58. Bandara, H. M.; Burdette, S. C., Photoisomerization in Different Classes of Azobenzene. *Chemical Society Reviews* **2012,** *41*, 1809.

59. Gagliardi, L.; Orlandi, G.; Bernardi, F.; Cembran, A.; Garavelli, M., A Theoretical Study of the Lowest Electronic States of Azobenzene: The Role of Torsion Coordinate in the *Cis-Trans* Photoisomerization. *Theoretical Chemistry Accounts* **2003,** *111*, 363.

60. Mostad, A.; Rømming, C.; Rømming, C.; Hammarström, S.; Lousberg, R. J. J. C.; Weiss, U., A Refinement of the Crystal Structure of *Cis*-Azobenzene. *Acta Chemica Scandinavica* **1971,** *25*, 3561.

61. Brown, C. J., A Refinement of the Crystal Structure of Azobenzene. *Acta Crystallographica* **1966,** *21*, 146.

62. Hartley, G. S., The *Cis*-Form of Azobenzene. *Nature* **1937,** *140*, 281.

63. de Wit, J.; van Ekenstein, G. A.; Polushkin, E.; Kvashnina, K.; Bras, W.; Ikkala, O.; ten Brinke, G., Self-Assembled Poly(4-Vinylpyridine)-Surfactant Systems Using Alkyl and Alkoxy Phenylazophenols. *Macromolecules* **2008,** *41*, 4200.

64. Yu, H., Recent Advances in Photoresponsive Liquid-Crystalline Polymers Containing Azobenzene Chromophores. *Journal of Materials Chemistry C* **2014,** *2*, 3047.

65. Mamiya, J.-i.; Yoshitake, A.; Kondo, M.; Yu, Y.; Ikeda, T., Is Chemical Crosslinking Necessary for the Photoinduced Bending of Polymer Films? *Journal of Materials Chemistry* **2008,** *18*, 63.

66. Stewart, D.; Imrie, C. T., Toward Supramolecular Side-Chain Liquid Crystal Polymers. 5. The Template Receptor Approach. *Macromolecules* **1997,** *30*, 877.

67. Cui, L.; Dahmane, S.; Tong, X.; Zhu, L.; Zhao, Y., Using Self-Assembly to Prepare Multifunctional Diblock Copolymers Containing Azopyridine Moiety. *Macromolecules* **2005,** *38*, 2076.

68. Wang, Y.; Han, P.; Xu, H.; Wang, Z.; Zhang, X.; Kabanov, A. V., Photocontrolled Self-Assembly and Disassembly of Block Ionomer Complex Vesicles: A Facile Approach toward Supramolecular Polymer Nanocontainers. *Langmuir* **2010,** *26*, 709.

69. Marcos, M.; Alcalá, R.; Barberá, J.; Romero, P.; Sánchez, C.; Serrano, J. L., Photosensitive Ionic Nematic Liquid Crystalline Complexes Based on Dendrimers and Hyperbranched Polymers and a Cyanoazobenzene Carboxylic Acid. *Chemistry of Materials* **2008,** *20*, 5209.

70. Kulikovska, O.; Goldenberg, L. M.; Kulikovsky, L.; Stumpe, J., Smart Ionic Sol-Gel-Based Azobenzene Materials for Optical Generation of Microstructures. *Chemistry of Materials* **2008,** *20*, 3528.

71. Kulikovsky, L.; Kulikovska, O.; Goldenberg, L. M.; Stumpe, J., Phenomenology of Photoinduced Processes in the Ionic Sol-Gel-Based Azobenzene Materials. *ACS Applied Materials & Interfaces* **2009,** *1*, 1739.

72. Fitzgerald, E. B.; Fuoss, R. M., Preparation and Fractionation of Poly-4-Vinylpyridine. *Industrial & Engineering Chemistry* **1950,** *42*, 1603.

73. Varshney, S. K.; Zhong, X. F.; Eisenberg, A., Anionic Homopolymerization and Block Copolymerization of 4-Vinylpyridine and Its Investigation by High-Temperature Size-Exclusion Chromatography in N-Methyl-2-Pyrrolidinone. *Macromolecules* **1993,** *26*, 701.

74. Creutz, S.; Teyssié, P.; Jérôme, R., Living Anionic Homopolymerization and Block Copolymerization of 4-Vinylpyridine at "Elevated" Temperature and Its Characterization by Size Exclusion Chromatography. *Macromolecules* **1997,** *30*, 1.

75. Bohrisch, J.; Wendler, U.; Jaeger, W., Controlled Radical Polymerization of 4-Vinylpyridine. *Macromolecular Rapid Communications* **1997,** *18*, 975.

76. Xia, J.; Zhang, X.; Matyjaszewski, K., Atom Transfer Radical Polymerization of 4-Vinylpyridine. *Macromolecules* **1999,** *32*, 3531.

77. Linnell, R., Notes- Dissociation Constants of 2-Substituted Pyridines. *The Journal of Organic Chemistry* **1960,** *25*, 290.

78. Vapaavuori, J.; Valtavirta, V.; Alasaarela, T.; Mamiya, J.-I.; Priimagi, A.; Shishido, A.; Kaivola, M., Efficient Surface Structuring and Photoalignment of Supramolecular Polymer-Azobenzene Complexes through Rational Chromophore Design. *Journal of Materials Chemistry* **2011,** *21*, 15437.

79. Saccone, M.; Dichiarante, V.; Forni, A.; Goulet-Hanssens, A.; Cavallo, G.; Vapaavuori, J.; Terraneo, G.; Barrett, C. J.; Resnati, G.; Metrangolo, P.; Priimagi, A., Supramolecular Hierarchy among Halogen and Hydrogen Bond Donors in Light-Induced Surface Patterning. *Journal of Materials Chemistry C* **2015,** *3*, 759.

80. Ruokolainen, J.; Tanner, J.; ten Brinke, G.; Ikkala, O.; Torkkeli, M.; Serimaa, R., Poly(4-Vinyl Pyridine)/Zinc Dodecyl Benzene Sulfonate Mesomorphic State due to Coordination Complexation. *Macromolecules* **1995,** *28*, 7779.

81. Viel, P.; Palacin, S.; Descours, F.; Bureau, C.; Le Derf, F.; Lyskawa, J.; Sallé, M., Electropolymerized Poly-4-Vinylpyridine for Removal of Copper from Wastewater. *Applied Surface Science* **2003,** *212-213*, 792.

82. Priimagi, A.; Lindfors, K.; Kaivola, M.; Rochon, P., Efficient Surface-Relief Gratings in Hydrogen-Bonded Polymer-Azobenzene Complexes. *ACS Applied Materials & Interfaces* **2009,** *1*, 1183.

83. Priimagi, A.; Vapaavuori, J.; Rodriguez, F. J.; Faul, C. F. J.; Heino, M. T.; Ikkala, O.; Kauranen, M.; Kaivola, M., Hydrogen-Bonded Polymer-Azobenzene Complexes: Enhanced

Photoinduced Birefringence with High Temporal Stability through Interplay of Intermolecular Interactions. *Chemistry of Materials* **2008,** *20*, 6358.

84. Vapaavuori, J.; Goulet-Hanssens, A.; Heikkinen, I. T. S.; Barrett, C. J.; Priimagi, A., Are Two Azo Groups Better Than One? Investigating the Photoresponse of Polymer-Bisazobenzene Complexes. *Chemistry of Materials* **2014,** *26*, 5089.

85. Wu, S.; Bubeck, C., Macro- and Microphase Separation in Block Copolymer Supramolecular Assemblies Induced by Solvent Annealing. *Macromolecules* **2013,** *46*, 3512.

86. Wang, X.; Vapaavuori, J.; Wang, X.; Sabat, R. G.; Pellerin, C.; Bazuin, C. G., Influence of Supramolecular Interaction Type on Photoresponsive Azopolymer Complexes: A Surface Relief Grating Formation Study. *Macromolecules* **2016,** *49*, 4923.

87. del Barrio, J.; Blasco, E.; Oriol, L.; Alcalá, R.; Sánchez-Somolinos, C., Diblock Copolymer-Azobenzene Complexes through Hydrogen Bonding: Self-Assembly and Stable Photoinduced Optical Anisotropy. *Journal of Polymer Science Part A: Polymer Chemistry* **2013,** *51*, 1716.

88. Brandys, F. A.; Bazuin, C. G., Mixtures of an Acid-Functionalized Mesogen with Poly(4-Vinylpyridine). *Chemistry of Materials* **1996,** *8*, 83.

89. Wang, X.; Bazuin, C. G.; Pellerin, C., Quantitative Analysis of Hydrogen Bonding in Electrospun Fibers of Poly(4-Vinyl Pyridine)/(4,4′-Biphenol) Complexes by ATR Using Liquid Blends as Models. *Vibrational Spectroscopy* **2014,** *71*, 18.

90. Roland, S.; Pellerin, C.; Bazuin, C. G.; Prud'homme, R. E., Evolution of Small Molecule Content and Morphology with Dip-Coating Rate in Supramolecular PS–P4VP Thin Films. *Macromolecules* **2012,** *45*, 7964.

91. Priimagi, A.; Cavallo, G.; Forni, A.; Gorynsztejn-Leben, M.; Kaivola, M.; Metrangolo, P.; Milani, R.; Shishido, A.; Pilati, T.; Resnati, G.; Terraneo, G., Halogen Bonding Versus Hydrogen Bonding in Driving Self-Assembly and Performance of Light-Responsive Supramolecular Polymers. *Advanced Functional Materials* **2012,** *22*, 2572.

92. Borah, K. J.; Dutta, P.; Borah, R., Synthesis, Characterization and Application of Poly(4-Vinylpyridine)-Supported Bronsted Acid as Reusable Catalyst for Acetylation Reaction. *Bulletin of the Korean Chemical Society* **2011,** *32*, 225.

93. Ikkala, O.; Ruokolainen, J.; ten Brinke, G.; Torkkeli, M.; Serimaa, R., Mesomorphic State of Poly(Vinylpyridine)-Dodecylbenzenesulfonic Acid Complexes in Bulk and in Xylene Solution. *Macromolecules* **1995,** *28*, 7088.

94. Zhu, X.; Beginn, U.; Moller, M.; Gearba, R. I.; Anokhin, D. V.; Ivanov, D. A., Self-Organization of Polybases Neutralized with Mesogenic Wedge-Shaped Sulfonic Acid Molecules: An Approach toward Supramolecular Cylinders. *Journal of the American Chemical Society* **2006,** *128*, 16928.

95. Xiao, S.; Lu, X.; Lu, Q., Photosensitive Polymer from Ionic Self-Assembly of Azobenzene Dye and Poly(Ionic Liquid) and Its Alignment Characteristic toward Liquid Crystal Molecules. *Macromolecules* **2007,** *40*, 7944.

96. Faul, C. F., Ionic Self-Assembly for Functional Hierarchical Nanostructured Materials. *Accounts of Chemical Research* **2014,** *47*, 3428.

97. Ube, T.; Ikeda, T., Photomobile Polymer Materials with Crosslinked Liquid-Crystalline Structures: Molecular Design, Fabrication, and Functions. *Angewandte Chemie, International Edition in English* **2014,** *53*, 10290.

98. Xiao, S.; Lu, X.; Lu, Q.; Su, B., Photosensitive Liquid-Crystalline Supramolecules Self-Assembled from Ionic Liquid Crystal and Polyelectrolyte for Laser-Induced Optical Anisotropy. *Macromolecules* **2008,** *41*, 3884.

99. Paterson, J.; Natansohn, A.; Rochon, P.; Callender, C. L.; Robitaille, L., Optically Inscribed Surface Relief Diffraction Gratings on Azobenzene-Containing Polymers for Coupling Light into Slab Waveguides. *Applied Physics Letters* **1996,** *69*, 3318.

100. Stockermans, R. J.; Rochon, P. L., Narrow-Band Resonant Grating Waveguide Filters Constructed with Azobenzene Polymers. *Applied Optics* **1999,** *38*, 3714.

101. Hvilsted, S.; Sánchez, C.; Alcalá, R., The Volume Holographic Optical Storage Potential in Azobenzene Containing Polymers. *Journal of Materials Chemistry* **2009,** *19*, 6641.

102. Natansohn, A.; Rochon, P., Photoinduced Motions in Azo-Containing Polymers. *Chemical Reviews* **2002,** *102*, 4139.

103. Utecht, M.; Klamroth, T.; Saalfrank, P., Optical Absorption and Excitonic Coupling in Azobenzenes Forming Self-Assembled Monolayers: A Study Based on Density Functional Theory. *Physical Chemistry Chemical Physics* **2011,** *13*, 21608.

104. Wang, X. Electrospinning and Characterization of Supramolecular Poly(4-Vinyl Pyridine)-Small Molecule Complexes. D*octoral Dissertation*, Université de Montréal, **2014**.

105. Fischer, M.; El Osman, A.; Blanche, P.-A.; Dumont, M., Photoinduce Dichroism as a Tool for Understanding Orientational Mobility of Photoisomerizable Dyes in Amorphous Matrices. *Synthetic Metals* **2000,** *115*, 139.

106. Yu, Y.; Ikeda, T., Alignment Modulation of Azobenzene-Containing Liquid Crystal Systems by Photochemical Reactions. *Journal of Photochemistry and Photobiology C: Photochemistry Reviews* **2004,** *5*, 247.

107. Yu, H.; Kobayashi, T., Photoresponsive Block Copolymers Containing Azobenzenes and Other Chromophores. *Molecules* **2010,** *15*, 570.

108. Yu, Y.; Nakano, M.; Ikeda, T., Photomechanics: Directed Bending of a Polymer Film by Light. *Nature* **2003,** *425*, 145.

109. Tanchak, O. M.; Barrett, C. J., Light-Induced Reversible Volume Changes in Thin Films of Azo Polymers: The Photomechanical Effect. *Macromolecules* **2005,** *38*, 10566.

110. Yager, K. G.; Tanchak, O. M.; Godbout, C.; Fritzsche, H.; Barrett, C. J., Photomechanical Effects in Azo-Polymers Studied by Neutron Reflectometry. *Macromolecules* **2006,** *39*, 9311.

111. Viswanathan, N. K.; Kim, D. Y.; Bian, S.; Williams, J.; Liu, W.; Li, L.; Samuelson, L.; Kumar, J.; Tripathy, S. K., Surface Relief Structures on Azo Polymer Films. *Journal of Materials Chemistry* **1999,** *9*, 1941.

112. Rochon, P.; Batalla, E.; Natansohn, A., Optically Induced Surface Gratings on Azoaromatic Polymer Films. *Applied Physics Letters* **1995,** *66*, 136.

113. Yager, K. G.; Barrett, C. J., Photomechanical Surface Patterning in Azo-Polymer Materials. *Macromolecules* **2006,** *39*, 9320.

114. Weigert, F., Photodichroismus Und Photoanisotropie. I. *Zeitschrift für Physikalische Chemie* **1929,** *3B*.

115. Kumar, G. S.; Neckers, D. C., Photochemistry of Azobenzene-Containing Polymers. *Chemical Reviews* **1989,** *89*, 1915.

116. Xie, S.; Natansohn, A.; Rochon, P., Recent Developments in Aromatic Azo Polymers Research. *Chemistry of Materials* **1993,** *5*, 403.

117. Ho, M.-S.; Natansohn, A.; Barrett, C.; Rochon, P., Azo Polymers for Reversible Optical Storage. 8. The Effect of Polarity of the Azobenzene Groups. *Canadian Journal of Chemistry* **1995,** *73*, 1773.

118. Ho, M. S.; Natansohn, A.; Rochon, P., Azo Polymers for Reversible Optical Storage. 7. The Effect of the Size of the Photochromic Groups. *Macromolecules* **1995,** *28*, 6124.

119. Barrett, C.; Choudhury, B.; Natansohn, A.; Rochon, P., Azocarbazole Polymethacrylates as Single-Component Electrooptic Materials. *Macromolecules* **1998,** *31*, 4845.

120. Cojocariu, C.; Rochon, P., Light-Induced Motions in Azobenzene-Containing Polymers. *Pure and Applied Chemistry* **2004,** *76*, 1479.

121. Koskela, J. E.; Vapaavuori, J.; Hautala, J.; Priimagi, A.; Faul, C. F. J.; Kaivola, M.; Ras, R. H. A., Surface-Relief Gratings and Stable Birefringence Inscribed Using Light of Broad Spectral Range in Supramolecular Polymer-Bisazobenzene Complexes. *The Journal of Physical Chemistry C* **2012,** *116*, 2363.

122. Rochon, P.; Gosselin, J.; Natansohn, A.; Xie, S., Optically Induced and Erased Birefringence and Dichroism in Azoaromatic Polymers. *Applied Physics Letters* **1992,** *60*, 4.

123. Nadtoka, O.; Syromyatnikov, V.; Tarasenko, V., Photoinduced Orientation of Azobenzene Groups in Polymer Films. Characterization by UV/Visible Spectroscopy. *Molecular Crystals and Liquid Crystals* **2011,** *536*, 122.

124. Natansohn, A.; Rochon, P.; Pezolet, M.; Audet, P.; Brown, D.; To, S., Azo Polymers for Reversible Optical Storage. 4. Cooperative Motion of Rigid Groups in Semicrystalline Polymers. *Macromolecules* **1994,** *27*, 2580.

125. Wiesner, U.; Reynolds, N.; Boeffel, C.; Spiess, H. W., An Infrared Spectroscopic Study of Photo-Induced Reorientation in Dye Containing Liquid-Crystalline Polymers. *Liquid Crystals* **1992,** *11*, 251.

126. Buffeteau, T.; Pézolet, M., In Situ Study of Photoinduced Orientation in Azopolymers by Time-Dependent Polarization Modulation Infrared Spectroscopy. *Applied Spectroscopy* **1996,** *50*, 948.

127. Marcott, C., Linear Dichroism of Polymer Films Using a Polarization-Modulation Fourier Transform Infrared Technique. *Applied Spectroscopy* **1984,** *38*, 442.

128. Buffeteau, T.; Lagugné Labarthet, F.; Pézolet, M.; Sourisseau, C., Photoinduced Orientation of Azobenzene Chromophores in Amorphous Polymers as Studied by Real-Time Visible and FTIR Spectroscopies. *Macromolecules* **1998,** *31*, 7312.

129. Buffeteau, T.; Desbat, B.; Besbes, S.; Nafati, M.; Bokobza, L., Molecular Orientation Studies in Polymer Films by Polarization Modulation FTI.R. Spectroscopy. *Polymer* **1994,** *35*, 2538.

130. Liang, Y.; Mauran, D.; Prud'homme, R. E.; Pellerin, C., A New Method for the Time-Resolved Analysis of Structure and Orientation: Polarization Modulation Infrared Structural Absorbance Spectroscopy. *Applied Spectroscopy* **2008,** *62*, 941.

131. Hvilsted, S.; Andruzzi, F.; Kulinna, C.; Siesler, H. W.; Ramanujam, P. S., Novel Side-Chain Liquid Crystalline Polyester Architecture for Reversible Optical Storage. *Macromolecules* **1995,** *28*, 2172.

132. Kulinna, C.; Hvilsted, S.; Hendann, C.; Siesler, H. W.; Ramanujam, P. S., Selectively Deuterated Liquid Crystalline Cyanoazobenzene Side-Chain Polyesters. 3. Investigations of Laser-Induced Segmental Mobility by Fourier Transform Infrared Spectroscopy. *Macromolecules* **1998,** *31*, 2141.

133. Han, M.; Kidowaki, M.; Ichimura, K.; Ramanujam, P. S.; Hvilsted, S., Influence of Structures of Polymer Backbones on Cooperative Photoreorientation Behavior of *P*-Cyanoazobenzene Side Chains. *Macromolecules* **2001,** *34*, 4256.

134. Zebger, I.; Rutloh, M.; Hoffmann, U.; Stumpe, J.; Siesler, H. W.; Hvilsted, S., Photoorientation of a Liquid Crystalline Polyester with Azobenzene Side Groups. 1. Effects of Irradiation with Linearly Polarized Blue Light. *The Journal of Physical Chemistry A* **2002,** *106*, 3454.

135. Tawa, K.; Kamada, K.; Sakaguchi, T.; Ohta, K., Photoinduced Anisotropy in a Polymer Doped with Azo Dyes in the Photostationary State Studied by Polarized FT-IR Spectroscopy. *Applied Spectroscopy* **1998,** *52*, 1536.

136. Tawa, K.; Kamada, K.; Sakaguchi, T.; Ohta, K., Local Environment Dependence of Photoinduced Anisotropy Observed in Azo-Dye-Doped Polymer Films. *Polymer* **2000,** *41*, 3235.

137. Tawa, K.; Zettsu, N.; Minematsu, K.; Ohta, K.; Namba, A.; Tran-Cong, Q., Photoinduced Reorientation of Azo-Dyes Covalently Linked to a Styrene Copolymer in Bulk State. *Journal of Photochemistry and Photobiology A: Chemistry* **2001,** *143*, 31.

138. Tawa, K.; Kamada, K.; Kiyohara, K.; Ohta, K.; Yasumatsu, D.; Sekkat, Z.; Kawata, S., Photoinduced Reorientation of Azo Dyes Bonded to Polyurethane Studied by Polarized FT-IR Spectroscopy. *Macromolecules* **2001,** *34*, 8232.

139. Labarthet, F. L.; Freiberg, S.; Pellerin, C.; Pézolet, M.; Natansohn, A.; Rochon, P., Spectroscopic and Optical Characterization of a Series of Azobenzene-Containing Side-Chain Liquid Crystalline Polymers. *Macromolecules* **2000,** *33*, 6815.

140. Wang, X.; Vapaavuori, J.; Bazuin, C. G.; Pellerin, C., Molecular-Level Study of Photoorientation in Hydrogen-Bonded Azopolymer Complexes. *Macromolecules* **2018,** *51*, 1077.

141. Kim, D. Y.; Tripathy, S. K.; Li, L.; Kumar, J., Laser-Induced Holographic Surface Relief Gratings on Nonlinear Optical Polymer Films. *Applied Physics Letters* **1995,** *66*, 1166.

142. Rochon, P.; Natansohn, A.; Callender, C. L.; Robitaille, L., Guided Mode Resonance Filters Using Polymer Films. *Applied Physics Letters* **1997,** *71*, 1008.

143. Li, X. T.; Natansohn, A.; Rochon, P., Photoinduced Liquid Crystal Alignment Based on a Surface Relief Grating in an Assembled Cell. *Applied Physics Letters* **1999,** *74*, 3791.

144. Kim, M.-H.; Kim, J.-D.; Fukuda, T.; Matsuda, H., Alignment Control of Liquid Crystals on Surface Relief Gratings. *Liquid Crystals* **2000,** *27*, 1633.

145. Yi, D. K.; Seo, E.-M.; Kim, D.-Y., Surface-Modulation-Controlled Three-Dimensional Colloidal Crystals. *Applied Physics Letters* **2002,** *80*, 225.

146. Liu, B.; Wang, M.; He, Y.; Wang, X., Duplication of Photoinduced Azo Polymer Surface-Relief Gratings through a Soft Lithographic Approach. *Langmuir* **2006,** *22*, 7405.

147. Na, S.-I.; Kim, S.-S.; Jo, J.; Oh, S.-H.; Kim, J.; Kim, D.-Y., Efficient Polymer Solar Cells with Surface Relief Gratings Fabricated by Simple Soft Lithography. *Advanced Functional Materials* **2008,** *18*, 3956.

148. Hubert, C.; Rumyantseva, A.; Lerondel, G.; Grand, J.; Kostcheev, S.; Billot, L.; Vial, A.; Bachelot, R.; Royer, P.; Chang, S. H.; Gray, S. K.; Wiederrecht, G. P.; Schatz, G. C., Near-Field Photochemical Imaging of Noble Metal Nanostructures. *Nano Letters* **2005,** *5*, 615.

149. Haggui, M.; Dridi, M.; Plain, J.; Marguet, S.; Perez, H.; Schatz, G. C.; Wiederrecht, G. P.; Gray, S. K.; Bachelot, R., Spatial Confinement of Electromagnetic Hot and Cold Spots in Gold Nanocubes. *ACS Nano* **2012,** *6*, 1299.

150. Ubukata, T.; Hara, M.; Ichimura, K.; Seki, T., Phototactic Mass Transport in Polymer Films for Micropatterning and Alignment of Functional Materials. *Advanced Materials* **2004,** *16*, 220.

151. Lee, S.; Kang, H. S.; Park, J. K., Directional Photofluidization Lithography: Micro/Nanostructural Evolution by Photofluidic Motions of Azobenzene Materials. *Advanced Materials* **2012,** *24*, 2069.

152. Barrett, C. J.; Natansohn, A. L.; Rochon, P. L., Mechanism of Optically Inscribed High-Efficiency Diffraction Gratings in Azo Polymer Films. *The Journal of Physical Chemistry* **1996,** *100*, 8836.

153. Holme, N. C. R.; Nikolova, L.; Hvilsted, S.; Rasmussen, P. H.; Berg, R. H.; Ramanujam, P. S., Optically Induced Surface Relief Phenomena in Azobenzene Polymers. *Applied Physics Letters* **1999,** *74*, 519.

154. Zettsu, N.; Ubukata, T.; Seki, T.; Ichimura, K., Soft Crosslinkable Azo Polymer for Rapid Surface Relief Formation and Persistent Fixation. *Advanced Materials* **2001,** *13*, 1693.

155. Zettsu, N.; Seki, T., Highly Efficient Photogeneration of Surface Relief Structure and Its Immobilization in Cross-Linkable Liquid Crystalline Azobenzene Polymers. *Macromolecules* **2004,** *37*, 8692.

156. Zettsu, N.; Ogasawara, T.; Arakawa, R.; Nagano, S.; Ubukata, T.; Seki, T., Highly Photosensitive Surface Relief Gratings Formation in a Liquid Crystalline Azobenzene Polymer: New Implications for the Migration Process. *Macromolecules* **2007,** *40*, 4607.

157. Seki, T., Meso- and Microscopic Motions in Photoresponsive Liquid Crystalline Polymer Films. *Macromolecular Rapid Communications* **2014,** *35*, 271.

158. Toshchevikov, V.; Saphiannikova, M.; Heinrich, G., Microscopic Theory of Light-Induced Deformation in Amorphous Side-Chain Azobenzene Polymers. *Journal of Physical Chemistry B* **2009,** *113*, 5032.

159. Saphiannikova, M.; Neher, D., Thermodynamic Theory of Light-Induced Material Transport in Amorphous Azobenzene Polymer Films. *Journal of Physical Chemistry B* **2005,** *109*, 19428.

160. Saphiannikova, M., Photoinduced Deformations in Azobenzene Polymer Films. *Nonlinear Optics and Quantum Optics* **2010,** *41*, 27.

161. Hurduc, N.; Donose, B. C.; Macovei, A.; Paius, C.; Ibanescu, C.; Scutaru, D.; Hamel, M.; Branza-Nichita, N.; Rocha, L., Direct Observation of Athermal Photofluidisation in Azo-Polymer Films. *Soft Matter* **2014,** *10*, 4640.

162. Yadavalli, N. S.; Loebner, S.; Papke, T.; Sava, E.; Hurduc, N.; Santer, S., A Comparative Study of Photoinduced Deformation in Azobenzene Containing Polymer Films. *Soft Matter* **2016,** *12*, 2593.

163. Ambrosio, A.; Marrucci, L.; Borbone, F.; Roviello, A.; Maddalena, P., Light-Induced Spiral Mass Transport in Azo-Polymer Films under Vortex-Beam Illumination. *Nature Communications* **2012,** *3*, 989.

164. Kim, D. Y.; Li, L.; Jiang, X. L.; Shivshankar, V.; Kumar, J.; Tripathy, S. K., Polarized Laser Induced Holographic Surface Relief Gratings on Polymer Films. *Macromolecules* **1995,** *28*, 8835.

165. Fabbri, F.; Garrot, D.; Lahlil, K.; Boilot, J. P.; Lassailly, Y.; Peretti, J., Evidence of Two Distinct Mechanisms Driving Photoinduced Matter Motion in Thin Films Containing Azobenzene Derivatives. *Journal of Physical Chemistry B* **2011,** *115*, 1363.

166. Sobolewska, A.; Bartkiewicz, S., Surface Relief Grating in Azo-Polymer Obtained for S-S Polarization Configuration of the Writing Beams. *Applied Physics Letters* **2012,** *101*, 193301.

167. Gao, J.; He, Y.; Liu, F.; Zhang, X.; Wang, Z.; Wang, X., Azobenzene-Containing Supramolecular Side-Chain Polymer Films for Laser-Induced Surface Relief Gratings. *Chemistry of Materials* **2007,** *19*, 3877.

168. Koskela, J. E.; Vapaavuori, J.; Ras, R. H. A.; Priimagi, A., Light-Driven Surface Patterning of Supramolecular Polymers with Extremely Low Concentration of Photoactive Molecules. *ACS Macro Letters* **2014,** *3*, 1196.

169. Börger, V.; Menzel, H.; Huber, M. R., Influence of the Molecular Weight of Azopolymers on the Photo-Induced Formation of Surface Relief Gratings. *Molecular Crystals and Liquid Crystals* **2005,** *430*, 89.

170. Buffeteau, T.; Pezolet, M., In Situ Study of Photoinduced Orientation in Azopolymers by Time-Dependent Polarization Modulation Infrared Spectroscopy. *Applied Spectroscopy* **1996,** *50*, 948.

171. Vapaavuori, J.; Valtavirta, V.; Alasaarela, T.; Mamiya, J.-I.; Priimagi, A.; Shishido, A.; Kaivola, M., Efficient Surface Structuring and Photoalignment of Supramolecular Polymer-Azobenzene Complexes through Rational Chromophore Design. *Journal of Materials Chemistry* **2011,** *21*, 15437.

172. Vapaavuori, J.; Heikkinen, I. T. S.; Dichiarante, V.; Resnati, G.; Metrangolo, P.; Sabat, R. G.; Bazuin, C. G.; Priimagi, A.; Pellerin, C., Photomechanical Energy Transfer to Photopassive Polymers through Hydrogen and Halogen Bonds. *Macromolecules* **2015,** *48*, 7535.

173. Zhang, Q.; Wang, X.; Barrett, C. J.; Bazuin, C. G., Spacer-Free Ionic Dye-Polyelectrolyte Complexes: Influence of Molecular Structure on Liquid Crystal Order and Photoinduced Motion. *Chemistry of Materials* **2009,** *21*, 3216.

174. Zhang, L.; Cole, J. M.; Dai, C., Variation in Optoelectronic Properties of Azo Dye-Sensitized TiO_2 Semiconductor Interfaces with Different Adsorption Anchors: Carboxylate, Sulfonate, Hydroxyl and Pyridyl Groups. *ACS Applied Materials & Interfaces* **2014,** *6*, 7535.

175. Kojima, M.; Nebashi, S.; Ogawa, K.; Kurita, N., Effect of Solvent on *Cis-to-Trans* Isomerization of 4-Hydroxyazobenzene Aggregated through Intermolecular Hydrogen Bonds. *Journal of Physical Organic Chemistry* **2005,** *18*, 994.

176. Moniruzzaman, M.; Talbot, J. D. R.; Sabey, C. J.; Fernando, G. F., The Use of ^{1}H NMR and UV-Vis Measurements for Quantitative Determination of *Trans/Cis* Isomerization of a Photo-Responsive Monomer and Its Copolymer. *Journal of Applied Polymer Science* **2006,** *100*, 1103.

177. Bortolus, P.; Monti, S., *Cis-Trans* Photoisomerization of Azobenzene. Solvent and Triplet Donors Effects. *The Journal of Physical Chemistry* **1979,** *83*, 648.

178. Karukstis, K. K.; Savin, D. A.; Loftus, C. T.; D'Angelo, N. D., Spectroscopic Studies of the Interaction of Methyl Orange with Cationic Alkyltrimethylammonium Bromide Surfactants. *Journal of Colloid and Interface Science* **1998,** *203*, 157.

179. Nandini, R.; Vishalakshi, B., A Study of Interaction of Methyl Orange with Some Polycations. *E-Journal of Chemistry* **2012,** *9*, 1.

180. Eisenbach, C. D., Effect of Polymer Matrix on the *Cis-Trans* Isomerization of Azobenzene Residues in Bulk Polymers. *Die Makromolekulare Chemie* **1978,** *179*, 2489.

181. Griffiths, P. R., De Haseth, J. A. , Fourier Transform Infrared Spectrometry. 2nd ed.; *John Wiley & Sons*: **2007**.

182. Roland, S.; Gaspard, D.; Prud'homme, R. E.; Bazuin, C. G., Morphology Evolution in Slowly Dip-Coated Supramolecular PS-b-P4VP Thin Films. *Macromolecules* **2012,** *45*, 5463.

183. de Santiago-Solís, C.; Rodríguez-González, R. J.; Larios-López, L.; Torres-Rocha, O. L.; Felix-Serrano, I.; Martínez-Ponce, G.; Navarro-Rodríguez, D., Liquid-Crystalline and Photo-Induced Properties of P4VP Quaternized with Bromo Derivative of Dialkyloxy-Phenyleneazobenzene Groups. *Journal of Applied Polymer Science* **2017,** *134*.

184. Vorontsov, Y. D.; Panov, V. P., Vibrational Spectra of Protonated Poly-4-Vinylpyridine. *Polymer Science U.S.S.R.* **1976,** *18*, 2752.

185. Blanche, P. A.; Lemaire, P. C.; Dumont, M.; Fischer, M., Photoinduced Orientation of Azo Dye in Various Polymer Matrices. *Optics Letters* **1999,** *24*, 1349.

186. Fischer, M.; El Osman, A.; Blanche, P. A.; Dumont, M., Photoinduce Dichroism as a Tool for Understanding Orientational Mobility of Photoisomerizable Dyes in Amorphous Matrices. *Synthetic Metals* **2000,** *115*, 139.

187. Lessard, R. A.; Dumont, M. L.; Sekkat, Z., Dynamical Study of Photoinduced Anisotropy and Orientational Relaxation of Azo Dyes in Polymeric Films: Poling at Room Temperature. **1993,** *1774*, 188.

188. Smith, M. A. G.; Mitchell, G. R.; O$rquot$Leary, S. V., Local Gratings Due to Angular Hole Burning in a Photorefractive Polymer. *Journal of Optics A: Pure and Applied Optics* **2002,** *4*, 474.

189. Kiselev, A. D.; Chigrinov, V. G.; Kwok, H. S., Kinetics of Photoinduced Ordering in Azo-Dye Films: Two-State and Diffusion Models. *Physical Review. E, Statistical, Nonlinear, and Soft Matter Physics* **2009,** *80*, 011706.

190. Kiselev, A. D.; Chigrinov, V. G.; Pasechnik, S. V.; Dubtsov, A. V., Photoinduced Reordering in Thin Azo-Dye Films and Light-Induced Reorientation Dynamics of the Nematic Liquid-Crystal Easy Axis. *Physical Review. E, Statistical, Nonlinear, and Soft Matter Physics* **2012,** *86*, 011706.

191. Laventure, A.; Bourotte, J.; Vapaavuori, J.; Karperien, L.; Sabat, R. G.; Lebel, O.; Pellerin, C., Photoactive/Passive Molecular Glass Blends: An Efficient Strategy to Optimize Azomaterials for Surface Relief Grating Inscription. *ACS Applied Materials & Interfaces* **2017,** *9*, 798.

192. Brown, D.; Natansohn, A.; Rochon, P., Azo Polymers for Reversible Optical Storage. 5. Orientation and Dipolar Interactions of Azobenzene Side Groups in Copolymers and Blends Containing Methyl Methacrylate Structural Units. *Macromolecules* **1995,** *28*, 6116.

193. Chien, F. S. S.; Lin, C. Y.; Huang, C. R.; Chang, C. S.; Hsu, C. C., Polar Orientation Induced by Local Photo-Assisted Poling in Azo Copolymer Films. *Journal of the Optical Society of America B* **2010,** *27*, 773.

194. Fuhrmann, T.; Kunze, M.; Wendorff, J. H., "Monte Carlo Kinetics" for the Simulation of Photoreactions in Polymers. *Macromolecular Theory and Simulations* **1998,** *7*, 421.

195. Chigrinov, V.; Pikin, S.; Verevochnikov, A.; Kozenkov, V.; Khazimullin, M.; Ho, J.; Huang, D. D.; Kwok, H. S., Diffusion Model of Photoaligning in Azo-Dye Layers. *Physical Review. E, Statistical, Nonlinear, and Soft Matter Physics* **2004,** *69*, 061713.

196. Cantatore, V.; Granucci, G.; Persico, M., The Photo-Orientation of Azobenzene in Viscous Solutions, Simulated by a Stochastic Model. *Physical Chemistry Chemical Physics* **2014,** *16*, 25081.

197. Van Leuven, P.; Cantatore, V.; Persico, M., Photo-Orientation of Axial Molecules. *Physical Chemistry Chemical Physics* **2012,** *14*, 1957.

198. Cusati, T.; Granucci, G.; Persico, M., Photodynamics and Time-Resolved Fluorescence of Azobenzene in Solution: A Mixed Quantum-Classical Simulation. *Journal of the American Chemical Society* **2011,** *133*, 5109.

199. Vapaavuori, J.; Laventure, A.; Bazuin, C. G.; Lebel, O.; Pellerin, C., Submolecular Plasticization Induced by Photons in Azobenzene Materials. *Journal of the American Chemical Society* **2015,** *137*, 13510.

200. Teboul, V.; Saiddine, M.; Nunzi, J. M.; Accary, J. B., An Isomerization-Induced Cage-Breaking Process in a Molecular Glass Former Below T_g . *Journal of Chemical Physics* **2011,** *134*, 114517.

201. Lagugné Labarthet, F.; Buffeteau, T.; Sourisseau, C., Analyses of the Diffraction Efficiencies, Birefringence, and Surface Relief Gratings on Azobenzene-Containing Polymer Films. *The Journal of Physical Chemistry B* **1998,** *102*, 2654.

202. Yager, K. G.; Barrett, C. J., Confinement of Surface Patterning in Azo-Polymer Thin Films. *Journal of Chemical Physics* **2007,** *126*, 094908.

203. Barrett, C. J.; Natansohn, A. L.; Rochon, P. L., Mechanism of Optically Inscribed High-Efficiency Diffraction Gratings in Azo Polymer Films. *Journal of Physical Chemistry* **1996,** *100*, 8836.

204. Börger, V.; Pohle, S.; Kuliskovska, O.; Gharaggozloo-Hubmann, K.; Stumpe, J.; Menzel, H., Azobenzene-Containing Polymers for Surface Relief Gratings. *Macromolecular Symposia* **2009,** *275-276*, 257.

205. Stumpel, J. E.; Saccone, M.; Dichiarante, V.; Lehtonen, O.; Virkki, M.; Metrangolo, P.; Priimagi, A., Surface-Relief Gratings in Halogen-Bonded Polymer-Azobenzene Complexes: A Concentration-Dependence Study. *Molecules* **2017,** *22*, 1.

206. Bertani, R.; Metrangolo, P.; Moiana, A.; Perez, E.; Pilati, T.; Resnati, G.; Rico-Lattes, I.; Sassi, A., Supramolecular Route to Fluorinated Coatings: Self-Assembly between Poly(4-Vinylpyridines) and Haloperfluorocarbons. *Advanced Materials* **2002,** *14*, 1197.